Article

From Fragment to Lead: De Novo Design and Development toward a Selective FGFR2 Inhibitor

Lewis D. Turner, Chi H. Trinh, Ryan A. Hubball, Kyle M. Orritt, Chi-Chuan Lin, Julie E. Burns, Margaret A. Knowles, and Colin W. G. Fishwick*

Read Online

ACCESS | Metrics & More | Article Recommendations | Supporting Information

ABSTRACT: Fibroblast growth factor receptors (FGFRs) are implicated in a range of cancers with several pan-kinase and selective-FGFR inhibitors currently being evaluated in clinical trials. Pan-FGFR inhibitors often cause toxic side effects and few examples of subtype-selective inhibitors exist. Herein, we describe a structure-guided approach toward the development of a selective FGFR2 inhibitor. De novo design was carried out on an existing fragment series to yield compounds predicted to improve potency against the FGFRs. Subsequent iterative rounds of synthesis and biological evaluation led to an inhibitor with nanomolar potency that exhibited moderate selectivity for FGFR2 over FGFR1/3. Subtle changes to the lead inhibitor resulted in a complete loss of selectivity for FGFR2. X-ray crystallographic studies revealed inhibitor-specific morphological differences in the P-loop which were posited to be fundamental to the selectivity of these compounds. Additional docking studies have predicted an FGFR2-selective H-bond which could be utilized to design more selective FGFR2 inhibitors.
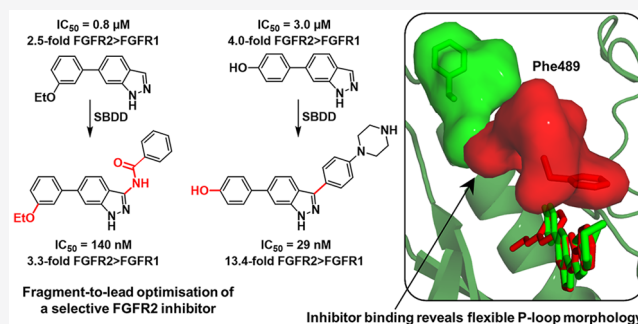
INTRODUCTION

FGFRs are transmembrane receptor tyrosine kinases that transmit cellular signaling by binding FGFs. The four known FGFRs (FGFR1−4) are implicated in various cellular processes such as development, tissue repair, and wound healing,[1] and have been shown to play crucial roles in the formation of cancer.[2−4] The general structure of all FGFRs is uniform, consisting of an extracellular binding domain, a single transmembrane domain, and an intracellular domain.[1] Binding of an FGF to the extracellular domain causes receptor dimerization and subsequent conformational changes which lead to order-specific transautophosphorylation of specific tyrosine residues within the intracellular kinase domain.[5,6] FGFR signal transduction leads to activation of a plethora of cascade pathways, including PI3K-PKB, RAS-MAPK, phospholipase C gamma (PLCγ), and signal transducer and activator of transcription proteins (STAT).[7]

Aberrant signaling of FGFRs is implicated in a multitude of cancer types, including bladder, endometrial, breast, and lung, with disease progression occurring through overexpression, point mutations, and/or chromosomal translocations.[8−11] The advancement of small molecule therapeutics for FGFR-implicated malignancies has illuminated several pan-angiokinase and FGFR-selective inhibitors which have been extensively documented over the past few years (Figure 1).[12−17]

Kinase inhibitors are classified into seven distinct categories (Type I, I1/2, II, III, IV, V, and VI) determined by their respective modes of inhibition.[18] Type I and I1/2 inhibitors occupy the ATP-binding site with the Asp-Phe-Gly (DFG) motif, a conserved region of the activation loop, exhibiting an "in" conformation (Figure S1A), with Type I and I1/2 inhibitors targeting the active and inactive forms of the kinase, respectively. Erdafitinib, a Type I1/2 inhibitor, was approved in the United States in 2019 for the treatment of locally advanced or metastatic FGFR2/3-driven urothelial carcinoma and is currently under investigation for a range of other FGFR-implicated cancers.[19] Type II inhibitors bind within the ATP binding pocket with a "DFG-out" conformation (Figure S1B) and solely bind the inactive form of the kinase. These inhibitors offer an advantage over Type I inhibitors in that their binding modes are noncompetitive with ATP and may overcome issues of selectivity arising from the structural similarities of kinase ATP binding pockets.[20] Ponatinib is a Type II inhibitor and gained accelerated FDA approval for the rare disease chronic myeloid leukemia in 2012, where
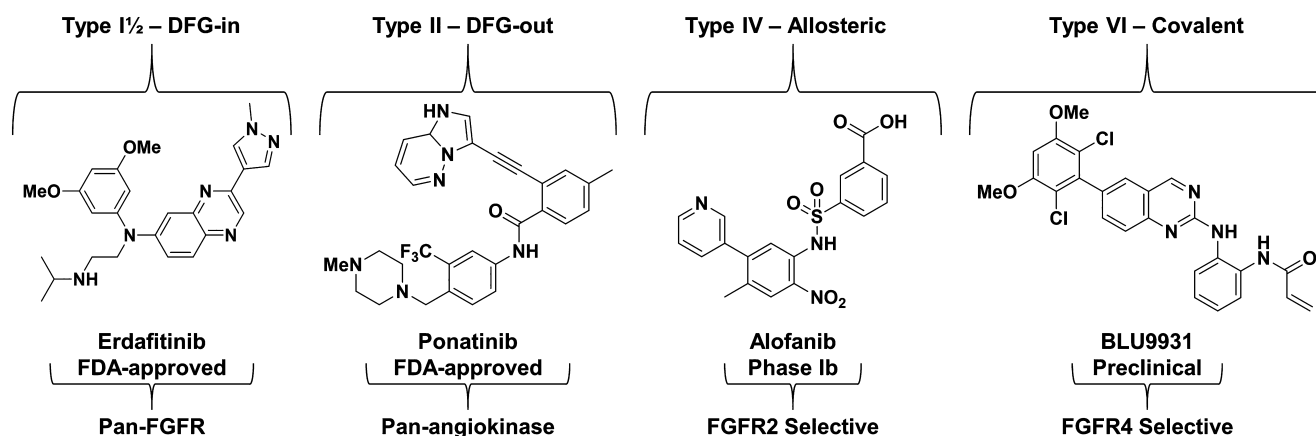
Figure 1. Examples of Type I1/2, II, IV, and VI small molecule kinase inhibitors currently approved or in development for FGFR-implicated malignancies.
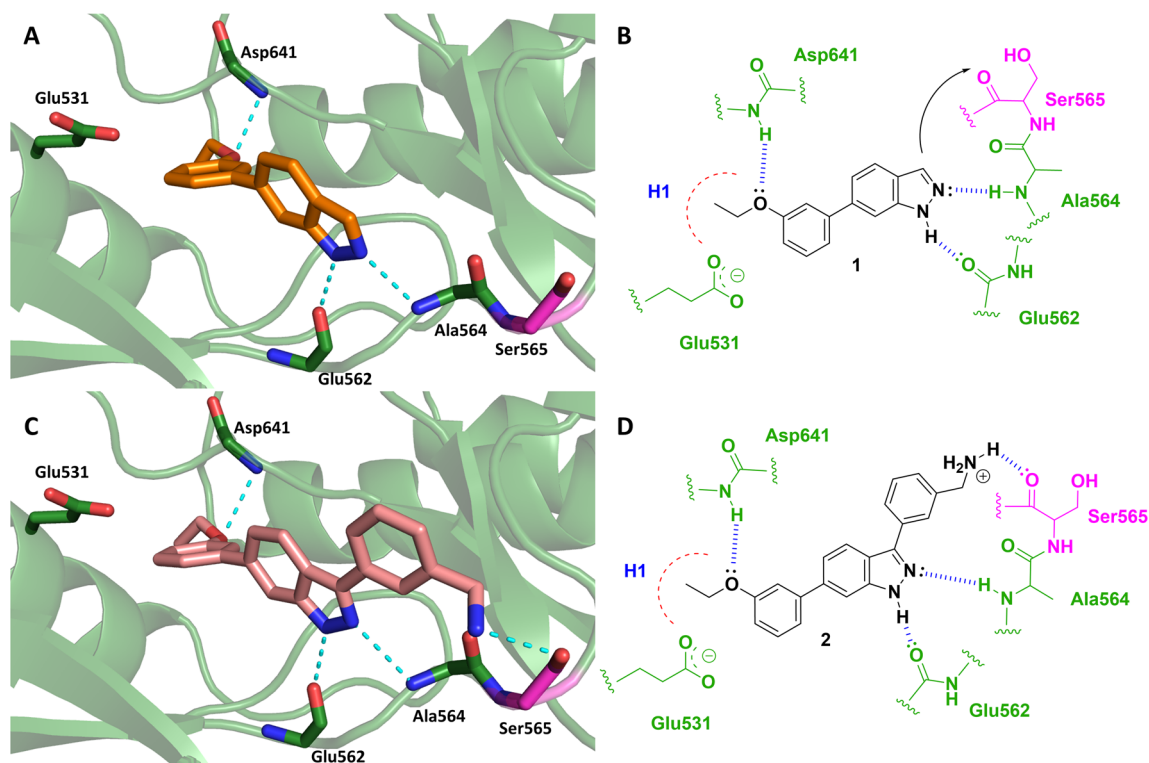

Figure 2. (A) Glide docking model of **1** (orange) bound within the FGFR1 active site. Predicted H-bonds are outlined by cyan hashed lines. (B) 2D representation of predicted binding mode of **1** bound within the FGFR1 active site. Hydrophobic pocket outlined by hashed red arc. Fragment growth can be carried out by extension at the 3-position toward Ser565. (C) Glide docking model of de novo designed compound **2** (pink). A new H-bond was predicted between the benzylamine and the backbone carbonyl of Ser565. (D) 2D representation of predicted binding mode of **2** bound within FGFR1. De novo design and docking were carried out using the FGFR1/CH5183284 cocrystal structure (PDB 5B7V).[49]

resistance or intolerance to at least two other kinase inhibitors was implicated.[21] Type III and IV inhibitors are allosteric in nature, with Type III inhibitors binding next to the ATP-binding pocket and Type IV inhibitors binding to other areas of the enzyme.[18] Alofanib is a selective FGFR2 Type IV inhibitor and binds to the extracellular domain of the kinase, disrupting signal transduction through prevention of FGF binding.[22] It is has been shown to have antitumor effects in preclinical ovarian cancer models and is currently being evaluated in Phase Ib for patients with metastatic gastric cancer.[23,24] Type V inhibitors are single entity, bivalent molecules that bind two distinct sites of the kinase simultaneously, e.g. the ATP-binding pocket and an allosteric

site joined by a linker.[18] Currently, no examples of FGFR inhibitors possess this type of inhibition, but this approach has been used for other kinases such as Src and Abl.[25−27] Type I−V are all reversible in nature, whereas the remaining category, Type VI, represents inhibitors with covalent modification potential.[18] The kinase domain of FGFR1−4 contains several conserved cysteine residues (Figure S2). Cys486 (in FGFR1) has been the target of several irreversible modifier campaigns owing to its close proximity to the ATP-binding pocket.[28−30] FGFR4 possesses a nonconserved cysteine (Cys552) at the entrance of the ATP-binding pocket and has also allowed the development of selective FGFR4 irreversible inhibitors (Figure S1C).[31,32] BLU9931 was one of the first selective irreversible

FGFR4 inhibitors and possesses exquisite selectivity; it is currently under investigation for the treatment of hepatocellular carcinomas.[33]

Although desired through their ability to treat various FGFR malignancies, pan-FGFR inhibitors often exhibit "FGFR1-specific" toxicity profiles that lead to adverse side effects, such as hyperphosphatemia and tissue mineralization, believed to stem from abnormal signaling of FGF23.[34] The development of exquisitely selective FGFR subtype inhibitors remains heavily biased toward FGFR4, through means outlined vide supra, as the high sequence homology (Table S1) of the FGFR1−3 kinase domains, particularly the active site residues, has made it very difficult to develop Type I, I1/2, or II subtype selective inhibitors. Of particular importance is the development of FGFR2 subtype selective inhibitors. Several studies have outlined the role of FGFR2 as an oncogenic driver in cholangiocarcinoma, a rare form of cancer that is difficult to diagnose and affects ∼8000 people in the United States each year.[35−37] FGFR2 has also been shown to play a role in promoting acquired resistance of human epidermal growth factor receptor 2 (HER2)-targeted treatments via indirect overactivation of FGFR2 from tumor-associated fibroblasts.[38] A recent breakthrough announced by Casaletto and coworkers has outlined the development of RLY-4008 (structure not publicly disclosed), an exquisitely selective FGFR2 inhibitor that possesses over 200-fold preference for FGFR2 over FGFR1.[39] These researchers reported that no structural differences in the X-ray cocrystal structures of RLY-4008 bound within FGFR1/2 were observed; however, molecular dynamic simulations revealed potential differences in a flexible loop region between FGFR1/2 and this was posited to be the source of the exquisite selectivity of this compound.[40] RLY-4008 is currently under Phase 1 clinical evaluation for FGFR2-implicated intrahepatic cholangiocarcinoma or other advanced solid tumors.[41] The acute lack of FGFR2 subtype selective inhibitors, coupled with the necessity to abrogate pan-FGFR inhibitor toxicity issues and FGFR-specific malignancies, warrants further research into the development of such inhibitors. Herein, we describe a structure-guide approach toward an FGFR2 subtype selective inhibitor.

■ RESULTS AND DISCUSSION

Our previous work outlined the identification of an indazole-based FGFR fragment inhibitor series that exhibited moderate activity against FGFR1−3.[42] Hit identification for this particular series was carried out using SPROUT, a de novo design software developed in the early 90s at The University of Leeds, UK.[43,44] Development of this series was also aided by the use of molecular modeling software Glide.[45] This method of inhibitor design was further incorporated within this project to design larger compounds predicted to inhibit FGFR1. Existing potent indazole-based inhibitors of FGFR kinases possess chemical functionality emanating from the 3-position of the indazole ring which, when bound to the FGFR kinase, has been shown to extend toward the solvent exposed region of the binding cavity.[46−48] We employed this approach and modeled molecular extensions from the indazole-3-position which could also target Ser565 as a potential H-bonding contact (Figure 2A, B).

Compound 1, the most potent fragment (IC$_{50}$ = 0.8 μM against FGFR2) identified previously,[42] was chosen as the template compound for de novo design using SPROUT. Appropriate target and spacer templates were chosen using the

modules available in SPROUT[43] and the resulting solutions (Table S2) were redocked using Glide (Table S3). We triaged the solutions based on a variety of parameters, some of which include docking score, synthetic tractability, and clogP. CH5183284 was also docked within its own crystal structure (PDB 5B7V) and found excellent agreement with the endogenous binding pose. Interestingly, CH5183284 scored lower (gscore = −8.432) than fragment 1 (gscore = −9.253) despite 1 being significantly less potent against the FGFRs. We attributed this to the predicted occupation of the H1 subpocket by the ethoxy group in 1, in which it not only improved lipophilic interactions but also formed an H-bond with Asp641. Compound 2, a benzylamine-based extension of the indazole core, was identified in the de novo screen and scored higher (gscore = −10.277) than both CH5183284 and 1. The benzylamine NH$_2$ was predicted to form an H-bond with the backbone carbonyl of Ser565 (Figure 2C/D) and was chosen as our initial target compound. To validate the existence of the new predicted H-bond with Ser565, we included the hydroxymethyl and ethyl analogues (Figure 3) to act as controls through their differing or absent H-bonding potential, respectively.
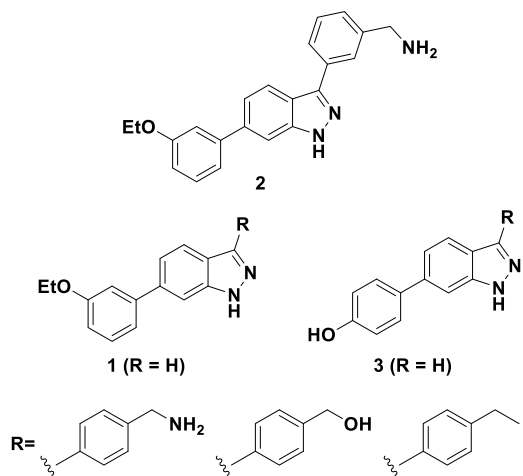
Figure 3. Focus library of extended versions of fragments.

Compound 3, a phenol-based fragment that exhibited similar potency (IC$_{50}$ = 3.0 μM against FGFR2) to 1 and slight FGFR2 selectivity (4-fold) over FGFR1 was also included. Compound 3 was predicted to form an H-bond between the phenol OH and Glu531 deep within the ATP binding pocket.[42] Several other ethoxy-fluoro-containing fragments were synthesized (Scheme S1) and biologically evaluated (Table S3). Details pertaining to these derivatives can be found in the Supporting Information. Synthesis of the "extended" ethoxy compounds began with a selective bromination at the 3-position of 6-iodoindazole (4) using NBS to give dihalogenated indazole 5 in an excellent yield (Scheme 1). Ethoxy derivatives were synthesized via selective Suzuki microwave (MW)-assisted chemistry with 5 to give brominated intermediate 6. Formation of small amounts of the bis-arylated product (9) was observed and provided an additional compound for biological evaluation.

Intermediate 6 then underwent a final Suzuki coupling to yield 2, 7 and 8, respectively. Synthesis of the phenol-based target compounds (15−17) proceeded in a similar fashion but required protection of the phenol moiety as the methoxy ether.

Scheme 1. Synthetic Route to Extended Ethoxy- and Phenol-Based Compounds[a]
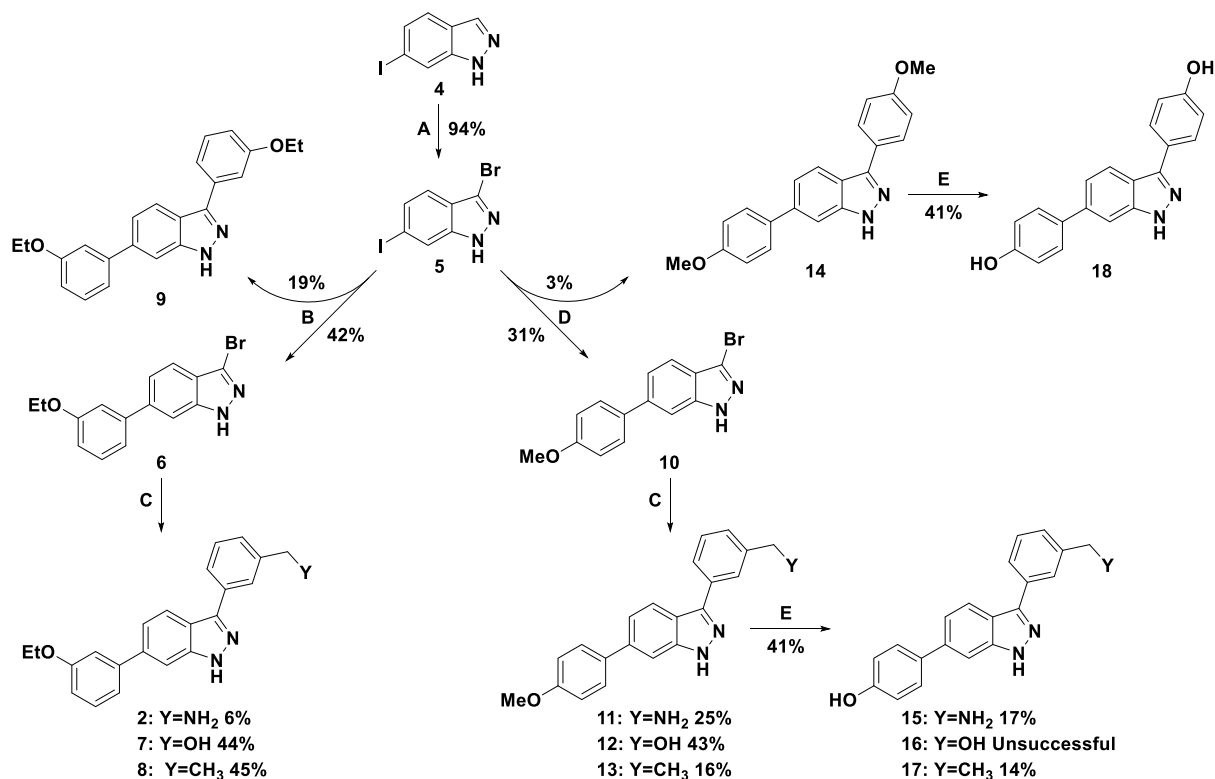
[a]Reagents and conditions: (A) NBS, DMF, 2 h. (B) 3-ethoxyphenylboronic acid, Pd(dppf)Cl$_2$), Na$_2$CO$_3$, dioxane:H$_2$O, 110 °C MW, 2 h. (C) 3-methylamino/3-methylhydroxy/3-ethyl-phenylboronic acid, Suzuki conditions. (D) 4-methoxyphenylboronic acid, Suzuki conditions. (E) BBr$_3$, DCM, 1 h.

This was easily dealkylated to reveal the phenol at the end of the synthesis using BBr$_3$. Attempts at using the unprotected phenol-based boronic acid were unsuccessful due to the rapid protodeboronation of ortho/para substituted phenolboronic acids.[50] Direct formation of **16** from **12** resulted in an Appel-like reaction with the methoxy group being converted to the alkyl bromide. This intermediate was subsequently transformed into the alcohol using harsh basic conditions (Scheme S2). Bis-arylated phenol **14** was also formed as a side product in the initial Suzuki coupling and was subsequently deprotected to yield **18**, which was also evaluated for FGFR1−3 inhibition.

Compounds were screened against FGFR1−3 (Table 1) using a FRET-based assay.[51] Unfortunately, **2** was inactive against FGFR1 and exhibited similar potencies as observed for fragment **1** against FGFR2/3. This was also reflected in the results obtained for **7**−**9** which all possessed greater docking scores when compared to fragment **1** (Table S3). In contrast to **2**, phenol **15** exhibited ~4-fold and ~5-fold increase in potency against FGFR1/2 and FGFR3, respectively, when compared to its corresponding fragment **3**. Despite having promising docking scores, compounds featuring an ethoxy moiety were invariably found to show disappointing levels of enzyme inhibition. Considering the improvement of potency for the phenol-based compounds, it was reasoned that the predicted interaction of the ethoxy group within the H1 subpocket (Figure 2) may not be occurring despite this being a prediction from the docking studies. Hydroxyethyl-containing **16** was also equipotent against FGFR1 with ethyl-containing **17** displaying a slight drop in potency in comparison to **15** and

16. This suggested the presence of H-bonding moieties in this area of the binding site is beneficial to potency. Surprisingly, bis-phenol **18**, which was isolated as a side product during the first Suzuki coupling (Scheme 1), exhibited an IC$_{50}$ of 0.25 μM against FGFR2, displaying a 2-fold increase in selectivity for FGFR2 over FGFR1 when compared to fragment **3** and benzylamine **15**. In addition to understanding why de novo-designed target compound **2** did not yield the expected results, we also wanted to further explore the potential for improving FGFR2 selectivity.

There are several examples of FGFR inhibitors that possess an indazole scaffold within the literature.[42,48,52,53] Liu et al. have reported an indazole-based FGFR inhibitor (**7n**, Figure S3) that possessed a similar pharmacophore to ours, with one major difference: the presence of an amide group between the indazole and the 3-position phenyl ring.[54] Structural data confirmed that the lead inhibitor described by Liu et al. occupies the ATP-binding pocket and reveals the amide NH to be involved in a H-bond donor interaction with the backbone carbonyl of Ala564 near the entrance of the pocket. To explore the importance of the amide and the phenyl ring, we designed a small library of control compounds containing these features (Figure 4).

Compounds **19**−**23** would establish SARs regarding flexibility, positioning of the carbonyl, and what degree of planarity is tolerated toward the entrance of the ATP-binding pocket. Synthesis began with formation of **25** from **24** via S$_N$Ar and intramolecular cyclization with hydrazine followed by Suzuki chemistry to yield **26** (Scheme 2). Direct reductive amination using sodium triacetoxyborohydride (STAB) in the

Table 1. Summary of the Biological Activities of Compounds 1−3, 7−9, and 15−18 against FGFR1−3
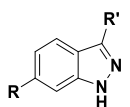
Cpd. No.	Structure		IC$_{50}$^{a} (µM) FGFR			FGFR2>FGFR1 Selectivity
	R	R'	1	2	3	
1	EtO-phenyl	H	2.0 ± 0.4	0.8 ± 0.3	4.5 ± 1.6	2.5
2	EtO-phenyl	H$_2$N-benzyl	>10	2.1 ± 0.9	2.6 ± 1.1	N/A^c
3	HO-phenyl	H	12 ± 1.6	3.0 ± 1.0	51 ± 1.2	4.0
7	EtO-phenyl	HO-benzyl	>10	>10	>10	N/A
8	EtO-phenyl	ethyl-phenyl	>10	ND^b	ND	N/A
9	EtO-phenyl	EtO-benzyl	>10	ND	ND	N/A
15	HO-phenyl	H$_2$N-benzyl	3.5 ± 0.03	0.8 ± 0.01	9.0 ± 0.10	4.4
16	HO-phenyl	HO-benzyl	3.0 ± 0.03	ND	ND	N/A
17	HO-phenyl	ethyl-phenyl	5.9 ± 0.06	ND	ND	N/A

^{a}IC$_{50}$ values are given as the mean $\pm$ SD of all data points, $n = 2$. ^{b}ND = not determined. ^{c}N/A = not applicable
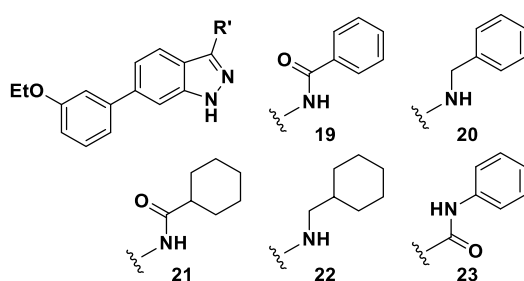

Figure 4. Library probing the importance of the amide and 3-position decoration.

formation of **22** from **26** proceeded in low yield, primarily because of preferential reaction at the 1-position NH over the 3-position NH$_2$.

Moving forward, we employed Boc protection of **26** to improve the efficiency of subsequent chemistry. Compound **27** was then subjected to amide coupling and reductive amination conditions to give **28−30** which were then deprotected to yield the final compounds. Notably, step E showed formation of the bis-amidated product which was also taken forward for deprotection (Scheme S3) and biological evaluation (Table S4). To obtain inverse amide **23**, bromoisatin **31** was subjected to basic hydrolysis followed by diazotization, reduction, and final ring closure to afford **32**. Formation of the amide bond was achieved by in situ acyl chlorination to obtain **33** which was then subjected to Suzuki coupling to yield the final compound. Compounds **19−23** were screened for activity against FGFR1−3 (Table 2).

The inclusion of the amide bond between the indazole and the 3-position phenyl ring appeared crucial. Compound **19** exhibited IC$_{50}$ values of 0.46, 0.14, and 2.2 µM against FGFR1−3, respectively, which was a significant increase in potency when compared to **1** and **2** (Table 1). Interestingly, removal of the amide carbonyl (**20**) resulted in a ∼7-fold loss of potency. The somewhat planar amide bond restricts the conformational flexibility at the 3-position, possibly placing the aromatic ring in a more favorable conformation when compared to the reduced amide version **20**. Compounds **21** and **22** were both inactive. This suggested that optimal substituents at the 3-position need to be planar and possess a linear trajectory, such as flat aromatic rings. Notably, testing of inverse amide **23** revealed a complete loss of potency which provided strong support for the importance of the H-bond between the amide carbonyl and the backbone NH of Ala564 (Figure S3).

Compound **19** exhibited a ∼3-fold selectivity preference for FGFR2 over FGFR1, a drop from the ∼8-fold preference that was observed with bis-phenol **18**. There were two major differences between these compounds: the substituent on the 6-position phenyl ring and the nature of the 3-position foliage. To determine the selectivity "handle" for **18**, we designed, synthesized (Scheme S4), and biologically evaluated compound **34** which incorporated the 3-position amide bond and the phenol simultaneously (Table 3).

Inclusion of an amide into the phenol-based compound resulted in a potency increase against FGFR1 and FGFR2. However, the selectivity preference for FGFR2 dropped from 8.4- to 3.6-fold for compounds **18** and **34**, respectively. This

Scheme 2. Synthetic Route to Amide-Based Control Compounds[a]
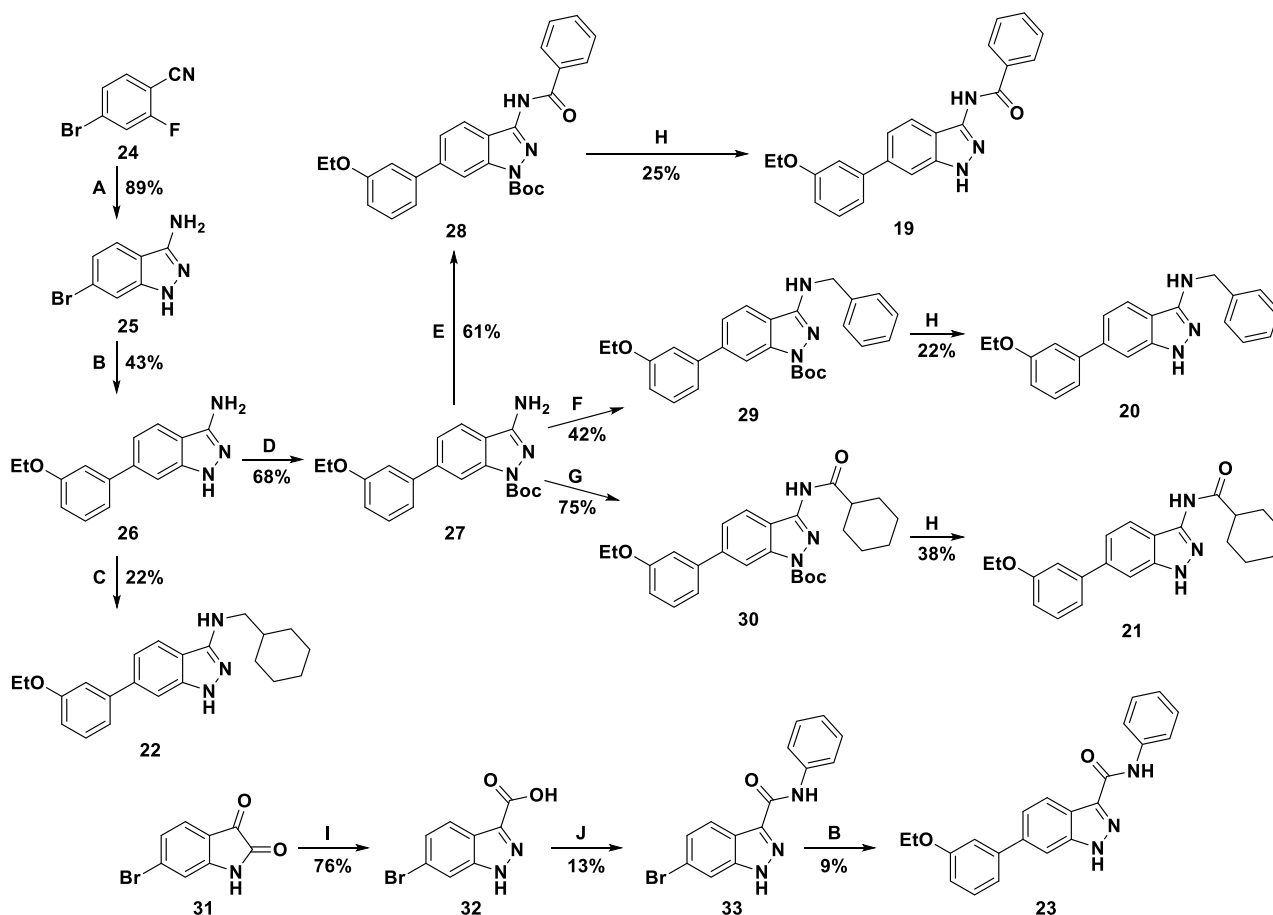
[a]Reagents and conditions: (A) N_2H_2, nBuOH, 100 °C, 2 h. (B) 3-Ethoxyphenylboronic acid, Pd(dppf)Cl$_2$), Na$_2$CO$_3$, dioxane:H$_2$O, 110 °C MW, 2 h. (C) Cyclohexanecarboxaldehyde, STAB, AcOH, DCM, 16 h. (D) Boc anhydride, DMAP, DCM, 2 h. (E) Benzoyl chloride, iPr$_2$NEt, DCM, 16 h. (F) Benzaldehyde, reductive amination conditions. (G) Cyclohexanecarbonyl chloride, acyl chloride conditions. (H) TFA, DCM, 1 h. (I) (i) NaOH$_{(aq)}$, 50 °C, 30 m; (ii) NaNO$_2$, 0 °C, 5 m; (iii) H$_2$SO$_4$, 0 °C, 20 m; (iv) SnCl$_2$, HCl, 0 °C, 1 h. (J) (i) SOCl$_2$, (ii) Et$_3$N, aniline, DCM, 45 °C, 4 h.

suggested that the most influential aspect governing FGFR2 selectivity for compound **18** was the linear trajectory of the 3-position foliage; however, it is a combination of both the phenol and the linear aryl–aryl bond that dictates FGFR2 selectivity. To further investigate the selectivity profile of **34**, we evaluated its inhibition against FGFR4, and it possessed no activity (IC$_{50}$ > 10 μM, data not shown). To further develop our inhibitors, we posited that substitution of a larger, linear, and more hydrophilic 3-position group would improve potency, solubility, and most importantly, the selectivity for FGFR2. Literature precedent outlined the use of piperazine as a useful group to improve the pharmacokinetic profile for inhibitors of FGFR kinases.[46,48] Using this rationale, we designed and synthesized **38** (Scheme 3).

Compound **10** was subjected to Suzuki chemistry to install the aniline functionality of **35**. This then underwent a double S$_N$2 reaction with **36** followed by a final deprotection with BBr$_3$ to afford the target compound **38**. Interestingly, during the S$_N$2 reaction an unknown side product was isolated, characterized, and determined to be compound **39** which was also taken forward for deprotection to obtain **40**. We have proposed a mechanism for the formation of **39** (Figure S4) and this is the first example of a one-pot synthesis of a piperazinyl-ethylene-oxazolidinone core from an aniline

precursor. In addition to **38** and **40**, several other piperazinyl derivatives (**41–44**) based on previous fluoro-phenol fragments[42] were also synthesized (Scheme S5) and evaluated for inhibition against FGFR1–3 (Table 4).

As hypothesized, the addition of the piperazine improved both the potency and selectivity with **38** possessing an IC$_{50}$ value of 29 nM and a ~13-fold inhibition preference for FGFR2 over FGFR1. Oxazolidinone **40** showed an improvement in potency when compared to **18** but was less potent and less selective than **38**. Unexpectedly, both **41** and **42**, which possess monosubstituted fluorines on the 6-position phenol, exhibited a dramatic loss in FGFR2 selectivity with **42** displaying no selectivity at all. The presence of the fluorine in **41** will likely cause an increase in the dihedral angle between the indazole ring and the 6-position phenyl ring by means of gauche interactions. We postulate that the disruption in planarity between the two ring systems is a likely cause for the selectivity drop. The FGFR1 active site may be more accommodating to such changes than the active site of FGFR2. We expect **42** to also have a similar effect, though we anticipate this fluorine to have a larger impact on the ability of the phenol to H-bond to Glu531, either through electron-withdrawing potential or via an intramolecular H-bond. We have shown previously that the phenol is an important feature

Table 2. Biological Results for Amide-Based Compounds 19−23
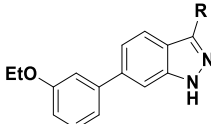
Cpd. No.	R	IC$_{50}$ (μM)[a] FGFR		
		1	2	3
19	(benzamide)	0.46 ± 0.01	0.14 ± 0.01	2.2 ± 0.02
20	(benzylamine)	3.2 ± 0.1	ND[b]	ND
21	(cyclohexanecarboxamide)	>10	ND	ND
22	(cyclohexylmethylamine)	>10	ND	ND
23	(anilide)	>10	ND	ND

[a]IC$_{50}$ values are given as the mean ± SD of all data points, n = 2. [b]ND = not determined.

Table 3. Biological Results for Compounds 18, 19, and 34 When Screened against FGFR1−3[a]
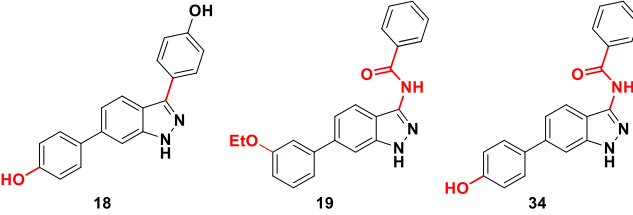
	FGFR IC$_{50}$ (μM)[b]			FGFR2 > FGFR1 Selectivity
Cpd. No.	1	2	3	
18	2.1 ± 0.03	0.25 ± 0.01	2.2 ± 0.02	8.4
19	0.46 ± 0.01	0.14 ± 0.01	2.2 ± 0.02	3.3
34	0.40 ± 0.01	0.11 ± 0.01	3.5 ± 0.03	3.6

[a]Areas implicated in selectivity differences are outlined in red. [b]IC$_{50}$ values are given as the mean ± SD of all data points, n = 2.

when aiming for FGFR2 selectivity (Table 3). This dramatic loss in selectivity was also observed for **43**. Conversely, **44** exhibited a large increase in FGFR2 selectivity. Using available structural information for FGFR1 and FGFR2, we conducted docking studies to rationalize these subtle SARs but unfortunately no points of selectivity were observed. To gain insight into these observations, we endeavored to obtain X-ray crystallographic evidence of inhibitor−enzyme complexes to unravel the structural requirements that dictate FGFR2 selectivity.

We performed crystallographic studies using a WT FGFR2 construct (residues 461−763) and an FGFR1 construct (residues 458−765) that harbored two mutations (C488A, C584S). This FGFR1 construct has been used extensively in the determination of ligand binding conformations.[55−57]

Compound **38** was successfully crystallized within FGFR1/2 to a resolution of 1.71 and 2.28 Å, respectively. In addition, **19** and **34** were also crystallized in FGFR1 to a resolution of 1.82 Å (Figure 5).

Consistent with other reported FGFR−inhibitor complex structures, FGFR1 with compounds **19**, **34**, and **38** occupied the ATP binding pocket and exhibited a "DFG-in" conformation. Compound **38** formed the crucial H-bond donor/acceptor interactions between the indazole nitrogen atoms and Ala567 and Glu565. The phenol participated in an H-bond network with Glu534 and Lys520 and confirmed predictions from earlier docking models that this was important for inhibition.[42] We observed the possible presence of either a partially occupied ethylene glycol or water molecules within the H1 pocket but did not include them in the final structure due to poor resolution of the electron density map. The binding mode of **38** within FGFR1 (PDB 7OZB, Figure S5) was identical to that of FGFR2 and did not indicate the presence of any selective inhibitor/enzyme interactions. For both the FGFR1 and FGFR2 structures, there were two molecules in the crystallographic asymmetric unit. One of the FGFR1 chains exhibited an alternate conformation for the piperazine ring (Figure S6) in which it had distorted inward to form an H-bond between the piperazine NH and the phenol of Tyr563, however, this conformation was not observed in the FGFR2 cocrystal structure. It was unclear whether this partial interaction had any effect on the selectivity profile of **38**. Compound **19** bound in a similar fashion to **38** with two major differences; the amide NH was involved in an H-bond with the backbone carbonyl of Ala564, and the ethoxy group occupied the H2 subpocket, contradicting earlier docking models (Figure 2) that predicted the ethoxy group to occupy the H1 subpocket. We conducted docking studies of **19** using our own FGFR1/**19** crystal structure (PDB 7OZF) to evaluate the accuracy of our model. Unexpectedly, the docked pose did not align with the crystal structure pose and placed the ethoxy group within the H1 subpocket (Figure S7). Glide predicted an H-bond between Asp641 and the ethoxy oxygen which was not observed in reality. This outlined a limitation of the current docking model and subsequent models should be modified accordingly. Compound **34** bound in the expected fashion, forming analogous H-bonds to those observed for both **38** and **19**.

The direct binding interactions of **19**, **34**, and **38** did not allude to any points of selectivity between FGFR1 and FGFR2. Analysis of the protein morphology surrounding the ATP binding pocket for FGFR1 and FGFR2 highlighted different conformations adopted by the P loop (residues 484−491) and the activation loop (residues 641−664) that appeared to be influenced by the bound ligand and intrinsic differences between FGFR1 and FGFR2, respectively (Figure 6).

The FGFR1/**19** complex possessed two alternate conformations within its crystal lattice (Figure 6A). One chain exhibited both an open and closed P loop conformation simultaneously, whereas its counterpart exclusively exhibited a closed-loop conformation. The closed P loop conformation has previously been observed using this construct, as was the case for FGFR1 in complex with AZD4547, a pan-FGFR inhibitor currently under clinical evaluation for FGFR-related cancers.[57,58] We posit that the closed P loop conformation was driven by an edge-to-face π−π stack between Phe489 and the 6-position phenyl ring of **19**. The presence of the 3-ethoxy group likely stabilized this conformation through an anchoring

Scheme 3. Synthetic Route Employed to Obtain 38[a]
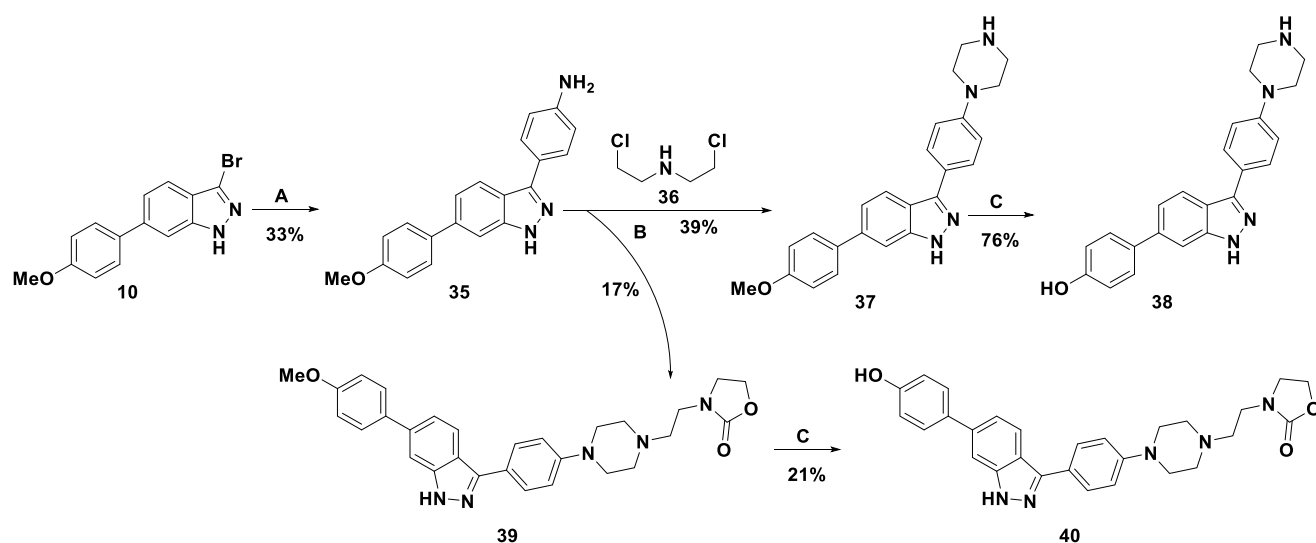
[a]Oxazolidinone **39** formed as a side product through over-substitution with **36**. Reagents and conditions: (A) 4-aminophenylboronic acid pinacol ester, Pd(dppf)Cl$_2$, Na$_2$CO$_3$, dioxane:H$_2$O, 110 °C MW, 2 h. (B) **36**, K$_2$CO$_3$, ^{t}BuOH, 100 °C, 100 h. (C) BBr$_3$, DCM, 1 h.

Table 4. Biological Results for Compounds 38 and 40−44 When Screened against FGFR1−3

Cpd. No.	Structure		IC$_{50}$[a] (nM) FGFR			FGFR2>FGFR1 Selectivity
	R	R'	1	2	3	
38	HO–phenyl	piperazine-NH	389 ± 2	29 ± 0.2	758 ± 3	13.4
40	HO–phenyl	piperazine-ethyl-oxazolidinone	449 ± 3	96 ± 1	ND[b]	4.68
41	F, HO–phenyl	piperazine-NH	204 ± 3	77 ± 1	915 ± 6	2.64
42	F, HO–phenyl	piperazine-NH	268 ± 1	258 ± 2	753 ± 5	1.04
43	HO–phenyl	piperazine-NEt	135 ± 7	77 ± 5	501 ± 2	1.75
44	HO–phenyl	NH$_2$	4200 ± 40	198 ± 2	>10000	21.21

[a]IC$_{50}$ values are given as the mean ± SD of all data points, $n = 2$. [b]ND = not determined.

effect via occupation of the H2 pocket. The electron density map for **19** was well-defined and indicated that rotation around the 6-position phenyl bond would be restricted as the ethoxy group would likely clash with Lys517 (Figure S8A). Compound **34** exhibited an open-loop conformation in one

of the crystal monomers. Notably, poor connectivity of the observed $2F_o−F_c$ electron density for the P loop in the other chain impeded our ability to reliably model this region. However, we did not observe evidence of a closed-loop conformation. We hypothesize that the lack of the ethoxy
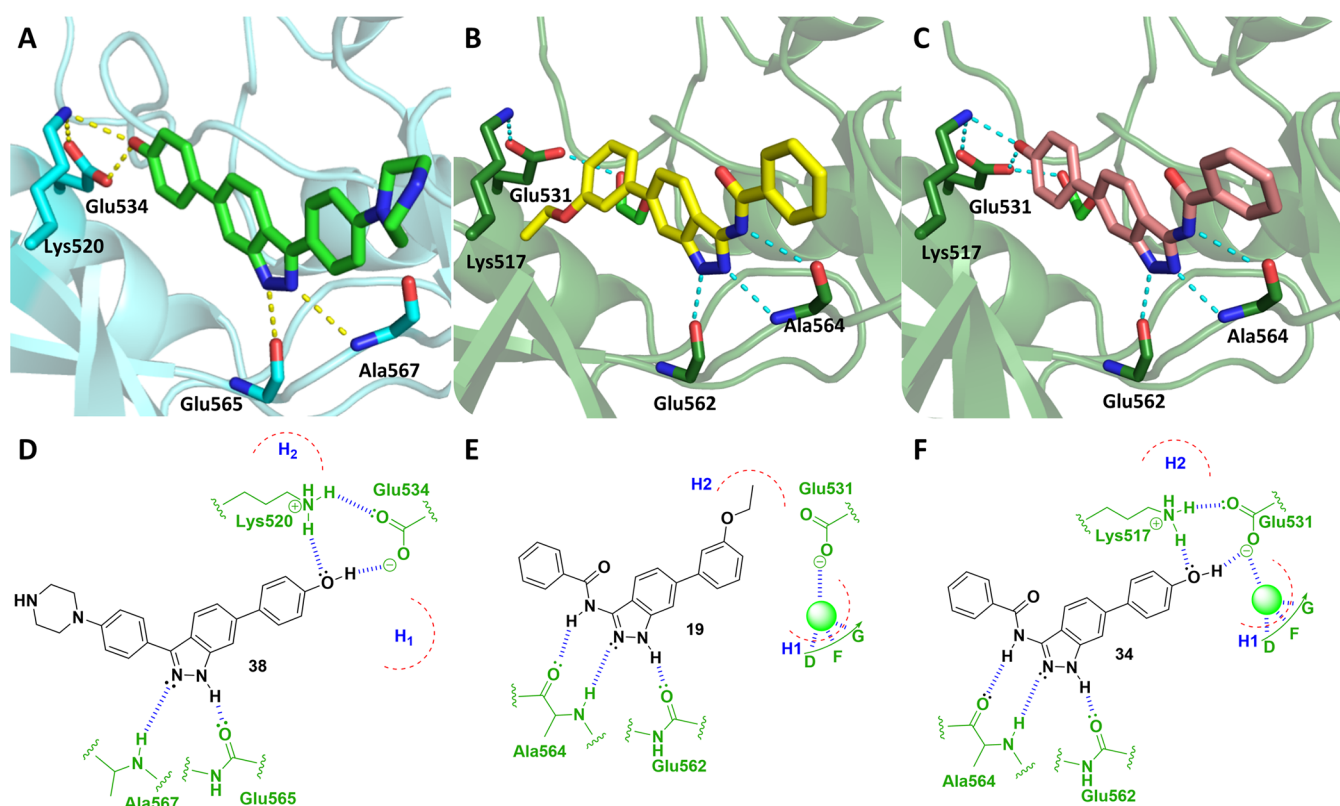
Figure 5. (A) Compound **38** (green) bound within the ATP binding pocket of FGFR2 (cyan) (PDB 7OZY). H-bonds are outlined as yellow hashed lines. The phenol is involved in an H-bond network with the side chains of Glu534 and Lys520. (B) Compound **19** (yellow) bound within the ATP binding pocket of FGFR1 (green) (PDB 7OZF). The ethoxy group occupies the H2 subpocket. Ethylene glycol occupies the H1 subpocket and forms H-bonds with the DFG motif. (C) Compound **34** (pink) bound within the ATP binding pocket of FGFR1 (PDB 7OZD). (D−F) 2D representations of the binding mode of **38**, **19**, and **34**, respectively.

"anchor" enables free rotation of the 6-position phenyl ring which in turn disrupts the edge-to-face π−π stack with Phe489 and therefore is less likely to adopt a closed-loop conformation. Furthermore, the electron density surrounding the 6-position phenyl ring in **34** was not as well-defined (Figure S8B) than for **19** which suggested more rotational freedom.

An open P loop conformation was also observed for one of the chains of the FGFR1/**38** crystal structure with the other chain also possessing a high degree of flexibility which again, we were unable to model. This was also reflected for one of the chains in the FGFR2/**38** crystal structure. It is apparent that this loop possesses a high degree of flexibility and likely exists in multiple conformations that are interchangeable. Nevertheless, we did observe an inward shift for this loop within one of the chains of the FGFR2/**38** crystal structure (Figure 6B). This inward shift may be indicative of a transitional state whereby the P loop moves from an open to a closed conformation. Assuming the closed P loop conformation is a more stable structure, it is possible that the observed selectivity preference of **38** for FGFR2 is due to a closed conformation being more favorable in FGFR2 than FGFR1. Flexibility in the P loop is well documented and is indicated as a determining factor for the selectivity of inhibitors of kinases MAP4K4, Abl, and Src.[59,60] In addition, Casaletto et al. reported that their highly selective FGFR2 inhibitor RLY-4008 did not show any structural differences between X-ray crystal structures of it bound within FGFR1/2.[40] Through molecular dynamic modeling, they hypothesized that the observed selectivity resulted from dynamic differences in a flexible loop present in

FGFR1 and FGFR2. Specifically, they predicted this flexible loop to switch between an open and closed conformation more rapidly in FGFR1 than FGFR2.[40] We believe that this hypothesis could refer to the flexibility of the P loop and may offer support for our hypothesis regarding **38** and its ability to stabilize a closed conformation more readily in FGFR2 over FGFR1. However, we acknowledge that our data is insufficient to support this hypothesis and further studies into the fluid dynamics of this region need to be carried out.

Another observed difference between FGFR1 and FGFR2 was the conformation of the activation loop between residues 641−664 (Figure 6C). The activation loop of FGFR1 was positioned over the active site, whereas in FGFR2, the loop was situated away from the active site. It is important to note that the activation loop in FGFR2 was packed against a symmetry-related molecule and likely played a role in the morphology of this portion of the protein. Furthermore, analysis of available crystal structures of FGFR1 and FGFR2 cocrystallized with pan-FGFR inhibitors (Figure S9) outlined that these differences are an intrinsic phenomenon that are specific to each enzyme and is unlikely to be a determining factor in the selectivity of **38**.

In addition to the differences in the P loop and activation loop, the selectivity preference of compound **38** for FGFR2 may also be explained via consideration of the ligand electron density maps within FGFR1/2 (Figure 7).

The ligand electron density map for compound **38** in FGFR2 was well-defined with flat edges flanking the planar 6-position phenyl ring. As was observed for **34** (Figure S8B), the
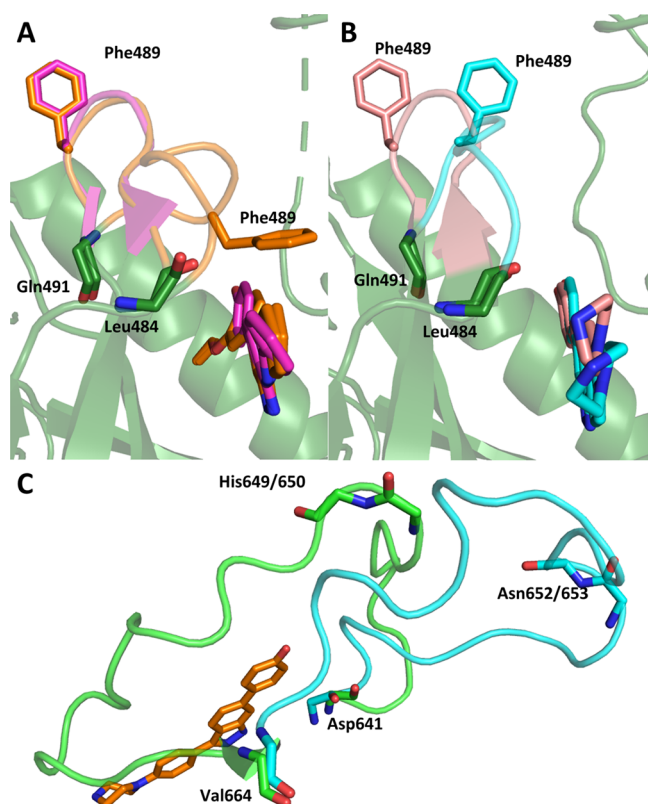
Figure 6. (A) P loop region, residues 484−491 (between β-strands 1 and 2 of the N-terminal domain). An open P loop conformation was observed for **19** (orange) and **34** (purple). A closed P loop conformation was only observed for compound **19** (orange) in one of the monomer chains. (B) P loop morphology for **38** bound within FGFR1 (pink) and FGFR2 (cyan). FGFR1 exhibited an open P loop morphology, whereas FGFR2 exhibited an inward shift. (C) Comparison of the activation loop morphology between FGFR1 (green) and FGFR2 (cyan); nonconserved residues are outlined. Labels for FGFR1/FGFR2 overlays refer to the FGFR1 amino acid number.
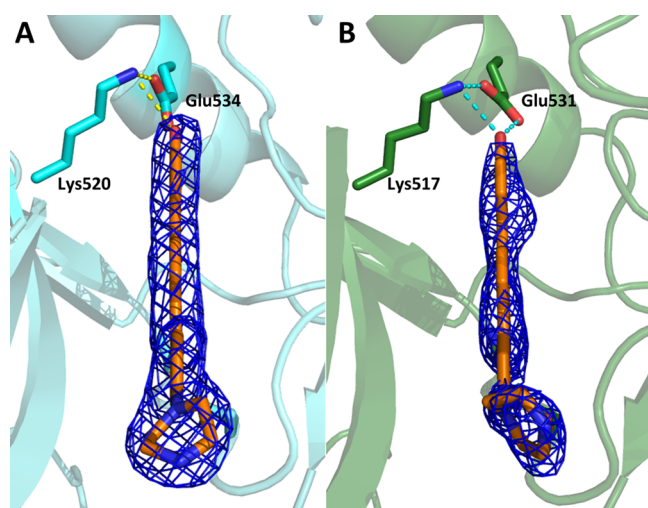

Figure 7. (A, B) $2F_o−F_c$ electron density maps (contour level 1.0 σ) for **38** bound within FGFR2 (cyan) and FGFR1 (green), respectively. FGFR1/**38** shows a slight spherical perturbation surrounding the 6-position phenyl ring.

electron density for **38** bound within FGFR1 exhibited a slight spherical perturbation which indicated more rotational freedom of the 6-position phenyl ring. This evidence bolsters the earlier hypothesis that an increase in the dihedral angle between the 6-position phenyl and indazole rings is tolerated more in FGFR1 than FGFR2, as exemplified by the lack of FGFR2 selectivity for **41** and **42** (Table 4). However, we acknowledge that the resolution difference between the FGFR1 and FGFR2 crystal structures may obscure the finer aspects of ligand binding and care should be taken when drawing these conclusions.

With our own FGFR1/2 structures in hand, we decided to revisit the docking studies of compound **44** (21-fold FGFR2-selective) which had previously not alluded to any selectivity differences between FGFR1/2. Using the cocrystallized ligand **38** as the template for grid generation, we performed Glide docking in both structures (Figure 8A, B).

As expected, compound **44** occupies the active site with the indazole nitrogen atoms predicted to maintain the crucial H-bond donor/acceptor interactions within the hinge region of the ATP binding pocket. Interestingly, the aniline NH_2 is predicted to form an H-bond with the backbone carbonyl of Ser568 in FGFR2 but is not predicted to form the same interaction within FGFR1. This was reflected in the docking scores (Table S3) which predicted an order of magnitude difference in binding energies between FGFR1 (gscore = −9.767) and FGFR2 (gscore = −10.857). Notably, the Glu residue at the back of the pocket possesses different orientations of the carboxylic acid side chain within FGFR1/2. To form an optimal H-bond between the phenol and Glu residue, the dihedral angle between the indazole ring and the 6-position phenolic ring are significantly different (FGFR2 = 33.5°, FGFR1 = 74.1°). This phenomenon also reflects the previous hypothesis regarding planarity of the ring systems and FGFR2 selectivity. The smaller dihedral angle in FGFR2 results in a downward shift of the 3-position appendage which allows for the aniline NH_2 to form an H-bond with Ser568. This predicted selective H-bond may explain the larger selectivity preference for **44** (21-fold) over **38** (13-fold) as **38** does not possess H-bond donor capability in this area of the binding pocket. This interaction could be utilized to design more selective FGFR2 inhibitors.

To establish whether FGFR2 selectivity was translatable to a cellular environment, we conducted cell viability assays for **38**, **41**, **42**, and PD173074 (Table 5). PD173074 is a potent pan-FGFR inhibitor and was included as a positive control.[61] Three cell lines were chosen: JMSU1[62] (FGFR1-driven[63]), SUM52[64] (FGFR2-driven[65]), and VMCUB3[66] (no evidence for FGFR activation).

Compound **38** exhibited modest potency against each of the cell lines with an IC_{50} value of 700 nM against SUM52. Compound **38** was more inhibitory to SUM52 than JMSU1 and VMCUB3 but displayed a significant drop in potency (~24-fold) from the enzyme inhibition data and therefore deductions about compound selectivity could not be made. The drop in potency was also reflected with **41** and **42** but not for PD173074 which was extremely potent against SUM52 (IC_{50} = 8 nM). Unexpectedly, PD173074 did not perform well against JMSU1, indicating that it may not be the best cell line to evaluate FGFR1 cellular efficacy. The reduction of potency for **38**, **41**, and **42** is likely due to poor cellular permeability. To investigate this, we conducted cell permeability predictions of **38**, **41**, **42** and PD173074 using PerMM[67] which is used to
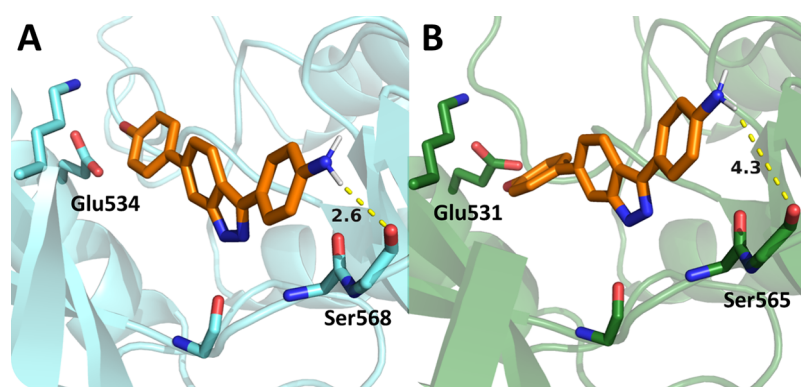
Figure 8. (A, B) Glide docking poses of **44** (orange) bound within FGFR2 (cyan) and FGFR1 (green), respectively. Distances between the aniline NH$_2$ and Ser568/565 are outlined by yellow dashes.

Table 5. Biological Evaluation of Compounds 38, 41, 42, and PD173074 against Various Cancer Cell Lines

Cpd. No.	SUM52 IC$_{50}$[a] (nM)	JMSU1 IC$_{50}$[a] (nM)	VMCUB3 IC$_{50}$[a] (nM)
38	700 ± 100	2100 ± 150	2000 ± 250
41	600 ± 150	2000 ± 150	1650 ± 100
42	1100 ± 200	3250 ± 150	2600 ± 150
PD173074	8.0 ± 1.0	1050 ± 250	4850 ± 600

[a]IC$_{50}$ values are given as the mean ± SD of all data points, n = 2.

evaluate the ability of a molecule to permeate four cell line models: black lipid membrane (BLM), parallel artificial membrane permeability assay (PAMPA), blood-brain barrier (BBB) and Caco2/MDCK cells (Table S5). In all models, PD173074 performed markedly better than **38**, **41**, and **42**, particularly for the BLM model where PD173074 exhibited >4.5-fold improvement in permeation coefficient. Future derivatives will look to improve cellular permeation while also maintaining FGFR2 selectivity.

CONCLUSION AND FUTURE OUTLOOK

This work described an extensive structure-guided medicinal chemistry campaign from a starting fragment (**1**) that exhibited submicromolar potency to a lead inhibitor (**38**) that possessed nM potency and >10-fold selectivity for FGFR2 over FGFR1. We used a combination of classical SAR studies and computational methods such as de novo design and docking to aid in the hit-to-lead process. We were able to show that subtle changes to the lead inhibitor, such as substitution of hydrogen for fluorine, resulted in a complete loss of selectivity for FGFR2. We posited that this phenomenon was due to an increase in the dihedral angle between the 6-position phenyl and indazole ring, which in turn would be better tolerated within FGFR1 over FGFR2. X-ray crystallographic studies outlined that ligand electron density surrounding the 6-position phenyl ring was more spherical in FGFR1 over FGFR2. This may indicate more rotational freedom and thus an improved tolerance for larger dihedral angles between both ring systems in FGFR1 than FGFR2. We have also demonstrated that ligand binding to FGFR1/2 resulted in significant morphological changes to the P loop. Static snapshots of this loop transitioning between an open- and closed-state, whereby the latter forms a lid above the active site, have alluded to a dynamic selectivity event between FGFR2 and **38**, and our findings may complement current

theories surrounding selective FGFR2 inhibition. Additionally, docking studies using our own crystal structures have revealed a potential FGFR2-selective H-bond with the backbone carbonyl of Ser568. Future derivatives will look to exploit this while also looking to deconvolute the structural aspects and requirements that govern the selectivity preference of **38** for FGFR2. We also determined that our lead inhibitor suffered from a large decrease in potency between enzyme- and cell-based assays. We concluded that it possessed poor cellular permeability and computational permeation calculations reflected this. In addition to improving cell permeability, we are utilizing our own crystal structures in iterative rounds of SBBD to yield more potent and more selective inhibitors of FGFR2 that house the potential to be used as therapeutics for the treatment of FGFR2-implicated cancers.

EXPERIMENTAL SECTION

Chemistry: General Procedures and Instrumentation. All reagents were obtained from commercial sources and were used without further purification unless otherwise stated. All microwave reactions were carried out in a CEM Explorer 48 Autosampler using a power of 200 W. Reactions were monitored using TLC and/or LC-MS. TLC was performed using aluminum precoated silica gel plates (Merck-chemicals) and visualized using either ultraviolet light (254 nm), dipping in KMnO$_4$ solution or ninhydrin solution and heated, or using an iodine tank. LC-MS was performed on a Bruker Daltronics instrument running a gradient of increasing MeCN/water (5−95%) containing 0.1% formic acid, at 1 mL min^{-1} on a 50 × 20 mm C$_{18}$ reverse phase (RP) column. Normal phase (NP) flash column chromatography was carried out using Geduran silica gel 60 4063 μm. Automated column chromatography (ACC) was performed on an Isolera Biotage using KP-C$_{18}$-HS SNAP 12/30/60 g cartridges using MeCN/water (0−95%) containing 0.1% TFA, at a flow rate of 12−50 mL min^{-1} for RP, or Thomson Single Step 12/40 g prepacked silica cartridges for NP. Preparative HPLC was performed on an Agilent 1100 Infinity Series equipped with a UV detector and Ascentis Express C$_{18}$ reverse phase column using MeCN/water (5−95%) containing 0.1% TFA, at a flow rate of 0.5 mL min^{-1} over a period of 15 min. Analytical HPLC was performed on an Agilent 1290 Infinity Series equipped with a UV detector and a Hyperclone-C$_{18}$RP column using MeCN/water (5−95%) containing 0.1% TFA, at either 0.5 mL min^{-1} over a period of 5 min, or 1.0 mL min^{-1} over a period of 30 min. All compounds are >95% pure by HPLC, unless otherwise stated. HRMS was carried out using a Bruker MaXis Impact Time of Flight spectrometer using ESI (±), giving masses correct to four decimal places.

^{1}H NMR spectra were recorded at 501, 500, or 400 MHz, respectively, and ^{13}C NMR spectra were recorded at 126 or 101 MHz on either a Bruker Advance 500 or 400 Fourier transform

spectrometer. Chemical shifts are reported in ppm and are reported with reference to the residual solvent peak. Multiplicities are reported with coupling constants and are given to the nearest 0.1 Hz. Where needed, COSY, HSQC, HMBC, and NOESY were used to aid assignment. Ar-q = aromatic quaternary carbon. IR spectra were recorded in the solid phase on a Bruker Alpha Platinum attenuated total reflectance FTIR spectrometer with vibrational frequencies given in cm^{-1}. Melting points were measured on a Stuart SMP30. Elemental analysis was carried out using a Carlo Erba 1108 Elemental Analyzer.

General Methods. *Method A: Microwave Suzuki Reactions.* A mixture of the chosen halogenated heterocycle (1.0 equiv), the chosen boronic acid (1.0−2.0 equiv), Pd(dppf)Cl$_2$·DCM (0.1 equiv) and Na$_2$CO$_3$ (3.0−5.0 equiv) were charged with nitrogen in a microwave vial (10 or 35 mL). A mixture of dioxane and water ((1:1) 5−20 mL) was degassed for 10 min and added to the reactants under nitrogen and the reaction mixture was heated to 110 °C for 1−6 h. The reaction mixture was cooled to 20 °C and diluted with EtOAc, and the reaction vessel sonicated, filtered through a Celite pad, and washed thoroughly with EtOAc. Where needed, DCM−MeOH (1:1) was used to wash the Celite pad. The filtrate was added to water and the organic layer separated. The aqueous layer was extracted with EtOAc (×3) and the combined organic layers were washed with brine, dried (MgSO$_4$), and concentrated in vacuo to reveal the crude product. The crude product was purified using either flash chromatography or NP ACC. See individual compounds for purification details.

Method B: Methoxy Deprotections. The chosen methoxy containing compound (1.0 equiv) was dissolved/suspended in DCM (5−15 mL) at 0 °C. One molar BBr$_3$ in DCM (2.0−8.0 equiv) was added slowly, and the reaction was stirred at room temperature for 1−24 h until complete. See individual compounds for workup and purification details.

Method C: Boc Deprotections. The chosen Boc-protected amine (1.0 equiv) was dissolved in DCM−TFA (1:1), and the reaction was stirred until complete. The reaction mixture was reduced in vacuo to reveal the crude product. See individual compounds for purification details.

Method D: Reductive Aminations. The chosen aldehyde (1.0−1.2 equiv) was dissolved in DCM (3−15 mL) and cooled to 0 °C. The chosen secondary amine (1.0−1.2 equiv) and glacial AcOH (1 drop) were added, and the reaction was stirred until complete (imine formation for some reactions required the use of 3 Å molecular sieves (MS) and heating to 40 °C). Sodium triacetoxyborohydride (STAB) (1.6 equiv) was added, and the reaction was warmed to 20 °C and stirred until complete. See individual compounds for workup and purification details.

Method E: Boc Protections. The chosen amine (1.0 equiv) was dissolved in THF (20−40 mL); DMAP (0.3 equiv) was added, and the reaction was stirred for 2 min. Di-*tert*-butyl dicarbonate (1.1−1.2 equiv) was added dropwise and the reaction was stirred until complete. The reaction mixture was reduced in vacuo to reveal the crude product which was purified by flash chromatography. See individual compounds for purification details.

Method F: Acyl Chloride Couplings. The chosen amine (1.0 equiv) was dissolved in DCM (5−20 mL); ^{i}Pr$_2$NEt (2.0−3.5 equiv) was added, and the reaction was stirred for 20 min. The chosen acid chloride (1.2−2.0 equiv) was added and the reaction stirred until complete. See individual compounds for workup and purification details.

Method G: Piperazine Cyclizations. The chosen aniline (1.0 equiv), bis(2-chloroethyl)amine hydrochloride (**36**, 1.2 equiv), and K$_2$CO$_3$ (2.4 equiv) were suspended in ^{t}BuOH (5−15 mL), and the reaction was heated to 100 °C and stirred until complete. See individual compounds for workup and purification details. CAUTION! **36** is a mustard gas precursor and presents significant risk, practice extreme caution when conducting this procedure.

Compounds. *{3-[6-(3-Ethoxyphenyl)-1H-indazol-3-yl]phenyl}-methanamine (2).* Synthesized by method A using **6** (150 mg, 0.47 mmol, 1.0 equiv), 3-(aminomethyl)phenylboronic acid·HCl (133 mg, 0.71 mmol, 1.5 equiv), Pd(dppf)Cl$_2$·DCM (39 mg, 0.05 mmol,

0.1 equiv), Na$_2$CO$_3$ (250 mg, 2.36 mmol, 5.0 equiv), dioxane (5 mL) and water (5 mL) and the reaction was heated for 2 h. The crude product was purified using flash column chromatography (isocratic: 3:10:87, 7.0 M NH$_3$ in MeOH−MeOH−EtOAc) and the resulting brown semisolid was triturated with DCM to give the titled compound (10 mg, 0.03 mmol, 6%) as colorless granules. ^{1}H NMR (500 MHz, DMSO-d_6): 8.16 (d, J = 8.5 Hz, 1H), 7.99 (d, J = 1.8 Hz, 1H), 7.85 (dt, J = 7.6, 1.5 Hz, 1H), 7.79−7.75 (m, 1H), 7.51 (dd, J = 8.6, 1.6 Hz, 1H), 7.46 (t, J = 7.6 Hz, 1H), 7.41 (t, J = 7.9 Hz, 1H), 7.38−7.34 (m, 1H), 7.31 (dt, J = 7.8, 1.2 Hz, 1H), 7.26 (t, J = 2.1 Hz, 1H), 6.98−6.94 (m, 1H), 4.13 (q, J = 6.9 Hz, 2H), 3.84 (s, 2H), 1.37 (t, J = 7.0 Hz, 3H). ^{13}C NMR (126 MHz, DMSO-d_6): 159.0, 144.9, 143.3, 142.3, 141.9, 138.3, 133.5, 130.0, 128.6, 126.5, 125.4, 124.6, 121.2, 120.8, 119.5, 119.4, 113.6, 113.2, 108.2, 63.1, 45.7, 30.7, 14.7. HPLC: RT = 2.27 min. HRMS (ESI+): Found: 366.1581 (M+Na$^+$), C$_{22}$H$_{21}$N$_3$NaO requires *MH* 366.1577.

3-Bromo-6-iodo-1H-indazole (5). 6-Iodo-1*H*-indazole (3.00 g, 12.3 mmol, 1.0 equiv) was dissolved in DMF (30 mL) and NBS (2.01 g, 13.5 mmol, 1.1 equiv) was added to the reaction mixture and the solution was stirred for 3 h. Water (60 mL) was added, and the resulting precipitate was filtered. The crude product was crystallized from EtOH and the titled compound (3.72 g, 11.5 mmol, 94%) was collected as yellow microcrystals. ^{1}H NMR (501 MHz, DMSO-d_6): 8.00 (t, J = 1.0 Hz, 1H), 7.50 (dd, J = 8.5, 1.3 Hz, 1H), 7.39 (dd, J = 8.5, 0.8 Hz, 1H). ^{13}C NMR (126 MHz, DMSO-d_6): 142.2, 130.0, 121.4, 121.0, 120.8, 119.5, 93.9. LC-MS (ESI+): RT = 1.95−2.10 min, m/z = 323.0 (M+H$^+$). mp: 230.4−231.7 °C. Anal. Calcd for C$_7$H$_4$BrIN$_2$: C, 26.3; H, 1.20; N, 8.7. Found: C, 26.4; H, 1.20; N, 8.7.

3-Bromo-6-(3-ethoxyphenyl)-1H-indazole (6). Synthesized by method A using **5** (500 mg, 1.55 mmol, 1.0 equiv), 3-ethoxyphenylboronic acid (385 mg, 2.32 mmol, 1.5 equiv), Pd-(dppf)Cl$_2$·DCM (126 mg, 0.155 mmol, 0.1 equiv), Na$_2$CO$_3$ (492 mg, 4.64 mmol, 3.0 equiv), dioxane (10 mL) and water (10 mL) and the reaction was heated for 3 h. The crude product was purified using flash column chromatography (isocratic: 1:4 EtOAc−hexane) and the resulting solid was crystallized from cyclohexane and the titled compound (207 mg, 0.65 mmol, 42%) was collected as colorless flakes. ^{1}H NMR (501 MHz, CDCl$_3$): 10.57 (br.s, 1H), 7.72−7.64 (m, 2H), 7.49 (dd, J = 8.4, 1.4 Hz, 1H), 7.38 (t, J = 7.9 Hz, 1H), 7.21 (ddd, J = 7.7, 1.7, 0.9 Hz, 1H), 7.17 (t, J = 2.2 Hz, 1H), 6.94 (ddd, J = 8.2, 2.6, 1.0 Hz, 1H), 4.12 (q, J = 7.0 Hz, 2H), 1.46 (t, J = 7.0 Hz, 3H). ^{13}C NMR (126 MHz, CDCl$_3$): 159.6, 142.4, 142.0, 141.9, 130.1, 123.2, 122.7, 122.4, 120.5, 120.1, 114.3, 113.9, 108.3, 63.8, 15.0. LC-MS (ESI+): RT = 1.95−2.01 min, m/z = 317.1 (M+H$^+$). mp: 132.9−133.4 °C. Anal. Calcd for C$_{15}$H$_{13}$BrN$_2$O: C,56.7; H, 4.10; N, 8.8. Found: C, 56.8; H, 4.13; N, 8.8.

{3-[6-(3-Ethoxyphenyl)-1H-indazol-3-yl]phenyl}methanol (7). Synthesized by method A using 3-(hydroxymethyl)phenylboronic acid (108 mg, 0.71 mmol, 1.5 equiv) and the same reagents and amounts that are outlined in the preparation of **2**, and the reaction was heated for 3 h. The crude product was purified using flash column chromatography (isocratic: 1:4 EtOAc−hexane) and the resulting yellow solid was triturated with DCM to give the titled compound (71 mg, 0.21 mmol, 44%) as a colorless solid.

^{1}H NMR (501 MHz, DMSO-d_6): 8.14 (d, J = 8.5 Hz, 1H), 8.00 (d, J = 1.8 Hz, 1H), 7.89 (dt, J = 7.7, 1.5 Hz, 1H), 7.78 (d, J = 1.6 Hz, 1H), 7.54−7.45 (m, 2H), 7.40 (t, J = 7.9 Hz, 1H), 7.35 (d, J = 7.6 Hz, 1H), 7.31 (dt, J = 7.8, 1.2 Hz, 1H), 7.26 (t, J = 2.1 Hz, 1H), 6.99−6.93 (m, 1H), 5.29 (t, J = 5.8 Hz, 1H), 4.63 (d, J = 5.8 Hz, 2H), 4.13 (q, J = 7.0 Hz, 2H), 1.37 (t, J = 6.9 Hz, 3H). ^{13}C NMR (126 MHz, DMSO-d_6): 159.0, 143.2, 143.2, 142.2, 141.9, 138.3, 133.5, 130.0, 128.6, 125.8, 125.0, 124.7, 121.1, 120.8, 119.5, 119.4, 113.6, 113.2, 108.2, 91.4, 63.1, 62.9, 30.6, 14.7. HPLC: RT = 2.88 min. HRMS (ESI+): Found: 345.1610 (M+H$^+$), C$_{22}$H$_{20}$N$_2$O$_2$ requires *MH* 345.1598.

6-(3-Ethoxyphenyl)-3-(3-ethylphenyl)-1H-indazole (8). Synthesized by method A using 3-ethylphenylboronic acid (106 mg, 0.71 mmol, 1.5 equiv) and the same reagents and amounts that are outlined in the preparation of **2** and the reaction was heated for 2.5 h. The crude product was purified using flash column chromatography

(isocratic: 1:4 EtOAc−hexane). The resulting colorless semisolid was dissolved in Et$_2$O and reduced in vacuo to give the titled compound (73 mg, 0.21 mmol, 45%) as a foamy off-white solid. ^{1}H NMR (501 MHz, CDCl$_3$): 8.06 (dd, J = 8.5, 0.8 Hz, 1H), 7.93−7.86 (m, 2H), 7.51−7.44 (m, 2H), 7.41−7.34 (m, 2H), 7.29 (dt, J = 7.7, 1.5 Hz, 1H), 7.18−7.12 (m, 2H), 6.93 (ddd, J = 8.4, 2.5, 1.2 Hz, 1H), 4.13 (q, J = 7.0 Hz, 2H), 2.73 (q, J = 7.6 Hz, 2H), 1.49 (t, J = 7.0 Hz, 3H), 1.26 (t, J = 7.6 Hz, 3H). ^{13}C NMR (126 MHz, CDCl$_3$): 159.4, 146.0, 145.2, 142.7, 142.5, 140.2, 133.6, 129.8, 129.1, 128.1, 127.4, 125.3, 121.7, 121.4, 120.5, 120.1, 114.3, 113.4, 108.6, 63.7, 29.1, 15.6, 15.1. HPLC: RT = 3.95 min. HRMS (ESI+): Found: 365.1628 (M+Na$^+$), C$_{23}$H$_{22}$N$_2$NaO requires MH 365.1624.

3,6-Bis(3-ethoxyphenyl)-1H-indazole (9). Synthesized as a side product and isolated in the purification of **6**. The titled compound (107 mg, 0.30 mmol, 19%) was collected as a fluffy beige powder. ^{1}H NMR (501 MHz, CDCl$_3$): 8.05 (dd, J = 8.6, 1.1 Hz, 1H), 7.68−7.63 (m, 1H), 7.63−7.60 (m, 1H), 7.48−7.42 (m, 2H), 7.39−7.32 (m, 2H), 7.17−7.11 (m, 2H), 6.98 (ddt, J = 8.2, 2.3, 1.1 Hz, 1H), 6.93 (ddt, J = 8.2, 2.3, 1.1 Hz, 1H), 4.16−4.09 (m, 2H), 4.09−3.98 (m, 2H), 1.55−1.45 (m, 3H), 1.43−1.35 (m, 3H). ^{13}C NMR (126 MHz, CDCl$_3$): 159.6, 159.4, 145.6, 142.7, 142.5, 140.3, 134.9, 130.2, 129.8, 121.7, 121.3, 120.4, 120.2, 120.1, 114.9, 114.2, 113.74, 113.72, 113.5, 108.68, 108.65, 63.7, 63.6, 15.0, 14.9. HPLC: RT = 3.14 min. HRMS (ESI+): Found: 359.1764 (M+H$^+$), C$_{23}$H$_{22}$N$_2$O$_2$ requires MH 359.1754.

3-Bromo-6-(4-methoxyphenyl)-1H-indazole (10). Synthesized by method A using **5** (500 mg, 1.55 mmol, 1.0 equiv), 4-methoxyphenylboronic acid (353 mg, 2.32 mmol, 1.5 equiv), Pd(dppf)Cl$_2$·DCM (126 mg, 0.155 mmol, 0.1 equiv), Na$_2$CO$_3$ (492 mg, 4.64 mmol, 3.0 equiv), dioxane (10 mL) and water (10 mL) and the reaction was heated for 5 h. The boronic acid was found to have the same R_f as the product, therefore **5** (250 mg, 0.77 mmol, 0.5 equiv) and Pd(dppf)Cl$_2$·DCM (63 mg, 0.077 mmol, 0.05 equiv) were added and the reaction was heated for 1 h. The crude product was purified using flash column chromatography (gradient: 20−50% EtOAc−hexane). The resulting off-white solid was crystallized from toluene and the titled compound (135 mg, 0.48 mmol, 31%) was collected as off-white shiny flakes. ^{1}H NMR (501 MHz, DMSO-d_6): 7.72−7.65 (m, 3H), 7.61 (dd, J = 8.5, 0.8 Hz, 1H), 7.49 (dd, J = 8.5, 1.4 Hz, 1H), 7.09−7.02 (m, 2H), 3.81 (s, 3H). ^{13}C NMR (126 MHz, DMSO-d_6): 159.2, 141.8, 139.5, 132.3, 128.4, 121.1, 121.0, 120.2, 119.5, 114.4, 107.5, 55.2. LC-MS (ESI+): RT = 2.01−2.09 min, m/z = 303.1 (M+H$^+$). mp: 213.2−214.1 °C. Anal. Calcd for C$_{14}$H$_{11}$BrN$_2$O: C, 55.7; H, 3.70; N, 9.2. Found: C, 55.5; H, 3.66; N, 9.2.

{3-[6-(4-Methoxyphenyl)-1H-indazol-3-yl]phenyl}-methanaminium Formate (11). Synthesized by method A using **10** (250 mg, 0.82 mmol, 1.0 equiv), 3-(aminomethyl)phenylboronic acid·HCl (232 mg, 1.24 mmol, 1.5 equiv), Pd(dppf)Cl$_2$·DCM (67 mg, 0.082 mmol, 0.1 equiv), Na$_2$CO$_3$ (437 mg, 4.12 mmol, 5.0 equiv), dioxane (2.5 mL) and water (2.5 mL) and the reaction was heated for 5 h. The Celite pad was washed with DCM−MeOH (1:1) and the workup was carried out using DCM instead of EtOAc. The crude product was purified using flash column chromatography (isocratic: 12% 7.0 M NH$_3$ in MeOH−EtOAc) and a brown semisolid was obtained. The semisolid was further purified using RP ACC (gradient: 0−40% MeCN−H$_2$O in 0.1% formic acid). Appropriate fractions were collected and reduced in vacuo to a volume of ~20 mL until precipitation was observed. The precipitate was filtered and triturated in hot MeOH and the filtrate was reduced in vacuo. The resulting solid was triturated in hot EtOAc and the titled compound (67 mg, 0.20 mmol, 25%) was collected as a colorless powder in the form of a 9/10 formate salt. ^{1}H NMR (500 MHz, DMSO-d_6): 8.42 (br.s, 1H), 8.21 (d, J = 8.5 Hz, 1H), 8.11−8.07 (m, 1H), 7.96 (dt, J = 7.7, 1.4 Hz, 1H), 7.75−7.67 (m, 3H), 7.52 (t, J = 7.7 Hz, 1H), 7.48 (dd, J = 8.6, 1.6 Hz, 1H), 7.44 (d, J = 7.6 Hz, 1H), 7.10−7.04 (m, 2H), 4.03 (s, 2H), 3.82 (s, 3H). ^{13}C NMR (126 MHz, DMSO-d_6): 165.2, 159.0, 142.8, 142.5, 138.9, 138.1, 133.9, 132.7, 128.9, 128.2, 127.5, 126.4, 125.7, 121.2, 120.5, 119.0, 114.4, 107.3, 55.2, 43.5. LC-MS (ESI+): RT = 0.5−0.5 min, m/z = 330.23 (M+H$^+$).

{3-[6-(4-Methoxyphenyl)-1H-indazol-3-yl]phenyl}methanol (12). Synthesized by method A using **10** (250 mg, 0.82 mmol, 1.0 equiv), 3-(hydroxymethyl)phenylboronic acid (188 mg, 1.24 mmol, 1.5 equiv), Pd(dppf)Cl$_2$·DCM (67 mg, 0.082 mmol, 0.1 equiv), Na$_2$CO$_3$ (262 mg, 2.47 mmol, 3.0 equiv), dioxane (2.5 mL) and water (2.5 mL) and the reaction was heated for 4.5 h. The crude product was purified using flash column chromatography (gradient: 60−70% EtOAc−hexane) and the resulting yellow solid was crystallized from EtOH to give the titled compound (118 mg, 0.36 mmol, 43%) as yellow microgranules. ^{1}H NMR (501 MHz, DMSO-d_6): 13.23 (br.s, 1H), 8.14−8.09 (m, 1H), 8.02−7.97 (m, 1H), 7.88 (dt, J = 7.7, 1.5 Hz, 1H), 7.74−7.67 (m, 3H), 7.51−7.45 (m, 2H), 7.35 (ddd, J = 7.6, 1.9, 1.1 Hz, 1H), 7.10−7.03 (m, 2H), 5.29 (t, J = 5.9 Hz, 1H), 4.63 (d, J = 5.8 Hz, 2H), 3.82 (s, 3H). ^{13}C NMR (126 MHz, DMSO-d_6): 159.0, 143.2, 143.2, 142.4, 138.1, 133.5, 132.7, 128.6, 128.2, 125.7, 125.0, 124.7, 121.1, 120.5, 119.0, 114.4, 107.3, 62.9, 55.2. LC-MS (ESI+): RT = 0.6−0.6 min, m/z = 331.20 (M+H$^+$). mp: 191.7−193.1 °C.

3-(3-Ethylphenyl)-6-(4-methoxyphenyl)-1H-indazole (13). Synthesized by method A using **10** (250 mg, 0.82 mmol, 1.0 equiv), 3-ethylphenylboronic acid (186 mg, 1.24 mmol, 1.5 equiv), Pd(dppf)Cl$_2$·DCM (67 mg, 0.082 mmol, 0.1 equiv), Na$_2$CO$_3$ (262 mg, 2.47 mmol, 3.0 equiv), dioxane (2.5 mL) and water (2.5 mL) and the reaction was heated for 3.5 h. The crude product was purified using flash column chromatography (isocratic: 7:3 hexane−EtOAc). The titled compound (26 mg, 0.07 mmol, 16%) was collected as colorless waxy platelets. ^{1}H NMR (501 MHz, DMSO-d_6): 13.21 (br.s, 1H), 8.09 (dd, J = 8.5, 1.0 Hz, 1H), 7.84 (d, J = 1.8 Hz, 1H), 7.82 (dt, J = 7.6, 1.4 Hz, 1H), 7.73−7.67 (m, 3H), 7.47 (dd, J = 8.5, 1.6 Hz, 1H), 7.44 (t, J = 7.6 Hz, 1H), 7.26 (dt, J = 7.9, 1.3 Hz, 1H), 7.10−7.03 (m, 2H), 3.82 (s, 3H), 2.73 (q, J = 7.6 Hz, 2H), 1.27 (t, J = 7.6 Hz, 3H). ^{13}C NMR (126 MHz, DMSO-d_6): 159.0, 144.3, 143.3, 142.4, 138.1, 133.7, 132.7, 128.8, 128.2, 127.2, 126.1, 124.1, 121.1, 120.5, 119.1, 114.4, 107.3, 55.2, 28.2, 15.7. LC-MS (ESI+): RT = 0.7−0.8 min, m/z = 329.23 (M+H$^+$).

3,6-Bis(4-methoxyphenyl)-1H-indazole (14). Synthesized as a side product and isolated in the purification **10**. The product was triturated in hot EtOH, decanting off the yellow solution, and the remaining solid was crystallized from EtOH. The titled compound (32 mg, 0.10 mmol, 3%) was collected as off-white microneedles. ^{1}H NMR (501 MHz, DMSO-d_6): 13.10 (s, 1H), 8.06 (dt, J = 8.6, 0.7 Hz, 1H), 7.97−7.91 (m, 2H), 7.73−7.66 (m, 3H), 7.45 (dd, J = 8.5, 1.6 Hz, 1H), 7.13−7.08 (m, 2H), 7.08−7.04 (m, 2H), 3.83 (s, 3H), 3.82 (s, 3H). ^{13}C NMR (126 MHz, DMSO-d_6): 159.0, 158.9, 143.0, 142.4, 138.0, 132.7, 128.2, 127.9, 126.3, 121.0, 120.3, 118.9, 114.4, 114.3, 107.2, 55.18, 55.15. LC-MS (ESI+): RT = 2.05−2.19 min, m/z = 331.2 (M+H$^+$). mp: 197.0−198.0 °C.

{3-[6-(4-Hydroxyphenyl)-1H-indazol-3-yl]phenyl}-methanaminium Bromide (15). Synthesized by method B using **11** (50 mg, 0.15 mmol, 1.0 equiv), 1 M BBr$_3$ in DCM (1.21 mL, 1.21 mmol, 8.0 equiv) and DCM (5 mL) and the reaction was stirred for 2 h. Water (10 mL) was added, and the biphasic mixture was left for 16 h. The resulting needles were filtered and dissolved in MeOH and reduced in vacuo to reveal the crude solid as an off-white solid. The crude solid was purified by mixed solvent crystallization from water using iso-propanol as the antisolvent. The titled compound (8 mg, 0.03 mmol, 17%) was collected as a colorless powder in the form of a bromide salt. ^{1}H NMR (501 MHz, DMSO-d_6): 13.30 (br.s, 1H), 9.58 (br.s, 1H), 8.30−8.19 (m, 4H), 8.15 (d, J = 1.8 Hz, 1H), 8.05 (dt, J = 7.8, 1.4 Hz, 1H), 7.69 (dd, J = 1.5, 0.8 Hz, 1H), 7.62−7.55 (m, 3H), 7.52−7.44 (m, 2H), 6.93−6.87 (m, 2H), 4.18 (q, J = 5.9 Hz, 2H). ^{13}C NMR (126 MHz, DMSO-d_6): 157.3, 142.51, 142.47, 138.6, 134.6, 134.2, 130.9, 129.2, 128.2, 127.0, 126.6, 121.1, 120.5, 118.8, 115.8, 107.0, 42.3, one Ar-q not observed. HPLC: RT = 1.95 min. HRMS (ESI+): Found: 316.1444 (M+H$^+$), C$_{20}$H$_{17}$N$_3$O requires MH 316.1444. mp: 191.2−195.8 °C.

4-{3-[3-(Hydroxymethyl)phenyl]-1H-indazol-6-yl}phenol (16). 4-{3-[3-(Bromomethyl)phenyl]-1H-indazol-6-yl}phenol* (83 mg, 0.22 mmol, 1.0 equiv) was suspended in saturated NaHCO$_3$ (3 mL) and the reaction was refluxed for 18 h. The mixture was diluted with DCM

(10 mL) and 2 M NaOH (20 mL) added, and the organic layer was separated. The aqueous layer was acidified to pH 1.0 (2 M HCl) and the solution was extracted with DCM (20 mL). The aqueous layer was neutralized to pH 7.0 and the solution was extracted with DCM (20 mL) and the combined organic layers were reduced in vacuo and the crude product was purified by RP ACC (gradient: 0−30% MeCN−H$_2$O). The titled compound (2 mg, 6×10^{-3} mmol, 3%) was collected as an off-white solid.

*Compound formed as an undesired product from BBr$_3$ deprotection of **12** and was not isolated. ^{1}H NMR (501 MHz, DMSO-d_6): 13.20 (br.s, 1H), 9.60 (br.s, 1H), 8.09 (d, J = 8.6 Hz, 1H), 7.98 (br.s, 1H), 7.87 (d, J = 7.9 Hz, 1H), 7.66 (br.s, 1H), 7.62−7.55 (m, 2H), 7.51−7.42 (m, 2H), 7.34 (d, J = 7.6 Hz, 1H), 6.92−6.86 (m, 2H), 5.28 (t, J = 5.8 Hz, 1H), 4.62 (d, J = 5.5 Hz, 2H). ^{13}C NMR (126 MHz, DMSO-d_6): 157.2, 143.2, 142.5, 131.0, 128.6, 128.2, 125.7, 125.0, 124.6, 120.9, 120.4, 118.8, 115.8, 106.9, 62.9, three Ar-qs not observed (weak signal due to limited material). HPLC: RT = 2.41 min. HRMS (ESI+): Found: 317.1283 (M+H$^+$), C$_{20}$H$_{16}$N$_2$O$_2$ requires MH 317.1285.

4-[3-(3-Ethylphenyl)-1H-indazol-6-yl]phenol (17). Synthesized by method B using **13** (100 mg, 0.30 mmol, 1.0 equiv), 1 M BBr$_3$ in DCM (2.44 mL, 2.44 mmol, 8.0 equiv) and DCM (5 mL) and the reaction was stirred for 2 h. Water (10 mL) was added, and the resulting precipitate was filtered, washed with water, dissolved in MeOH, and reduced in vacuo to reveal the crude solid as an off-white solid. The crude solid was triturated in hot EtOAc to give the titled compound (13 mg, 0.04 mmol, 14%) as a colorless powder. ^{1}H NMR (501 MHz, DMSO-d_6): 8.07 (d, J = 8.6 Hz, 1H), 7.85−7.78 (m, 2H), 7.66 (d, J = 1.5 Hz, 1H), 7.61−7.55 (m, 2H), 7.47−7.40 (m, 2H), 7.25 (d, J = 7.6 Hz, 1H), 6.93−6.86 (m, 2H), 2.73 (q, J = 7.6 Hz, 2H), 1.26 (t, J = 7.6 Hz, 3H). ^{13}C NMR (126 MHz, DMSO-d_6): 157.2, 144.3, 143.2, 142.5, 138.5, 133.7, 131.0, 128.8, 128.2, 127.2, 126.0, 124.1, 121.0, 120.5, 118.9, 115.8, 106.9, 28.2, 15.7. HPLC: RT = 3.48 min (97%). HRMS (ESI+): Found: 315.1490 (M+H$^+$), C$_{21}$H$_{18}$N$_2$O requires MH 315.1492.

3,6-Bis(4-hydroxyphenyl)-1H-indazole (18). Synthesized by method B using **14** (194 mg, 0.59 mmol, 1.0 equiv), 1 M BBr$_3$ in DCM (4.70 mL, 4.70 mmol, 8.0 equiv) and DCM (15 mL) and the reaction was stirred for 23 h. Water (20 mL) was added, and the resulting precipitate was filtered and washed with DCM. The solid was dissolved in MeOH and reduced in vacuo to yield the crude product as a brown solid. The crude product was triturated with small amounts of cold MeOH and filtered to give the titled compound (73 mg, 0.24 mmol, 41%) as an off-white solid. ^{1}H NMR (501 MHz, DMSO-d_6): 12.98 (s, 1H), 9.58 (s, 1H), 9.56 (s, 1H), 8.01 (d, J = 8.5 Hz, 1H), 7.85−7.78 (m, 2H), 7.62 (dd, J = 1.5, 0.8 Hz, 1H), 7.60−7.54 (m, 2H), 7.40 (dd, J = 8.6, 1.6 Hz, 1H), 6.95−6.90 (m, 2H), 6.90−6.86 (m, 2H). ^{13}C NMR (126 MHz, DMSO-d_6): 157.18, 157.16, 143.3, 142.4, 138.3, 131.1, 128.1, 128.0, 124.8, 121.0, 120.0, 118.7, 115.8, 115.6, 106.7. HPLC: RT = 2.41 min. HRMS (ESI+): Found: 303.1138 (M+H$^+$), C$_{19}$H$_{15}$N$_2$O$_2$ requires MH 303.1128.

N-(6-(3-Ethoxyphenyl)-1H-indazol-3-yl)benzamide (19). Synthesized by method C using **28** (176 mg, 0.38 mmol, 1.0 equiv), TFA (1 mL) and DCM (1 mL) and the reaction was stirred for 1.5 h. The crude brown solid was triturated with MeOH and filtered to give the titled compound as an off-white solid (45 mg, 0.10 mmol, 25%). ^{1}H NMR (501 MHz, DMSO-d_6): 10.83 (s, 1H), 8.12−8.07 (m, 2H), 7.80 (dd, J = 8.5, 0.8 Hz, 1H), 7.68 (dd, J = 1.4, 0.8 Hz, 1H), 7.66−7.59 (m, 1H), 7.59−7.51 (m, 2H), 7.43−7.36 (m, 2H), 7.29 (ddd, J = 7.7, 1.7, 1.0 Hz, 1H), 7.26−7.22 (m, 1H), 6.95 (ddd, J = 8.2, 2.5, 1.0 Hz, 1H), 4.13 (q, J = 7.0 Hz, 2H), 1.37 (t, J = 7.0 Hz, 3H). ^{13}C NMR (126 MHz, DMSO-d_6): 165.5, 159.0, 142.0, 141.7, 140.1, 138.6, 133.8, 131.8, 130.0, 128.4, 127.9, 122.4, 119.5, 119.4, 116.3, 113.6, 113.1, 107.8, 63.1, 14.7. HPLC: RT = 3.21 min. HRMS (ESI+): Found: 380.1365 (M+Na$^+$), C$_{22}$H$_{19}$N$_3$NaO$_2$ requires MNa 380.1369.

N-Benzyl-6-(3-ethoxyphenyl)-1H-indazol-3-amine (20). Synthesized by method C using **29** (80 mg, 0.18 mmol, 1.0 equiv), TFA (0.5 mL) and DCM (0.5 mL) and the reaction was stirred for 2.5 h. The crude product was purified by flash column chromatography (gradient: 10−20% EtOAc−hexane) to give the titled compound as

a red semisolid (18 mg, 0.04 mmol, 22%). ^{1}H NMR (501 MHz, CDCl$_3$): 7.54 (dd, J = 8.3, 0.8 Hz, 1H), 7.47−7.42 (m, 3H), 7.38−7.30 (m, 3H), 7.30−7.24 (m, 2H), 7.18 (ddd, J = 7.7, 1.8, 1.0 Hz, 1H), 7.14 (t, J = 2.1 Hz, 1H), 6.88 (ddd, J = 8.2, 2.6, 0.9 Hz, 1H), 4.64 (s, 2H), 4.09 (q, J = 7.0 Hz, 2H), 1.43 (t, J = 7.0 Hz, 3H). ^{13}C NMR (126 MHz, CDCl$_3$): 159.5, 150.7, 143.3, 143.0, 141.1, 139.7, 129.9, 128.8, 128.0, 127.5, 120.1, 119.6, 119.5, 114.1, 113.6, 108.1, 63.7, 48.5, 23.5, 15.0. HPLC: RT = 2.92 min (71%*). HRMS (ESI+): Found: 344.1757 (M+H$^+$), C$_{22}$H$_{22}$N$_3$O requires MH 344.1757. *Pure at time of testing (see ^{1}H NMR), HPLC performed after degradation took place.

N-(6-(3-Ethoxyphenyl)-1H-indazol-3-yl)-cyclohexanecarboxamide (21). Synthesized by method C using **30** (110 mg, 0.24 mmol, 1.0 equiv), TFA (1 mL) and DCM (1 mL) and the reaction was stirred for 1.5 h. The crude brown solid was triturated with MeOH and filtered to give the titled compound as a pink solid (43 mg, 0.09 mmol, 38%). ^{1}H NMR (501 MHz, DMSO-d_6): 12.65 (br.s, 1H), 10.21 (br.s, 1H), 7.79 (dd, J = 8.5, 0.8 Hz, 1H), 7.61 (t, J = 1.2 Hz, 1H), 7.43−7.31 (m, 2H), 7.29−7.23 (m, 1H), 7.21 (t, J = 2.1 Hz, 1H), 6.94 (ddd, J = 8.2, 2.5, 0.9 Hz, 1H), 4.12 (q, J = 7.0 Hz, 2H), 1.88 (d, J = 12.7 Hz, 2H), 1.78 (d, J = 12.5 Hz, 2H), 1.67 (d, J = 12.1 Hz, 1H), 1.48 (qd, J = 12.2, 3.1 Hz, 2H), 1.36 (t, J = 7.0 Hz, 4H), 1.32−1.16 (m, 3H). ^{13}C NMR (126 MHz, DMSO-d_6): 174.4, 159.0, 142.1, 141.6, 140.4, 138.5, 130.0, 122.7, 119.4, 119.1, 115.7, 113.5, 113.1, 107.6, 63.0, 43.8, 29.2, 25.4, 25.2, 14.7. HPLC: RT = 3.39 min. HRMS (ESI+): Found: 386.1835 (M+Na$^+$), C$_{22}$H$_{25}$N$_3$NaO$_2$ requires MNa 386.1839.

N-(Cyclohexylmethyl)-6-(3-ethoxyphenyl)-1H-indazol-3-amine (22). Synthesized by method D using **26** (100 mg, 0.39 mmol, 1.0 equiv), cyclohexane carboxaldehyde (57 μL, 0.47 mmol, 1.2 equiv), glacial AcOH (1 drop), STAB (134 mg, 0.63 mmol, 1.6 equiv) and DCM (3 mL). Imine formation took 10 min, and the reduction was stirred for 18 h. The reaction mixture was added to water and the aqueous phase was extracted with DCM (×3) and the combined organic layers were washed with brine, dried (MgSO$_4$), and reduced in vacuo to reveal a colorless oil. The crude product was purified using flash column chromatography (isocratic: 0.25% 7.0 M NH$_3$ in MeOH−DCM) to give the titled compound (30 mg, 0.086 mmol, 22%) as a colorless oil that solidified upon standing. ^{1}H NMR (501 MHz, DMSO-d_6): 11.35 (s, 1H), 7.79 (d, J = 8.3 Hz, 1H), 7.41 (dd, J = 1.6, 0.8 Hz, 1H), 7.35 (t, J = 7.9 Hz, 1H), 7.22 (ddd, J = 7.7, 1.7, 1.0 Hz, 1H), 7.20−7.15 (m, 2H), 6.91 (ddd, J = 8.2, 2.5, 0.9 Hz, 1H), 5.93 (t, J = 5.9 Hz, 1H), 4.11 (q, J = 7.0 Hz, 2H), 3.14−3.05 (m, 2H), 1.82 (d, J = 12.9 Hz, 2H), 1.74−1.67 (m, 3H), 1.67−1.61 (m, 1H), 1.36 (t, J = 7.0 Hz, 3H), 1.27−1.11 (m, 3H), 1.01−0.90 (m, 2H). ^{13}C NMR (126 MHz, DMSO-d_6): 158.9, 150.2, 142.5, 142.3, 138.5, 129.9, 120.6, 119.3, 117.0, 113.3, 113.2, 112.9, 107.0, 63.0, 49.8, 37.0, 30.9, 26.3, 25.6, 14.7. HPLC: RT = 3.08 min. HRMS (ESI+): Found: 350.2240 (M+H$^+$), C$_{22}$H$_{27}$N$_3$O requires MH 350.2232.

6-(3-Ethoxyphenyl)-1H-indazole-3-phenylcarboxamide (23). Synthesized by method A using **33** (120 mg, 0.38 mmol, 1.0 equiv), 3-ethoxyphenylboronic acid (95 mg, 0.57 mmol, 1.5 equiv), Pd(dppf)Cl$_2$·DCM (31 mg, 0.038 mmol, 0.1 equiv), Na$_2$CO$_3$ (121 mg, 1.14 mmol, 3.0 equiv), dioxane (2 mL) and water (2 mL) and the reaction was heated for 1.5 h. The crude product was purified using flash column chromatography (4:1 petrol−EtOAc) to give a brown solid that was crystallized from EtOH. The resulting brown needles were recrystallized from CHCl$_3$ to give the titled compound (11 mg, 0.03 mmol, 9%) as pearlescent white platelets. ^{1}H NMR (501 MHz, DMSO-d_6): 10.31 (s, 1H), 8.30−8.24 (m, 1H), 7.93−7.87 (m, 2H), 7.84 (dd, J = 1.5, 0.8 Hz, 1H), 7.61 (dd, J = 8.5, 1.5 Hz, 1H), 7.41 (t, J = 7.9 Hz, 1H), 7.38−7.34 (m, 2H), 7.31 (ddd, J = 7.7, 1.7, 1.0 Hz, 1H), 7.27 (t, J = 2.1 Hz, 1H), 7.14−7.07 (m, 1H), 6.97 (ddd, J = 8.2, 2.6, 1.0 Hz, 1H), 4.14 (q, J = 6.9 Hz, 2H), 1.37 (t, J = 6.9 Hz, 3H). ^{13}C NMR (126 MHz, DMSO-d_6): 160.8, 159.0, 142.0, 141.7, 139.0, 138.8, 138.3, 130.1, 128.6, 123.4, 122.3, 121.9, 121.2, 120.2, 119.5, 113.8, 113.2, 108.4, 63.1, 14.7. HPLC: RT = 3.65 min. HRMS (ESI+): Found: 356.1395 (M+H$^+$), C$_{22}$H$_{19}$N$_3$O$_2$ requires MH 356.1404. mp: >250 °C.

3-Amino-6-bromo-1H-indazole (25). 4-Bromo-2-fluorobenzonitrile (5.0 g, 25.0 mmol, 1.0 equiv) was dissolved in ^{n}BuOH (25 mL) and 50−60% N_2H_2 in water (5.20 mL, 100.0 mmol, 4.0 equiv) was added and the reaction heated to 100 °C for 2 h. The reaction mixture was allowed to cool slowly, and the resulting crystals were filtered and washed with MeOH to give the titled compound (4.17 g, 19.7 mmol, 79%) as colorless microneedles. A second batch crystallized in the filtrate overnight and was collected as off-white microneedles (505 mg, 2.38 mmol, 10%). ^{1}H NMR (501 MHz, DMSO-d_6): 11.49 (br.s, 1H), 7.63 (d, J = 8.5 Hz, 1H), 7.42 (dd, J = 1.6, 0.6 Hz, 1H), 7.02 (dd, J = 8.5, 1.6 Hz, 1H), 5.44 (br.s, 2H). ^{13}C NMR (126 MHz, DMSO-d_6): 149.3, 142.0, 122.1, 120.3, 119.8, 113.1, 111.8. LC-MS (ESI+): RT = 27.7−30.2 s, m/z = 213.96 (M+H$^+$).

3-Amino-6-(3-ethoxyphenyl)-1H-indazole (26). Synthesized by method A using **25** (500 mg, 2.36 mmol, 1.0 equiv), 3-ethoxyphenyl boronic acid (587 mg, 3.54 mmol, 1.5 equiv), Pd(dppf)Cl$_2$·DCM (193 mg, 0.236 mmol, 0.1 equiv), Na$_2$CO$_3$ (750 mg, 7.07 mmol, 3.0 equiv), dioxane (10 mL) and water (10 mL) and the reaction was heated for 4 h. The crude product was purified using flash column chromatography (isocratic: 50:49:1 EtOAc−hexane−7.0 M NH$_3$ in MeOH) and the resulting off-white solid was crystallized from EtOAc. The titled compound (519 mg, 2.05 mmol, 43%) was collected as shiny off-white crystals. ^{1}H NMR (501 MHz, DMSO-d_6): 11.42 (s, 1H), 7.74 (dd, J = 8.3, 0.9 Hz, 1H), 7.42 (dd, J = 1.5, 0.8 Hz, 1H), 7.36 (t, J = 7.9 Hz, 1H), 7.23 (ddd, J = 7.7, 1.7, 1.0 Hz, 1H), 7.21−7.17 (m, 2H), 6.91 (ddd, J = 8.2, 2.6, 0.9 Hz, 1H), 5.35 (s, 2H), 4.11 (q, J = 6.9 Hz, 2H), 1.36 (t, J = 7.0 Hz, 3H). ^{13}C NMR (126 MHz, DMSO-d_6): 158.9, 149.1, 142.5, 142.0, 138.3, 129.9, 120.6, 119.3, 117.2, 113.5, 113.3, 113.0, 107.1, 63.0, 14.7. LC-MS (ESI+): RT = 31.3−34.2 s, m/z = 254.15 (M+H$^+$). mp: 185.4−186.0 °C.

tert-Butyl 3-Amino-6-(3-ethoxyphenyl)-1H-indazole-1-carboxylate (27). Synthesized by method E using **27** (700 mg, 2.76 mmol, 1.0 equiv), DMAP (101 mg, 0.83 mmol, 0.3 equiv), di-*tert*-butyl dicarbonate (698 μL, 3.04 mmol, 1.1 equiv) and THF (20 mL) and the reaction stirred for 2 h. The crude product was purified using flash column chromatography (gradient: 25−40% EtOAc−hexane) to give the titled compound (667 mg, 1.89 mmol, 68%) as a yellow foamy solid. ^{1}H NMR (501 MHz, CDCl$_3$): 8.30 (br.s, 1H), 7.57 (dd, J = 8.2, 0.8 Hz, 1H), 7.47 (dd, J = 8.2, 1.5 Hz, 1H), 7.35 (t, J = 7.9 Hz, 1H), 7.23 (ddd, J = 7.6, 1.7, 0.9 Hz, 1H), 7.19 (dd, J = 2.5, 1.7 Hz, 1H), 6.91 (ddd, J = 8.2, 2.5, 0.9 Hz, 1H), 4.82 (br.s, 2H), 4.10 (q, J = 7.0 Hz, 2H), 1.70 (s, 9H), 1.44 (t, J = 7.0 Hz, 3H). ^{13}C NMR (126 MHz, CDCl$_3$): 159.5, 151.6, 149.7, 142.9, 142.4, 141.3, 129.9, 122.6, 120.1, 119.5, 118.0, 114.0, 113.9, 113.6, 83.8, 63.6, 28.4, 15.0. LC-MS (ESI+): RT = 39.3−43.3 s, m/z = 296.20 (M-^{t}Bu).

tert-Butyl 3-Benzamido-6-(3-ethoxyphenyl)-1H-indazole-1-carboxylate (28). Synthesized by method F using **27** (152 mg, 0.43 mmol, 1.0 equiv), freshly distilled benzoyl chloride (60 μL, 0.52 mmol, 1.2 equiv), ^{i}Pr$_2$NEt (150 μL, 0.86 mmol, 2.0 equiv) and DCM (5 mL) and the reaction was stirred for 16 h. The reaction mixture was reduced in vacuo to reveal the crude product as a yellow oil which was purified using flash column chromatography (gradient: 10−20% EtOAc−hexane). The titled compound (120 mg, 0.26 mmol, 61%) was collected as a colorless oil. ^{1}H NMR (501 MHz, CDCl$_3$): 9.28 (br.s, 1H), 8.40 (br.s, 1H), 8.29 (d, J = 8.5 Hz, 1H), 8.05−7.99 (m, 2H), 7.63−7.54 (m, 2H), 7.51 (dd, J = 8.4, 7.0 Hz, 2H), 7.38 (t, J = 7.9 Hz, 1H), 7.30−7.25 (m, 1H), 7.23 (t, J = 2.1 Hz, 1H), 6.94 (ddd, J = 8.2, 2.5, 0.9 Hz, 1H), 4.12 (q, J = 7.0 Hz, 2H), 1.69 (s, 9H), 1.46 (t, J = 7.0 Hz, 3H). ^{13}C NMR (126 MHz, CDCl$_3$): 165.7, 159.5, 149.1, 145.6, 143.2, 142.4, 142.0, 133.3, 132.7, 130.0, 129.0, 127.8, 124.8, 123.5, 120.2, 118.8, 114.2, 114.0, 112.9, 85.2, 63.7, 28.3, 15.0. LC-MS (ESI+): RT = 45.3−50.1 s, m/z = 458.27.

tert-Butyl 3-(Benzylamino)-6-(3-ethoxyphenyl)-1H-indazole-1-carboxylate (29). Synthesized by method D using **27** (150 mg, 0.42 mmol, 1.0 equiv), freshly distilled benzaldehyde (52 μL, 0.51 mmol, 1.2 equiv), glacial AcOH (1 drop), STAB (144 mg, 0.68 mmol, 1.6 equiv), and DCM (3 mL). Imine formation required heating to 40 °C and the addition of 4 Å MS. STAB was added, and the reaction was stirred for 16 h. The reaction mixture was reduced in vacuo to

reveal a yellow solid which was triturated with EtOAc and then filtered. The filtrate was reduced in vacuo to give a yellow oil that was further purified by flash column chromatography (isocratic: 9:1 hexane−EtOAc) to give the titled compound as a colorless semisolid (80 mg, 0.18 mmol, 42%). ^{1}H NMR (501 MHz, CDCl$_3$): 8.28 (s, 1H), 7.53 (dd, J = 8.3, 0.7 Hz, 1H), 7.49−7.42 (m, 3H), 7.40−7.34 (m, 3H), 7.34−7.27 (m, 1H), 7.26−7.21 (m, 1H), 7.19 (t, J = 2.1 Hz, 1H), 6.92 (ddd, J = 8.3, 2.6, 0.9 Hz, 1H), 4.73 (s, 2H), 4.11 (q, J = 7.0 Hz, 2H), 1.72 (s, 9H), 1.45 (t, J = 7.0 Hz, 3H). ^{13}C NMR (126 MHz, CDCl$_3$): 159.5, 152.3, 142.8, 142.5, 139.0, 130.0, 128.8, 128.4, 127.7, 122.4, 120.0, 119.2, 118.0, 114.00, 113.98, 113.7, 102.9, 63.7, 47.9, 28.5, 15.0, two Ar-qs not observed. LC-MS (ESI+): RT = 0.8−0.9 min, m/z = 444.31 (M+H$^+$).

tert-Butyl 3-Cyclohexaneamido-6-(3-ethoxyphenyl)-1H-indazole-1-carboxylate (30). Synthesized by method F using **27** (152 mg, 0.43 mmol, 1.0 equiv), freshly distilled cyclohexanecarbonyl chloride (69 μL, 0.52 mmol, 1.2 equiv), ^{i}Pr$_2$NEt (150 μL, 0.86 mmol, 2.0 equiv) and DCM (5 mL) and the reaction was stirred for 16 h. The reaction mixture was reduced in vacuo to reveal the crude product as a yellow oil which was purified by flash column chromatography (gradient: 10−20% EtOAc−hexane) to give the titled compound (150 mg, 0.33 mmol, 75%) as shiny off-white crystals. ^{1}H NMR (501 MHz, CDCl$_3$): 8.34 (s, 1H), 8.26−8.18 (m, 2H), 7.53 (dd, J = 8.5, 1.6 Hz, 1H), 7.37 (t, J = 7.9 Hz, 1H), 7.25 (ddd, J = 7.7, 1.7, 0.9 Hz, 2H), 7.20 (dd, J = 2.5, 1.7 Hz, 1H), 6.93 (ddd, J = 8.2, 2.5, 0.9 Hz, 1H), 4.11 (q, J = 7.0 Hz, 2H), 2.39 (s, 1H), 2.08−2.00 (m, 2H), 1.86 (dt, J = 12.6, 3.4 Hz, 2H), 1.74−1.69 (m, 10H), 1.60−1.56 (m, 2H), 1.45 (t, J = 7.0 Hz, 3H), 1.36−1.25 (m, 3H). ^{13}C NMR (126 MHz, CDCl$_3$): 174.6, 159.6, 149.2, 145.5, 143.0, 142.4, 141.9, 123.0, 123.3, 120.1, 118.7, 114.2, 114.0, 112.8, 112.7, 85.1, 63.7, 45.8, 29.7, 28.4, 25.8, 25.7, 15.0. LC-MS (ESI+): RT = 47.3−50.9 s, m/z = 464.35 (M+H$^+$).

6-Bromo-1H-indazole-3-carboxylic Acid (32). 6-Bromoisatin (100 mg, 0.44 mmol, 1.0 equiv) was suspended in water (0.5 mL) and 2 M NaOH (0.5 mL) and the suspension was heated at 55 °C for 30 min followed by stirring at 20 °C for 30 min. A solution of NaNO$_2$ (31 mg, 0.44 mmol, 1.0 equiv) in water (0.5 mL) was cooled to 0 °C and added to the reaction mixture and stirred for 5 min. This solution was then added slowly over 5 min to a solution of H$_2$SO$_4$ (0.1 mL) in water (0.9 mL) via a pipet submerged beneath the liquid surface and the reaction was maintained at 0 °C for 20 min. SnCl$_2$·2H$_2$O (240 mg, 1.06 mmol, 2.4 equiv) was dissolved in HCl (1 mL) and added in one portion to the reaction and the mixture was warmed to 20 °C and stirred for 1 h. The resulting orange precipitate was filtered and washed with water. The crude solid was triturated with hot AcOH, and the insoluble impurities removed via filtration and the filtrate was reduced in vacuo to give the titled compound (81 mg, 0.34 mmol, 76%) as an orange powder. ^{1}H NMR (400 MHz, DMSO-d_6): 8.02 (d, J = 8.6 Hz, 1H), 7.88 (d, J = 1.6 Hz, 1H), 7.39 (dd, J = 8.6, 1.7 Hz, 1H). ^{13}C NMR (101 MHz, DMSO-d_6)*: 164.0, 143.2**, 137.2**, 126.0, 123.7, 121.7, 120.2, 114.3**. LC-MS (ESI+): RT = 0.5−0.5 min, m/z = 483.11 (2M+H$^+$). *Compound highly insoluble, weak signals. **Peaks visible on HMBC spectra.

6-Bromo-1H-indazole-3-phenylcarboxamide (33). Compound **32** (750 mg, 3.0 mmol, 1.0 equiv) was dissolved in freshly distilled SOCl$_2$ (3.0 mL, 41.4 mmol, 13.8 equiv) and refluxed for 1.5 h. The reaction mixture was reduced in vacuo and the resulting solid dissolved in DCM (9 mL) and Et$_3$N (360 μL, 3.6 mmol, 1.2 equiv) and the reaction was stirred 5 min. Aniline (720 μL, 7.5 mmol, 2.5 equiv) was added and the reaction was heated to 45 °C for 4 h. The reaction mixture was added to 2 M HCl and the aqueous layer was extracted with DCM (×3) and the combined organic layers were washed with 2 M NaOH, brine, dried (MgSO$_4$), and concentrated in vacuo to reveal a crude red solid that was purified by flash column chromatography (isocratic: 0.5% MeOH−DCM) to give a brown solid. The solid was crystallized from EtOAc and the titled compound (94 mg, 0.30 mmol, 13%) was collected as brown needles. ^{1}H NMR (501 MHz, DMSO-d_6): 10.36 (s, 1H), 8.16 (d, J = 8.6 Hz, 1H), 7.93−7.85 (m, 3H), 7.43 (dd, J = 8.6, 1.6 Hz, 1H), 7.39−7.31 (m, 2H), 7.10 (tt, J = 7.4, 1.2 Hz, 1H). ^{13}C NMR (126 MHz, DMSO-d_6): 160.5, 142.1, 138.7, 138.6,

128.5, 125.6, 123.5, 123.3, 120.7, 120.3, 120.2, 113.5. LC-MS (ESI+): RT = 0.6−0.6 min, m/z = 316.05 (M+H⁺). mp: >250 °C.

3-({4-[6-(4-Hydroxyphenyl)-1H-indazol-3-yl]phenyl}amino)-piperidin-1-ium Formate (34). Synthesized by method B using **S16** (100 mg, 0.29 mmol, 1.0 equiv), 1 M BBr₃ in DCM (2.33 mL, 2.33 mmol, 8.0 equiv) and DCM (7 mL) and the reaction was stirred for 20 h. Water (10 mL) was added, and the resulting yellow precipitate was collected by filtration and washed with water. The crude solid was dissolved in MeOH and reduced in vacuo to reveal an off-white solid which was crystallized from EtOH to give the titled compound (36 mg, 0.11 mmol, 38%) as a fluffy colorless solid. ¹H NMR (500 MHz, DMSO-d_6): 12.76 (s, 1H), 10.80 (s, 1H), 9.57 (s, 1H), 8.12−8.06 (m, 2H), 7.76 (d, J = 8.5 Hz, 1H), 7.64−7.60 (m, 1H), 7.59−7.52 (m, 5H), 7.33 (dd, J = 8.6, 1.5 Hz, 1H), 6.91−6.85 (m, 2H). ¹³C NMR (101 MHz, DMSO-d_6): 165.5, 157.2, 141.9, 140.1, 138.8, 133.8, 131.8, 131.2, 128.4, 128.2, 127.9, 122.3, 119.2, 115.8, 115.7, 106.5. HPLC RT = 2.46 min. HRMS (ESI+): Found: 330.1236 (M+H⁺), C₂₀H₁₅N₃O₂ requires *MH* 330.1237. mp: >250 °C.

4-[6-(4-Methoxyphenyl)-1H-indazol-3-yl]aniline (35). Synthesized by method A using **10** (500 mg, 1.65 mmol, 1.0 equiv), 4-aminophenylboronic acid·HCl (723 mg, 3.30 mmol, 2.0 equiv), Pd(dppf)Cl₂·DCM (135 mg, 0.17 mmol, 0.1 equiv), Na₂CO₃ (524 mg, 4.95 mmol, 3.0 equiv), dioxane (10 mL) and water (10 mL) and the reaction was heated for 6 h. The crude product was purified using column chromatography (isocratic: 2% 7.0 M NH₃ in MeOH−DCM) and an orange solid was obtained. The product was further purified using RP ACC (gradient: 0−50% MeCN−H₂O) and the resulting off-white solid was crystallized from EtOH to give the titled compound (33 mg, 0.10 mmol, 4%) as shiny brown needles. Coeluted fractions from the column were reduced in vacuo (151 mg, 0.48 mmol, 29%) and used without further purification. ¹H NMR (501 MHz, DMSO-d_6): 12.88 (s, 1H), 8.02 (d, J = 8.5 Hz, 1H), 7.71−7.65 (m, 4H), 7.64 (dd, J = 1.6, 0.8 Hz, 1H), 7.40 (dd, J = 8.5, 1.6 Hz, 1H), 7.09−7.02 (m, 2H), 6.74−6.67 (m, 2H), 5.26 (s, 2H), 3.81 (s, 3H). ¹³C NMR (126 MHz, DMSO-d_6): 158.9, 148.5, 144.0, 142.3, 137.8, 132.8, 128.1, 127.6, 121.4, 121.3, 119.8, 118.9, 114.4, 114.0, 107.0, 55.2. LC-MS (ESI+): RT = 0.5−0.6 min, m/z = 316.39 (M+H⁺). mp: 224.7−225.2 °C

6-(4-Methoxyphenyl)-3-[4-(piperazin-1-yl)phenyl]-1H-indazole (37). Synthesized by method G using **35** (715 mg, 2.27 mmol, 1.0 equiv), **36** (486 mg, 2.72 mmol, 1.2 equiv), K₂CO₃ (752 mg, 5.44 mmol, 2.4 equiv) and ᵗBuOH (15 mL) and the reaction was heated for 111 h. The reaction mixture was concentrated in vacuo to reveal a green/yellow solid. The solid was dissolved in DMSO, and the solution was decanted from the insoluble impurities. The crude product was purified by RP ACC (gradient: 0−30% MeCN−H₂O in 0.1% formic acid) and a brown/orange solid (432 mg) was obtained. The product was further purified by suspending the solid in 2 M NaOH (20 mL) and DCM (40 mL) with small additions of MeOH until dissolution was observed. The aqueous layer was extracted with DCM (2 × 15 mL) and the combined organic layers washed with brine (50 mL), dried (MgSO₄) and reduced in vacuo to reveal a yellow solid. The crude solid was purified by column chromatography (isocratic: 7% 7.0 M NH₃ in MeOH−DCM) to give the titled compound (304 mg, 0.79 mmol, 39%) as an off-white powder. ¹H NMR (501 MHz, DMSO-d_6): 13.02 (s, 1H), 8.05 (d, J = 8.5 Hz, 1H), 7.89−7.82 (m, 2H), 7.72−7.65 (m, 3H), 7.43 (dd, J = 8.5, 1.6 Hz, 1H), 7.09−7.03 (m, 4H), 3.82 (s, 3H), 3.16−3.10 (m, 4H), 2.90−2.84 (m, 4H). ¹³C NMR (126 MHz, DMSO-d_6): 158.9, 151.1, 146.3, 142.4, 137.9, 132.8, 128.2, 127.3, 124.0, 121.1, 120.1, 118.9, 115.2, 114.4, 107.1, 55.2, 49.0, 45.5. LC-MS (ES): RT = 0.5−0.5 min, m/z = 385.48 (M+H⁺).

4-{4-[6-(4-Hydroxyphenyl)-1H-indazol-3-yl]phenyl}piperazin-1-ium Formate (38). Synthesized by method B using **37** (49 mg, 0.13 mmol, 1.0 equiv), 1 M BBr₃ in DCM (1.02 mL, 1.02 mmol, 8.0 equiv) and DCM (5 mL) and the reaction was stirred for 1 h. Water (10 mL) was added and the resulting suspension was added to MeOH (10 mL) and the reaction mixture was washed with DCM (×3) and the combined organic layers were extracted with water (×3), adding MeOH to aid dissolution. The aqueous layer was reduced in vacuo to

reveal a brown solid which was purified by RP ACC (gradient: 0−40% MeCN−H₂O in 0.1% formic acid) to give the titled compound (36 mg, 0.1 mmol, 76%) as a colorless solid in the form of 3/10 formate salt. ¹H NMR (501 MHz, DMSO-d_6): 13.02 (br.s, 1H), 8.20 (br.s, 1H), 8.03 (d, J = 8.5 Hz, 1H), 7.92−7.86 (m, 2H), 7.65−7.61 (m, 1H), 7.60−7.54 (m, 2H), 7.41 (dd, J = 8.6, 1.5 Hz, 1H), 7.15−7.08 (m, 2H), 6.92−6.85 (m, 2H), 3.35 (t, J = 5.2 Hz, 4H), 3.16 (dd, J = 6.8, 3.8 Hz, 4H). ¹³C NMR (126 MHz, DMSO-d_6): 163.6, 157.2, 149.8, 143.0, 142.5, 138.3, 131.1, 128.1, 127.4, 125.1, 121.0, 120.1, 118.7, 115.8, 115.8, 106.8, 46.4, 43.5. HPLC: RT = 1.82 min. HRMS (ESI+): Found: 371.1869 (M+H⁺), C₂₃H₂₂N₄O requires *MH* 371.1866.

3-[2-(4-{4-[6-(4-Methoxyphenyl)-1H-indazol-3-yl]phenyl}-piperazin-1-yl)ethyl]-1,3-oxazolidin-2-one (39). Synthesized as a side product and isolated in the purification of **37**. The titled compound (193 mg, 0.39 mmol, 17%) was collected as an off-white solid. ¹H NMR (501 MHz, DMSO-d_6): 13.02 (br.s, 1H, indazole N<u>H</u>), 8.05 (d, J = 8.5 Hz, 1H, 4-H), 7.86 (d, J = 8.6 Hz, 2H, 2′′′-H and 6′′′-H), 7.72−7.65 (m, 3H, 2′′-H, 6′′-H and 7-H), 7.43 (dd, J = 8.5, 1.6 Hz, 1H, 5-H), 7.08−7.03 (m, 4H, 3′′-H, 5′′-H, 3′′′-H and 5′′′-H), 4.25 (dd, J = 9.0, 7.0 Hz, 2H, oxazolidinone OC<u>H</u>₂), 3.82 (s, 3H, C<u>H</u>₃), 3.62 (dd, J = 9.0, 7.1 Hz, 2H, oxazolidinone NC<u>H</u>₂), 3.33 (t, J = 6.4 Hz, 2H, piperazine-C<u>H</u>₂CH₂-oxazolidinone), 3.24−3.19 (m, 4H, piperazine C<u>H</u>₂), 2.60 (t, J = 5.0 Hz, 4H, piperazine C<u>H</u>₂), 2.54 (t, J = 6.2 Hz, 2H, piperazine-C<u>H</u>₂CH₂−oxazolidinone). ¹³C NMR (101 MHz, DMSO-d_6): 159.0 (4′′-C), 157.9 (oxazolidinone C═O), 150.4 (1′′′-C), 143.3 (3-C), 142.4 (3′-C), 137.9 (6-C), 132.8 (1′′-C), 128.2 (2′′-C and 6′′-C), 127.4 (3′′′-C and 5′′′-C), 124.2 (4′′′-C), 121.1 (4-C), 120.1 (5-C), 118.9 (7′-C), 115.3 (2′′′-C and 6′′′-C), 114.4 (3′′-C and 5′′-C), 107.1 (7-C), 61.6 (oxazolidinone OC<u>H</u>₂), 55.2 (OC<u>H</u>₃), 54.9 (piperazine-C<u>H</u>₂CH₂−oxazolidinone), 52.5 (piperazine C<u>H</u>₂), 48.0 (piperazine C<u>H</u>₂), 44.3 (oxazolidinone NC<u>H</u>₂), 40.6 (piperazine-CH₂C<u>H</u>₂-oxazolidinone). LC-MS (ESI+): RT = 0.6−0.6 min, m/z = 498.61 (M+H⁺). IR: ν_{max}/cm⁻¹ (solid): 3234 (N−H), 2939, 2833, 1723 (C═O), 1608.

4-{4-[6-(4-Hydroxyphenyl)-1H-indazol-3-yl]phenyl}-1-[2-(2-oxo-1,3-oxazolidin-3-yl)ethyl]piperazin-1-ium Formate (40). Synthesized by method B using **39** (70 mg, 0.14 mmol, 1.0 equiv), 1 M BBr₃ in DCM (1.13 mL, 1.13 mmol, 8.0 equiv) and DCM (3 mL) and the reaction was stirred for 45 min. MeOH (10 mL) was added, and the reaction mixture was reduced in vacuo to reveal the crude product as an orange solid. The crude product was purified by RP ACC (gradient: 0−40% MeCN−H₂O in 0.1% formic acid) to give an orange glassy solid that was further purified by flash column chromatography (gradient: 2−5% MeOH−DCM). The titled compound (14 mg, 0.029 mmol, 21%) was collected as a colorless solid. ¹H NMR (501 MHz, DMSO-d_6): 12.99 (br.s, 1H), 8.18 (br.s, 1H), 8.02 (dd, J = 8.6, 0.8 Hz, 1H), 7.89−7.82 (m, 2H), 7.64−7.60 (m, 1H), 7.60−7.54 (m, 2H), 7.40 (dd, J = 8.6, 1.5 Hz, 1H), 7.11−7.04 (m, 2H), 6.92−6.85 (m, 2H), 4.29−4.22 (m, 2H), 3.65−3.58 (m, 2H), 3.33 (t, J = 6.4 Hz, 2H), 3.21 (t, J = 5.0 Hz, 4H), 2.59 (t, J = 5.0 Hz, 4H), 2.53 (t, J = 5.7 Hz, 2H). ¹³C NMR (101 MHz, DMSO-d_6): 163.4, 157.9, 157.2, 150.4, 142.5, 138.3, 131.1, 128.1, 127.3, 124.3, 121.0, 120.0, 118.7, 115.8, 115.3, 106.8, 61.6, 54.9, 52.5, 48.0, 44.3, 40.6. HPLC: RT = 1.94 min (96%). HRMS (ESI+): Found: 484.2345 (M+H⁺), C₂₈H₂₉N₅O₃ requires *MH* 484.2343.

4-{4-[6-(2-Fluoro-4-hydroxyphenyl)-1H-indazol-3-yl]phenyl}-piperazin-1-ium Formate (41). Synthesized by method B using **S21** (16 mg, 0.04 mmol, 1.0 equiv), 1 M BBr₃ in DCM (0.32 mL, 0.32 mmol, 8.0 equiv) and DCM (1 mL) and the reaction was stirred for 1 h. The reaction mixture was concentrated in vacuo and the resulting solid was purified by RP ACC (gradient: 20−28% MeCN−H₂O in 0.1% formic acid). Appropriate fractions were combined and concentrated in vacuo to a volume of ~3 mL until a white precipitate had formed which was then filtered to give the titled compound (15 mg, 0.04 mmol, 96%) as a white powder in the form of a formate salt. ¹H NMR (501 MHz, DMSO-d_6): 8.30 (s, 1H), 8.05 (d, J = 8.5 Hz, 1H), 7.91−7.85 (m, 2H), 7.59 (d, J = 1.8 Hz, 1H), 7.42 (dd, J = 9.5, 8.4 Hz, 1H), 7.28 (dt, J = 8.5, 1.6 Hz, 1H), 7.12−7.06 (m, 2H), 6.75 (dd, J = 8.4, 2.4 Hz, 1H), 6.71 (dd, J = 12.8, 2.4 Hz, 1H), 3.28−3.22

(m, 4H), 3.05−2.99 (m, 4H). ^{13}C NMR (126 MHz, DMSO-d_6): 164.4, 159.8 (d, J = 245.0 Hz), 158.6 (d, J = 11.8 Hz), 150.4, 143.2, 142.0, 133.2, 131.4 (d, J = 5.3 Hz), 127.4, 124.5, 121.9 (d, J = 2.6 Hz), 120.7, 118.84 (d, J = 13.4 Hz), 118.82, 115.6, 112.2 (d, J = 2.7 Hz), 109.8 (d, J = 3.1 Hz), 103.1 (d, J = 25.0 Hz), 47.6, 44.2. HPLC: RT = 1.50 min. HRMS (ESI+): Found: 389.1775 (M+H$^+$), $C_{23}H_{21}FN_4O$ requires MH 389.1772.

4-{4-[6-(3-Fluoro-4-hydroxyphenyl)-1H-indazol-3-yl]phenyl}-piperazin-1-ium Formate (42). Synthesized by method B using **S22** (33 mg, 0.082 mmol, 1.0 equiv), 1 M BBr$_3$ in DCM (0.65 mL, 0.65 mmol, 8.0 equiv) and DCM (5 mL) and the reaction was stirred for 16 h. The reaction mixture was reduced in vacuo and the crude product was purified by RP ACC (gradient: 0−40% MeCN−H$_2$O in 0.1% formic acid) to give the titled compound (9 mg, 0.02 mmol, 25%) as an off-white solid in the form of a 4/5 formate salt. ^{1}H NMR (501 MHz, DMSO-d_6): 8.29 (br.s, 1H), 8.04 (dd, J = 8.6, 0.8 Hz, 1H), 7.91−7.83 (m, 2H), 7.68 (dd, J = 1.5, 0.8 Hz, 1H), 7.55 (dd, J = 12.7, 2.2 Hz, 1H), 7.45−7.39 (m, 2H), 7.12−7.02 (m, 3H), 3.28−3.21 (m, 4H), 3.04−2.96 (m, 5H). ^{13}C NMR (101 MHz, DMSO-d_6): 163.7, 151.3 (d, J = 240.6 Hz), 149.6, 144.7 (d, J = 12.1 Hz), 143.0, 142.4, 137.1 (d, J = 1.7 Hz), 131.8 (d, J = 6.2 Hz), 127.5, 125.2, 123.1 (d, J = 2.9 Hz), 121.1, 120.1, 119.0, 118.2 (d, J = 3.3 Hz), 116.0, 114.6 (d, J = 19.0 Hz), 107.3, 45.6, 42.8. HPLC: RT = 1.94 min (95%). m/z (ES+): Found: 389.1789 (M+H$^+$), $C_{23}H_{21}FN_4O$ requires MH 389.1772.

1-Ethyl-4-{4-[6-(4-hydroxyphenyl)-1H-indazol-3-yl]phenyl}-piperazin-1-ium Formate (43). Synthesized by method B using **S23** (68 mg, 0.16 mmol, 1.0 equiv), 1 M BBr$_3$ in DCM (1.32 mL, 1.32 mmol, 8.0 equiv) and DCM (3 mL) and the reaction was stirred for 1 h. Water was added, and the reaction mixture was transferred to a separating funnel. MeOH−DCM (1:1) was added to aid dissolution and the organic layer was separated. The aqueous layer was extracted with DCM (×2) with addition of MeOH to aid dissolution of precipitate in aqueous layer. The combined organic layers were dried (MgSO$_4$) and reduced in vacuo to reveal the crude product as a yellow solid. LC-MS analysis of the aqueous layer showed product and therefore the aqueous layer was reduced in vacuo and combined with the yellow solid. The crude product was purified by RP ACC (gradient: 0−40% MeCN−H$_2$O in 0.1% formic acid) to give the titled compound (41 mg, 0.10 mmol, 62%) as an off-white solid in the form of a 9/10 formate salt. ^{1}H NMR (501 MHz, DMSO-d_6): 12.98 (br.s, 1H), 8.15 (br.s, 1H), 8.02 (d, J = 8.5 Hz, 1H), 7.86 (d, J = 8.4 Hz, 2H), 7.63 (s, 1H), 7.57 (d, J = 8.5 Hz, 2H), 7.40 (dd, J = 8.6, 1.5 Hz, 1H), 7.08 (d, J = 8.5 Hz, 2H), 6.88 (d, J = 8.4 Hz, 2H), 3.24 (t, J = 5.1 Hz, 4H), 2.59 (t, J = 5.0 Hz, 4H), 2.45 (q, J = 7.1 Hz, 2H), 1.07 (t, J = 7.2 Hz, 3H). ^{13}C NMR (101 MHz, DMSO-d_6): 163.2, 157.2, 150.3, 143.2, 142.5, 138.3, 131.1, 128.2, 127.4, 124.3, 121.0, 120.1, 118.7, 115.8, 115.3, 106.8, 52.1, 51.5, 47.7, 11.7. HPLC: RT = 1.92 min. HRMS (ESI+): Found: 399.2174 (M+H$^+$), $C_{25}H_{26}N_4O$ requires MH 399.2179.

4-[3-(4-Aminophenyl)-1H-indazol-6-yl]phenol (44). Synthesized by method B using **35** (50 mg, 0.16 mmol, 1.0 equiv), 1 M BBr$_3$ in DCM (1.27 mL, 1.27 mmol, 8.0 equiv) and DCM (5 mL) and the reaction was stirred for 1 h. The workup proceeded in the same manner as was outlined in the preparation of **43**. The crude product was purified by RP ACC (gradient: 0−40% MeCN−H$_2$O in 0.1% formic acid). Appropriate fractions were combined and reduced in vacuo to a volume of ∼5 mL and the resulting solid was filtered and washed with water to give the titled compound (11 mg, 0.04 mmol, 23%) as a fluffy colorless solid. ^{1}H NMR (501 MHz, DMSO-d_6): 12.84 (s, 1H), 9.54 (s, 1H), 7.99 (d, J = 8.5 Hz, 1H), 7.71−7.65 (m, 2H), 7.59 (d, J = 1.6 Hz, 1H), 7.58−7.53 (m, 2H), 7.37 (dd, J = 8.5, 1.6 Hz, 1H), 6.91−6.85 (m, 2H), 6.73−6.67 (m, 2H), 5.25 (s, 2H). ^{13}C NMR (126 MHz, DMSO-d_6): 157.1, 148.5, 144.0, 142.4, 138.2, 131.2, 128.1, 127.5, 121.4, 121.2, 119.7, 118.7, 115.7, 114.0, 106.6. HPLC: RT = 1.66 min. HRMS (ESI+): Found: 302.1283 (M+H$^+$), $C_{19}H_{15}N_3O$ requires MH 302.1288.

Supporting Compounds. 3-Bromo-6-(3-ethoxy-5-fluorophenyl)-1H-indazole (S1). Synthesized by method A using **5** (500 mg, 1.55 mmol, 1.0 equiv), 3-ethoxy-5-fluorophenylboronic acid (427 mg, 2.32

mmol, 1.5 equiv), Pd(dppf)Cl$_2$·DCM (126 mg, 0.155 mmol, 0.1 equiv), Na$_2$CO$_3$ (492 mg, 4.64 mmol, 3.0 equiv), dioxane (10 mL) and water (10 mL) and the reaction was heated for 3 h. The crude product was purified using column chromatography (isocratic: 1:9 EtOAc−hexane) to give a colorless solid which was crystallized from cyclohexane to give the titled compound (166 mg, 0.50 mmol, 32%) as colorless flakes. ^{1}H NMR (501 MHz, CDCl$_3$): 10.64 (br.s, 1H), 7.69 (dd, J = 8.4, 0.8 Hz, 1H), 7.65 (dd, J = 1.5, 0.8 Hz, 1H), 7.44 (dd, J = 8.5, 1.4 Hz, 1H), 6.96 (t, J = 1.9 Hz, 1H), 6.92 (ddd, J = 9.5, 2.3, 1.5 Hz, 1H), 6.64 (dt, J = 10.6, 2.3 Hz, 1H), 4.09 (q, J = 7.0 Hz, 2H), 1.46 (t, J = 7.0 Hz, 3H). ^{13}C NMR (126 MHz, CDCl$_3$): 164.0 (d, J = 244.9 Hz), 160.7 (d, J = 11.6 Hz), 143.5 (d, J = 9.9 Hz), 141.8, 140.8 (d, J = 2.7 Hz), 123.2, 123.0, 122.1, 120.7, 110.2 (d, J = 2.6 Hz), 108.4, 106.9 (d, J = 22.7 Hz), 101.4 (d, J = 25.3 Hz), 64.2, 14.9. LC-MS (ESI+): RT = 2.11−2.25 min, m/z = 335.0 (M+H$^+$). mp: 166.4−167.6 °C. Anal. Calcd for $C_{15}H_{12}BrFN_2O$: C, 53.8; H, 3.60; N, 8.4. Found: C, 53.8; H, 3.61; N, 8.4.

3-Bromo-6-(3-ethoxy-2-fluorophenyl)-1H-indazole (S2). Synthesized by method A using **5** (500 mg, 1.55 mmol, 1.0 equiv), 3-ethoxy-2-fluorophenylboronic acid (429 mg, 2.33 mmol, 1.5 equiv), Pd(dppf)Cl$_2$·DCM (126 mg, 0.155 mmol, 0.1 equiv), Na$_2$CO$_3$ (492 mg, 4.65 mmol, 3.0 equiv), dioxane (10 mL) and water (10 mL) and the reaction heated was for 2 h. The crude product was purified using flash column chromatography (isocratic: 3:7 EtOAc−hexane) and the resulting colorless solid was crystallized from cyclohexane to give the titled compound (239 mg, 0.72 mmol, 46%) as colorless plates. ^{1}H NMR (501 MHz, CDCl$_3$): 10.39 (br.s, 1H), 7.70 (dd, J = 8.4, 0.8 Hz, 1H), 7.67−7.64 (m, 1H), 7.42 (dt, J = 8.4, 1.5 Hz, 1H), 7.14 (td, J = 8.0, 1.4 Hz, 1H), 7.07−6.97 (m, 2H), 4.18 (q, J = 7.0 Hz, 2H), 1.49 (t, J = 7.0 Hz, 3H). ^{13}C NMR (126 MHz, CDCl$_3$): 150.1 (d, J = 247.7 Hz), 147.8 (d, J = 11.3 Hz), 141.5, 136.1, 129.6 (d, J = 11.2 Hz), 124.2 (d, J = 4.9 Hz), 123.7 (d, J = 2.4 Hz), 123.3, 122.7, 122.4 (d, J = 2.1 Hz), 120.2, 114.3 (d, J = 2.0 Hz), 110.6 (d, J = 3.7 Hz), 65.3, 15.0. LC-MS (ESI+): RT = 1.88−2.16 min, m/z = 337.5 (M+H$^+$). mp: 148.6−150.3 °C. Anal. Calcd for $C_{15}H_{12}BrFN_2O$: C, 53.6; H, 3.50; N, 8.3. Found C, 53.8; H, 3.61; N, 8.4.

3,6-Bis(3-ethoxy-5-fluorophenyl)-1H-indazole (S3). Synthesized as a side product and isolated in the purification of **S1**. The titled compound (87 mg, 0.22 mmol, 14%) was collected as a fluffy colorless solid. ^{1}H NMR (501 MHz, CDCl$_3$): 11.15 (s, 1H), 8.05 (dd, J = 8.5, 0.8 Hz, 1H), 7.51 (dd, J = 1.6, 0.8 Hz, 1H), 7.44 (dd, J = 8.6, 1.5 Hz, 1H), 7.36 (t, J = 1.8 Hz, 1H), 7.32 (ddd, J = 9.3, 2.3, 1.3 Hz, 1H), 6.95 (t, J = 1.9 Hz, 1H), 6.90 (ddd, J = 9.5, 2.3, 1.5 Hz, 1H), 6.68 (dt, J = 10.6, 2.3 Hz, 1H), 6.64 (dt, J = 10.5, 2.2 Hz, 1H), 4.08 (dq, J = 13.9, 7.0 Hz, 4H), 1.47 (t, J = 6.9 Hz, 3H), 1.42 (t, J = 7.0 Hz, 3H). ^{13}C NMR (126 MHz, CDCl$_3$): 164.1 (d, J = 244.6 Hz), 164.0 (d, J = 244.6 Hz), 160.9 (d, J = 11.6 Hz), 160.7 (d, J = 11.6 Hz), 144.9 (d, J = 3.3 Hz), 143.7 (d, J = 9.9 Hz), 142.4, 139.6 (d, J = 2.6 Hz), 135.8 (d, J = 10.7 Hz), 121.9, 121.4, 120.6, 110.1 (d, J = 2.6 Hz), 109.7 (d, J = 2.6 Hz), 108.5, 106.9, 106.8, 102.2 (d, J = 24.9 Hz), 101.2 (d, J = 25.0 Hz), 64.0*, 14.7, 14.7. HPLC: RT = 3.87 min. HRMS (ESI+): Found: 395.1577 (M+H$^+$), $C_{23}H_{20}F_2N_2O_2$ requires MH 395.1566. *Two overlapping peaks.

3,6-Bis(3-ethoxy-2-fluorophenyl)-1H-indazole (S4). Synthesized as a side product and isolated in the purification of **S2** to give a glassy solid. The glassy solid was dissolved in Et$_2$O and reduced in vacuo to give the titled compound (9 mg, 0.02 mmol, 2%) as a pale purple powder. ^{1}H NMR (501 MHz, CDCl$_3$): 10.52 (br.s, 1H), 7.93 (ddd, J = 8.5, 3.3, 0.8 Hz, 1H), 7.65 (q, J = 1.2 Hz, 1H), 7.43−7.36 (m, 2H), 7.18 (td, J = 8.0, 1.4 Hz, 1H), 7.13 (td, J = 7.9, 1.4 Hz, 1H), 7.10−7.03 (m, 2H), 6.99 (td, J = 7.9, 1.7 Hz, 1H), 4.18 (p, J = 7.0 Hz, 4H), 1.50 (td, J = 7.0, 2.6 Hz, 6H). ^{13}C NMR (126 MHz, CDCl$_3$): 150.6 (d, J = 249.7 Hz), 150.2 (d, J = 247.7 Hz), 147.8* (t, J = 11.4 Hz), 141.7 (d, J = 13.2 Hz), 134.8, 130.1 (d, J = 11.1 Hz), 124.3 (d, J = 4.6 Hz), 124.1 (d, J = 4.8 Hz), 123.2, 122.5 (d, J = 2.1 Hz), 122.4 (d, J = 2.9 Hz), 122.0 (d, J = 12.2 Hz), 121.9 (d, J = 7.5 Hz), 121.5, 115.0 (d, J = 2.1 Hz), 114.1 (d, J = 2.0 Hz), 110.3 (d, J = 3.4 Hz), 65.4, 65.3, 15.02, 15.01. HPLC: RT = 2.99 min. HRMS (ESI+): Found: 395.1575 (M+H$^+$), $C_{23}H_{21}F_2N_2O_2$ requires MH 395.1571. *Two overlapping peaks.

{3-[6-(3-Ethoxy-5-methylphenyl)-1H-indazol-3-yl]phenyl}-methanaminium Formate (S5). Synthesized by method A using **S1** (100 mg, 0.30 mmol, 1.0 equiv), 3-(aminomethyl)phenylboronic acid·HCl (112 mg, 0.60 mmol, 2.0 equiv), Pd(dppf)Cl$_2$·DCM (24 mg, 0.03 mmol, 0.1 equiv), Na$_2$CO$_3$ (158 mg, 1.50 mmol, 5.0 equiv), dioxane (5 mL) and water (5 mL) and the reaction was heated for 3 h. The crude product was purified using flash column chromatography (isocratic: 1:10:89, 7.0 M NH$_3$ in MeOH−MeOH−EtOAc) and the resulting brown solid was further purified using preparative HPLC (gradient: 50−80% MeOH−H$_2$O in 0.1% formic acid). Appropriate fractions were reduced in vacuo to ∼3 mL and the compound was left to precipitate overnight. The titled compound (4 mg, 0.01 mmol, 4%) was collected as a colorless solid in the form of a formate salt. ^{1}H NMR (501 MHz, DMSO-d_6): 8.36 (br.s, 1H), 8.22 (d, J = 8.6 Hz, 1H), 8.07 (s, 1H), 7.95 (d, J = 7.7 Hz, 1H), 7.83 (d, J = 1.6 Hz, 1H), 7.56−7.49 (m, 2H), 7.43 (d, J = 7.6 Hz, 1H), 7.17 (dt, J = 9.9, 1.9 Hz, 1H), 7.13 (t, J = 1.9 Hz, 1H), 6.85 (dt, J = 11.0, 2.3 Hz, 1H), 4.15 (q, J = 7.0 Hz, 2H), 4.01 (br.s, 2H), 1.37 (t, J = 6.9 Hz, 3H). ^{13}C NMR (126 MHz, DMSO-d_6): 164.7, 163.4 (d, J = 241.9 Hz), 160.3 (d, J = 12.4 Hz), 143.3 (d, J = 10.0 Hz), 143.0, 142.1, 139.6, 137.1, 133.7, 128.9, 127.5, 126.3, 125.6, 121.3, 120.7, 119.8, 109.6, 108.6, 106.0 (d, J = 22.6 Hz), 100.9 (d, J = 26.2 Hz), 63.7, 43.8, 14.5. HPLC: RT = 0.60 min. HRMS (ESI+): Found: 384.1486 (M-formate$^+$), C$_{22}$H$_{20}$FN$_3$NaO requires *MH* 384.1483.

{3-[6-(3-Ethoxy-5-fluorophenyl)-1H-indazol-3-yl]phenyl}-methanol (S6). Synthesized by method A using **S1** (100 mg, 0.30 mmol, 1.0 equiv), 3-(hydroxymethyl)phenylboronic acid (68 mg, 0.45 mmol, 1.5 equiv), Pd(dppf)Cl$_2$·DCM (24 mg, 0.03 mmol, 0.1 equiv), Na$_2$CO$_3$ (95 mg, 0.90 mmol, 3.0 equiv), dioxane (5 mL) and water (5 mL) and the reaction was heated for 2 h. The crude product was purified using flash column chromatography (isocratic: 3:2 EtOAc−hexane) to give a yellow solid which was crystallized from toluene to give the titled compound (34 mg, 0.094 mmol, 31%) as colorless fluffy microneedles. ^{1}H NMR (501 MHz, DMSO-d_6): 8.14 (dd, J = 8.6, 0.8 Hz, 1H), 7.99 (d, J = 1.9 Hz, 1H), 7.88 (dt, J = 7.7, 1.6 Hz, 1H), 7.82 (t, J = 1.1 Hz, 1H), 7.53 (dd, J = 8.6, 1.6 Hz, 1H), 7.48 (t, J = 7.6 Hz, 1H), 7.35 (ddd, J = 7.6, 1.8, 1.1 Hz, 1H), 7.20−7.15 (m, 1H), 7.15−7.11 (m, 1H), 6.85 (dt, J = 11.0, 2.3 Hz, 1H), 5.29 (t, J = 6.0 Hz, 1H), 4.62 (d, J = 4.2 Hz, 2H), 4.15 (q, J = 6.9 Hz, 2H), 1.37 (t, J = 7.0 Hz, 3H). ^{13}C NMR (126 MHz, DMSO-d_6): 163.4 (d, J = 241.9 Hz), 160.3 (d, J = 12.0 Hz), 143.28 (d, J = 10.2 Hz), 143.25 (d, J = 7.8 Hz), 142.1, 137.1, 133.4, 128.6, 125.8, 125.0, 124.7, 121.2, 120.7, 119.8, 109.6, 108.5, 106.0 (d, J = 22.6 Hz), 100.9 (d, J = 25.1 Hz), 63.7, 62.9, 14.5. HPLC: RT = 1.77 min. HRMS (ESI+): Found: 363.1515 (M+H$^+$), C$_{22}$H$_{19}$FN$_2$O$_2$ requires *MH* 363.1503. mp: 171.2−171.8 °C. Anal. Calcd for C$_{22}$H$_{19}$FN$_2$O$_2$: C,73.1; H, 5.30; N, 7.8. Found: C, 72.9; H, 5.28; N, 7.7.

6-(3-Ethoxy-5-fluorophenyl)-3-(3-ethylphenyl)-1H-indazole (S7). Synthesized by method A using **S1** (100 mg, 0.30 mmol, 1.0 equiv), 3-ethylphenylboronic acid (67 mg, 0.45 mmol, 1.5 equiv), Pd(dppf)Cl$_2$·DCM (24 mg, 0.03 mmol, 0.1 equiv), Na$_2$CO$_3$ (95 mg, 0.90 mmol, 3.0 equiv), dioxane (5 mL) and water (5 mL) and the reaction was heated for 2 h. The crude product was purified using flash column chromatography (isocratic: 1:9 EtOAc−hexane) and the resulting colorless glassy solid was dissolved in Et$_2$O and reduced in vacuo to give the titled compound (28 mg, 0.08 mmol, 25%) as an off-white hygroscopic foamy solid. ^{1}H NMR (501 MHz, CDCl$_3$): 11.87 (br.s, 1H), 8.05 (dd, J = 8.5, 0.8 Hz, 1H), 7.91−7.84 (m, 2H), 7.49 (t, J = 7.6 Hz, 1H), 7.42 (dd, J = 8.5, 1.5 Hz, 1H), 7.34−7.27 (m, 2H), 6.92 (t, J = 1.9 Hz, 1H), 6.85 (ddd, J = 9.6, 2.3, 1.5 Hz, 1H), 6.64 (dt, J = 10.6, 2.3 Hz, 1H), 4.10 (q, J = 7.0 Hz, 2H), 2.73 (q, J = 7.6 Hz, 2H), 1.48 (t, J = 7.0 Hz, 3H), 1.26 (t, J = 7.6 Hz, 3H). ^{13}C NMR (126 MHz, CDCl$_3$): 164.0 (d, J = 244.4 Hz), 160.6 (d, J = 11.5 Hz), 146.1, 145.2, 143.8 (d, J = 9.9 Hz), 142.4, 139.2 (d, J = 2.6 Hz), 133.4, 129.2, 128.3, 127.4, 125.3, 121.6, 121.4, 120.8, 110.2 (d, J = 2.5 Hz), 108.6, 106.9 (d, J = 22.6 Hz), 101.0 (d, J = 25.0 Hz), 64.1, 29.1, 15.6, 14.9. HPLC: RT = 3.35 min (97%). HRMS (ESI+): Found: 383.1529 (M+Na$^+$), C$_{23}$H$_{21}$FN$_2$NaO requires *MH* 383.1530.

{3-[6-(3-Ethoxy-2-fluorophenyl)-1H-indazol-3-yl]phenyl}-methanamine (S8). Synthesized by method A using **S2** (150 mg,

0.45 mmol, 1.0 equiv), 3-(aminomethyl)phenylboronic acid·HCl (126 mg, 0.67 mmol, 1.5 equiv), Pd(dppf)Cl$_2$·DCM (37 mg, 0.045 mmol, 0.1 equiv), Na$_2$CO$_3$ (237 mg, 2.24 mmol, 5.0 equiv), dioxane (5 mL) and water (5 mL) and the reaction was heated for 2 h. The crude product was purified using flash column chromatography (isocratic: 3:10:87 7.0 M NH$_3$ in MeOH−MeOH−EtOAc) and the resulting brown solid was crystallized from toluene to give the titled compound (37 mg, 0.10 mmol, 23%) as pale brown crystals. ^{1}H NMR (501 MHz, DMSO-d_6): 8.18 (dd, J = 8.5, 0.8 Hz, 1H), 8.00 (d, J = 1.9 Hz, 1H), 7.85 (dt, J = 7.6, 1.5 Hz, 1H), 7.71−7.67 (m, 1H), 7.46 (t, J = 7.6 Hz, 1H), 7.40−7.33 (m, 2H), 7.28−7.17 (m, 2H), 7.13 (td, J = 6.8, 2.0 Hz, 1H), 4.17 (q, J = 7.0 Hz, 2H), 3.84 (s, 2H), 1.39 (t, J = 7.0 Hz, 3H). ^{13}C NMR (126 MHz, DMSO-d_6): 148.9 (d, J = 245.5 Hz), 147.0 (d, J = 11.1 Hz), 145.0, 143.4, 141.8, 133.4, 132.9, 129.2 (d, J = 10.6 Hz), 128.6, 126.5, 125.4, 124.6, 124.5 (d, J = 4.7 Hz), 122.3 (d, J = 2.6 Hz), 121.9 (d, J = 2.2 Hz), 120.9, 119.5, 114.0, 110.6 (d, J = 3.0 Hz), 64.4, 45.7, 14.6. HPLC: RT = 3.39 min. HRMS (ESI +): Found: 362.1675 (M+H$^+$), C$_{22}$H$_{21}$FN$_3$O requires *MH* 362.1669. mp: 164.9−165.3 °C.

{3-[6-(3-Ethoxy-2-fluorophenyl)-1H-indazol-3-yl]phenyl}-methanol (S9). Synthesized by method A using **S2** (150 mg, 0.45 mmol, 1.0 equiv), 3-hydroxymethylphenylboronic acid (102 mg, 0.68 mmol, 1.5 equiv), Pd(dppf)Cl$_2$·DCM (37 mg, 0.045 mmol, 0.1 equiv), Na$_2$CO$_3$ (142 mg, 1.34 mmol, 3.0 equiv), dioxane (5 mL) and water (5 mL) and the reaction was heated for 1 h. The crude product was purified using flash column chromatography (gradient: 50−60% EtOAc−hexane) and the resulting off-white solid was triturated with DCM and filtered. The solid was crystallized from propan-2-ol to give the titled compound (26 mg, 0.07 mmol, 16%) as colorless crystals. ^{1}H NMR (501 MHz, DMSO-d_6): 8.16 (dd, J = 8.6, 0.8 Hz, 1H), 8.02−7.98 (m, 1H), 7.89 (dt, J = 7.7, 1.5 Hz, 1H), 7.72−7.67 (m, 1H), 7.48 (t, J = 7.6 Hz, 1H), 7.36 (ddt, J = 7.9, 4.6, 1.3 Hz, 2H), 7.27−7.17 (m, 2H), 7.17−7.10 (m, 1H), 5.29 (t, J = 5.9 Hz, 1H), 4.62 (d, J = 5.8 Hz, 2H), 4.17 (q, J = 7.0 Hz, 2H), 1.39 (t, J = 7.0 Hz, 3H). ^{13}C NMR (126 MHz, DMSO-d_6): 148.9 (d, J = 245.8 Hz), 147.0 (d, J = 10.9 Hz), 143.3, 143.2, 141.7, 133.4, 132.9, 129.2 (d, J = 10.9 Hz), 128.6, 125.8, 125.0, 124.7, 124.5 (d, J = 4.7 Hz), 122.3 (d, J = 2.4 Hz), 121.9 (d, J = 1.9 Hz), 120.8, 119.5, 114.0, 110.6 (d, J = 3.2 Hz), 64.4, 62.9, 14.6. HPLC: RT = 3.81 min. HRMS (ESI+): Found: 363.1513 (M+H$^+$), C$_{22}$H$_{20}$FN$_2$O$_2$ requires *MH* 363.1509. mp: 190.3−192.5 °C.

6-(3-Ethoxy-2-fluorophenyl)-3-(3-ethylphenyl)-1H-indazole (S10). Synthesized by method A using **S2** (110 mg, 0.33 mmol, 1.0 equiv), 3-ethylphenylboronic acid (74 mg, 0.49 mmol, 1.5 equiv), Pd(dppf)Cl$_2$·DCM (27 mg, 0.033 mmol, 0.1 equiv), Na$_2$CO$_3$ (104 mg, 0.98 mmol, 3.0 equiv), dioxane (5 mL) and water (5 mL) and the reaction was heated for 2 h. The crude product was purified using flash column chromatography (isocratic: 1:4 EtOAc−hexane) and the resulting glassy solid was dissolved in Et$_2$O and reduced in vacuo to give the titled compound (37 mg, 0.10 mmol, 31%) as a colorless foamy solid. ^{1}H NMR (501 MHz, CDCl$_3$): 10.59 (s, 1H), 8.07 (dd, J = 8.5, 0.8 Hz, 1H), 7.88−7.85 (m, 1H), 7.85−7.80 (m, 1H), 7.62−7.58 (m, 1H), 7.45 (t, J = 7.6 Hz, 1H), 7.42 (dt, J = 8.5, 1.5 Hz, 1H), 7.30−7.24 (m, 2H), 7.14 (td, J = 8.0, 1.4 Hz, 1H), 7.08−6.96 (m, 2H), 4.18 (q, J = 7.0 Hz, 2H), 2.76 (q, J = 7.6 Hz, 2H), 1.50 (t, J = 7.0 Hz, 3H), 1.31 (t, J = 7.6 Hz, 3H). ^{13}C NMR (126 MHz, CDCl$_3$): 150.2 (d, J = 247.5 Hz), 147.7 (d, J = 11.4 Hz), 146.2, 145.1, 142.1, 134.7, 133.5, 130.0 (d, J = 11.3 Hz), 129.0, 128.0, 127.2, 125.1, 124.1 (d, J = 4.8 Hz), 123.2 (d, J = 2.5 Hz), 122.5 (d, J = 2.2 Hz), 121.2, 120.6, 114.1, 110.5 (d, J = 3.3 Hz), 65.3, 29.1, 15.7, 15.0. HPLC: RT = 1.49 min. HRMS (ESI+): Found: 361.1710 (M+H$^+$), C$_{23}$H$_{22}$FN$_2$O requires *MH* 361.1716.

tert-Butyl 3-(N-Benzoylbenzamido)-6-(3-ethoxyphenyl)-1H-inda-zole-1-carboxylate (S12). Synthesized as a side product and isolated in the purification of **28** to give a colorless semisolid. The colorless solid was dissolved in MeOH and reduced in vacuo to give the titled compound (45 mg, 0.08 mmol, 19%) as a white solid. ^{1}H NMR (501 MHz, CDCl$_3$): 8.35 (t, J = 1.1 Hz, 1H), 7.89−7.83 (m, 4H), 7.56 (qd, J = 8.4, 1.1 Hz, 2H), 7.49 (ddt, J = 8.7, 7.1, 1.3 Hz, 2H), 7.40−7.34 (m, 5H), 7.21 (ddd, J = 7.7, 1.7, 0.9 Hz, 1H), 7.17 (dd, J = 2.5, 1.7

Hz, 1H), 6.93 (ddd, J = 8.3, 2.6, 0.9 Hz, 1H), 4.10 (q, J = 7.0 Hz, 2H), 1.45 (t, J = 7.0 Hz, 3H). ^{13}C NMR (126 MHz, CDCl$_3$): 172.2, 159.6, 148.8, 146.1, 143.1, 142.2, 141.8, 134.1, 132.9, 130.1, 129.4, 128.8, 124.4, 120.4, 120.1, 119.8, 114.2, 114.1, 113.8, 85.3, 63.7, 28.2, 15.0. LC-MS (ESI+): RT = 48.3−54.3 s, m/z = 562.32 (M+H$^+$).

3-(N-Benzoylbenzamido)-6-(3-ethoxyphenyl)-1H-indazol-2-ium Trifluoroacetate (S13). Synthesized by method C using **S12** (95 mg, 0.17 mmol, 1.0 equiv), TFA (1 mL) and DCM (1 mL) and the reaction was stirred for 45 min. The crude product was purified by flash column chromatography (isocratic: 1:1 EtOAc−hexane) to give the titled compound (45 mg, 0.08 mmol, 46%) as a colorless gummy solid. ^{1}H NMR (501 MHz, CDCl$_3$): 10.23 (br.s, 1H), 7.88−7.82 (m, 4H), 7.57 (dd, J = 8.4, 0.8 Hz, 1H), 7.48−7.42 (m, 2H), 7.39 (t, J = 1.1 Hz, 1H), 7.37−7.29 (m, 6H), 7.08 (ddd, J = 7.6, 1.7, 0.9 Hz, 1H), 7.05 (dd, J = 2.5, 1.6 Hz, 1H), 6.89 (ddd, J = 8.3, 2.5, 0.9 Hz, 1H), 4.06 (q, J = 7.0 Hz, 2H), 1.43 (t, J = 7.0 Hz, 3H). ^{13}C NMR (101 MHz, CDCl$_3$): 172.6, 159.5, 142.4, 134.3, 132.8, 130.9, 130.0, 129.3, 129.1, 128.8, 128.2, 127.8, 122.6, 120.1, 117.4, 114.1, 113.8, 108.8, 63.7, 15.0. HPLC: RT = 3.89 min (84%)*. HRMS (ES+): Found: 484.1630 (M+Na$^+$), C$_{29}$H$_{23}$N$_3$NaO$_3$ requires MNa 484.1632. *Pure at time of biological evaluation (see ^{1}H NMR), HPLC performed after degradation took place.

tert-Butyl 3-Amino-6-bromo-1H-indazole-1-carboxylate (S14). Synthesized by method E using **25** (2.28 g, 10.8 mmol, 1.0 equiv), DMAP (395 mg, 3.23 mmol, 0.3 equiv), di-*tert*-butyl dicarbonate (2.97 mL, 12.9 mmol, 1.2 equiv) and THF (40 mL) and the reaction was stirred for 1 h. The crude product was purified by flash column chromatography (gradient: 20−50% EtOAc−hexane) and the resulting off-white solid was crystallized from iso-propanol to give the titled compound (1.36 g, 4.36 mmol, 40%) as colorless granules. The filtrate was reduced in vacuo to give a colorless solid (1.30 g, 4.16 mmol, 39%) which was used without further purification. ^{1}H NMR (500 MHz, DMSO-d_6): 8.12 (br.s, 1H), 7.80 (dd, J = 8.3, 0.6 Hz, 1H), 7.46 (dd, J = 8.4, 1.7 Hz, 1H), 6.41 (s, 2H), 1.58 (s, 9H). ^{13}C NMR (125 MHz, DMSO-d_6): 152.1, 140.6, 125.5, 122.6, 122.5, 118.4, 116.7, 104.5, 82.9, 27.8. LC-MS (ESI+): RT = 0.6−0.7 min, m/z = 257.97 (M-^{t}Bu+H$^+$). mp: 167.5−168.3 °C.

tert-Butyl 3-benzamido-6-bromo-1H-indazole-1-carboxylate (S15). Synthesized by method F using **S14** (1.0 g, 3.20 mmol, 1.0 equiv), freshly distilled benzoyl chloride (446 μL, 3.84 mmol, 1.2 equiv), ^{i}Pr$_2$NEt (1.12 mL, 6.41 mmol, 2.0 equiv) and DCM (20 mL) and the reaction was stirred for 20 h. The crude product was purified by flash column chromatography (gradient: 5−10% EtOAc−hexane then flush with 1:1 EtOAc−hexane) to give the titled compound (592 mg, 1.42 mmol, 44%) as an off-white glassy solid. ^{1}H NMR (501 MHz, CDCl$_3$): 8.89 (br.s, 1H), 8.38 (br.s, 1H), 8.17 (dd, J = 8.7, 0.6 Hz, 1H), 7.99−7.93 (m, 2H), 7.64−7.57 (m, 1H), 7.55−7.49 (m, 2H), 7.45 (dd, J = 8.7, 1.7 Hz, 1H), 1.70 (s, 9H). ^{13}C NMR (126 MHz, CDCl$_3$): 165.6, 148.8, 145.4, 133.1, 132.9, 129.1, 127.7, 127.2, 125.9, 124.7, 118.3, 117.7, 105.1, 85.8, 28.3. LC-MS (ESI+): RT = 0.7−0.8 min, m/z = 362.07 (M-^{t}Bu+Br^{81+}).

N-[6-(4-Methoxyphenyl)-1H-indazol-3-yl]benzamide (S16). Synthesized by method A using **S15** (229 mg, 0.55 mmol, 1.0 equiv), 4-methoxyphenylboronic acid (125 mg, 0.82 mmol, 1.5 equiv), Pd(dppf)Cl$_2$·DCM (45 mg, 0.055 mmol, 0.1 equiv), Na$_2$CO$_3$ (175 mg, 1.65 mmol, 3.0 equiv), dioxane (2 mL) and water (2 mL) and the reaction was heated for 3 h. The crude product was purified by flash column chromatography (gradient: 50−60% EtOAc−hexane) and the resulting solid was crystallized from propan-2-ol to give the titled compound (94 mg, 0.27 mmol, 50%) as colorless microneedles. The filtrate was reduced in vacuo to reveal an off-white solid (55 mg, 0.16 mmol, 29%) which was used without further purification. ^{1}H NMR (501 MHz, DMSO-d_6): 12.79 (s, 1H), 10.81 (s, 1H), 8.12−8.07 (m, 2H), 7.79 (dd, J = 8.7, 0.9 Hz, 1H), 7.72−7.65 (m, 2H), 7.65−7.58 (m, 2H), 7.58−7.51 (m, 2H), 7.36 (dd, J = 8.6, 1.5 Hz, 1H), 7.09−7.02 (m, 2H), 3.81 (s, 3H). ^{13}C NMR (126 MHz, DMSO-d_6): 165.5, 159.0, 141.9, 140.1, 138.4, 133.8, 132.8, 131.8, 128.4, 128.2, 127.9, 122.4, 119.2, 115.9, 114.4, 106.9, 104.5, 55.2. LC-MS (ES): RT = 0.6−0.6 min, m/z = 344.20 (M+H$^+$). mp: 213.5−215.0 °C.

3-Bromo-6-(2-fluoro-4-methoxyphenyl)-1H-indazole (S17). Synthesized by method A using **5** (750 mg, 2.3 mmol, 1.0 equiv), 2-fluoro-4-methoxyphenylboronic acid (395 mg, 2.32 mmol, 1.0 equiv), Pd(dppf)Cl$_2$·DCM (190 mg, 0.23 mmol, 0.1 equiv), Na$_2$CO$_3$ (738 mg, 7.0 mmol, 6.0 equiv), dioxane (10 mL) and water (10 mL) and the reaction was heated for 6 h. The crude product was purified using flash column chromatography (gradient: 20−30% EtOAc−petrol) to give the titled compound (182 mg, 0.57 mmol, 25%) as colorless microcrystals. ^{1}H NMR (501 MHz, DMSO-d_6): 13.46 (s, 1H), 7.66−7.61 (m, 2H), 7.54 (t, J = 9.0 Hz, 1H), 7.36 (dt, J = 8.5, 1.6 Hz, 1H), 6.98 (dd, J = 13.0, 2.5 Hz, 1H), 6.92 (dd, J = 8.6, 2.6 Hz, 1H), 3.83 (s, 3H). ^{13}C NMR (126 MHz, DMSO-d_6): 160.4 (d, J = 11.3 Hz), 159.7 (d, J = 246.0 Hz), 141.2, 134.4, 131.5 (d, J = 4.9 Hz), 122.8 (d, J = 2.7 Hz), 121.2, 120.2, 120.1 (d, J = 13.3 Hz), 119.2, 111.0 (d, J = 2.9 Hz), 110.3 (d, J = 3.5 Hz), 102.1 (d, J = 26.5 Hz), 55.7. LC-MS (ES): RT = 0.6−0.7 min, m/z = 321.27 (M+H$^+$).

3-Bromo-6-(3-fluoro-4-methoxyphenyl)-1H-indazole (S18). Synthesized by method A using **5** (750 mg, 2.32 mmol, 1.0 equiv), 3-fluoro-4-methoxyphenylboronic acid (395 mg, 2.32 mmol, 1.0 equiv), Pd(dppf)Cl$_2$·DCM (190 mg, 0.23 mmol, 0.1 equiv), Na$_2$CO$_3$ (738 mg, 6.96 mmol, 3.0 equiv), dioxane (10 mL) and water (10 mL) and the reaction was heated for 6 h. The crude product was purified using flash column chromatography (gradient: 20−30% EtOAc−petrol) to give the titled compound (237 mg, 0.74 mmol, 32%) as an off-white powder. ^{1}H NMR (501 MHz, DMSO-d_6): 13.47 (s, 1H), 7.75 (t, J = 1.1 Hz, 1H), 7.65 (dd, J = 12.9, 2.3 Hz, 1H), 7.62 (d, J = 8.5 Hz, 1H), 7.55 (ddd, J = 8.6, 2.4, 1.1 Hz, 1H), 7.52 (dd, J = 8.5, 1.5 Hz, 1H), 7.28 (t, J = 8.8 Hz, 1H), 3.90 (s, 3H). ^{13}C NMR (126 MHz, DMSO-d_6): 151.7 (d, J = 243.9 Hz), 146.9 (d, J = 10.8 Hz), 141.6, 138.3, 132.9 (d, J = 6.6 Hz), 123.4 (d, J = 3.2 Hz), 121.0, 120.2, 119.6, 114.7, 114.6, 114.3 (d, J = 2.3 Hz), 107.9, 56.1. LC-MS (ES): RT = 0.6−0.7 min, m/z = 321.24 (M+H$^+$).

4-[6-(2-Fluoro-4-methoxyphenyl)-1H-indazol-3-yl]aniline (S19). Synthesized by method A using **S17** (170 mg, 0.53 mmol, 1.0 equiv), 4-aminophenylboronic acid pinacol ester (232 mg, 1.06 mmol, 2.0 equiv), Pd(dppf)Cl$_2$·DCM (43 mg, 0.053 mmol, 0.1 equiv), Na$_2$CO$_3$ (168 mg, 1.59 mmol, 3.0 equiv), dioxane (2.5 mL) and water (2.5 mL) and the reaction was heated for 3 h. The crude product was purified using flash column chromatography (isocratic: 2% 7.0 M NH$_3$ in MeOH−DCM) to give the titled compound (115 mg, 0.36 mmol, 69%) as a yellow powder. ^{1}H NMR (501 MHz, DMSO-d_6): 12.92 (br.s, 1H), 8.04 (d, J = 8.5 Hz, 1H), 7.71−7.62 (m, 2H), 7.59 (s, 1H), 7.54 (t, J = 9.0 Hz, 1H), 7.27 (dt, J = 8.5, 1.6 Hz, 1H), 6.97 (dd, J = 12.9, 2.5 Hz, 1H), 6.92 (dd, J = 8.6, 2.6 Hz, 1H), 6.74−6.67 (m, 2H), 5.27 (s, 2H), 3.83 (br.s, 3H). ^{13}C NMR (126 MHz, DMSO-d_6): 160.1 (d, J = 11.1 Hz), 159.8 (d, J = 245.5 Hz), 148.5, 144.1, 141.8, 132.6, 131.4 (d, J = 5.2 Hz), 127.6, 121.5, 121.3, 121.0, 120.6 (d, J = 13.7 Hz), 118.9, 114.0, 110.9 (d, J = 2.8 Hz), 109.8 (d, J = 3.4 Hz), 102.1 (d, J = 26.5 Hz), 55.7. LC-MS (ESI+): RT = 0.5−0.6 min, m/z = 334.36 (M+H$^+$).

4-[6-(3-Fluoro-4-methoxyphenyl)-1H-indazol-3-yl]aniline (S20). Synthesized by method A using **S18** (214 mg, 0.67 mmol, 1.0 equiv), 4-aminophenylboronic acid pinacol ester (292 mg, 1.33 mmol, 2.0 equiv), Pd(dppf)Cl$_2$·DCM (54 mg, 0.067 mmol, 0.1 equiv), Na$_2$CO$_3$ (212 mg, 2.00 mmol, 3.0 equiv), dioxane (2.5 mL) and water (2.5 mL) and the reaction was heated for 3 h. The crude oil was purified using flash column chromatography (isocratic: 2% MeOH−DCM) and the resulting brown solid was further purified using RP ACC (gradient: 20−49% MeCN−H$_2$O in 0.1% formic acid). Appropriate fractions were combined and concentrated in vacuo to a volume of ~3 mL until a white precipitate had formed which was then filtered to give the titled compound (108 mg, 0.32 mmol, 49%) as an off-white powder. ^{1}H NMR (501 MHz, DMSO-d_6): 12.93 (br.s, 1H), 8.02 (d, J = 8.5 Hz, 1H), 7.68 (d, J = 8.5 Hz, 3H), 7.63 (dd, J = 12.9, 2.3 Hz, 1H), 7.54 (ddd, J = 8.6, 2.4, 1.1 Hz, 1H), 7.42 (dd, J = 8.5, 1.6 Hz, 1H), 7.27 (t, J = 8.8 Hz, 1H), 6.74−6.67 (m, 2H), 5.27 (br.s, 2H), 3.90 (s, 3H). ^{13}C NMR (126 MHz, DMSO-d_6): 151.8 (d, J = 243.5 Hz), 148.5, 146.6 (d, J = 10.5 Hz), 144.0, 142.2, 136.5, 133.5 (d, J = 6.5 Hz), 123.1 (d, J = 3.2 Hz), 121.4, 121.3, 119.7, 119.1,

114.5, 114.4, 114.3 (d, J = 2.2 Hz), 114.0, 107.4, 56.1. LC-MS (ESI+): RT = 0.6−0.6 min, m/z = 334.38 (M+H$^+$).

6-(2-Fluoro-4-methoxyphenyl)-3-[4-(piperazin-1-yl)phenyl]-1H-indazole (S21). Synthesized by method G using **S19** (106 mg, 0.34 mmol, 1.0 equiv), **36** (73 mg, 0.40 mmol, 1.2 equiv) and K$_2$CO$_3$ (112 mg, 0.81 mmol, 2.4 equiv) and ^{t}BuOH (5 mL) and the reaction was heated for 159 h. The reaction mixture was concentrated in vacuo and the resulting solid was purified by flash column chromatography (isocratic: 4% 7.0 M NH$_3$ in MeOH−DCM) to give the titled compound (16 mg, 0.04 mmol, 12%) as a brown solid. Due to time constraints, all available material was carried through immediately without full characterization. LC-MS (ES): RT = 1.4−1.5 min, m/z = 334.18 (M+H$^+$).

4-{4-[6-(3-Fluoro-4-methoxyphenyl)-1H-indazol-3-yl]phenyl}-piperazin-1-ium Formate (S22). Synthesized by method G using **S20** (98 mg, 0.29 mmol, 1.0 equiv), **36** (63 mg, 0.35 mmol, 1.2 equiv), K$_2$CO$_3$ (98 mg, 0.71 mmol, 2.4 equiv) and ^{t}BuOH (5 mL) and the reaction was heated for 152 h. The reaction mixture was concentrated in vacuo to reveal a yellow solid which was dissolved in DMSO, and the solution was decanted from the insoluble impurities. The crude product was purified by RP ACC (gradient: 5−50% MeCN−H$_2$O in 0.1% formic acid) and the resulting orange solid was triturated with MeOH to give the titled compound (17 mg, 0.042 mmol, 14%) as a pink solid. The filtrate from the trituration was reduced in vacuo to give an orange solid (59 mg) which was used without further purification. ^{1}H NMR (500 MHz, DMSO-d_6): 8.28 (br.s, 1H), 8.06 (d, J = 8.5 Hz, 1H), 7.87 (d, J = 8.4 Hz, 2H), 7.73 (br.s, 1H), 7.65 (dd, J = 12.9, 2.2 Hz, 1H), 7.56 (d, J = 8.5 Hz, 1H), 7.49−7.43 (m, 1H), 7.28 (t, J = 8.8 Hz, 1H), 7.09 (d, J = 8.4 Hz, 2H), 3.90 (s, 3H), 3.24 (br.s, 5H), 3.01 (br.s, 4H). ^{13}C NMR (101 MHz, DMSOd$_6$): 164.3, 151.8 (d, J = 243.5 Hz), 150.5, 146.8, 146.6, 143.2, 142.3, 136.7, 133.4, 124.4, 123.2 (d, J = 3.2 Hz), 121.2, 120.1, 119.2, 115.6, 114.5 (d, J = 18.8 Hz), 114.3, 107.6, 56.1, 47.7, 44.3. LC-MS (ESI+): RT = 0.5−0.6 min, m/z = 403.47 (M+H$^+$).

3-[4-(4-Ethylpiperazin-1-yl)phenyl]-6-(4-methoxyphenyl)-1H-indazole (S23). Synthesized using method D using **37** (100 mg, 0.26 mmol, 1.0 equiv), ethanol (18 μL, 0.31 mmol, 1.2 equiv), AcOH (1 drop), STAB (88 mg, 0.42 mmol, 1.6 equiv) and DCM (3 mL) and the reaction was stirred for 1 h. The reaction mixture was reduced in vacuo and the crude product was purified flash column chromatography (isocratic: 3% 7.0 M NH$_3$ in MeOH−DCM) to give the titled compound (90 mg, 0.22 mmol, 84%) as a colorless semisolid. ^{1}H NMR (501 MHz, CDCl$_3$): 11.88 (s, 1H), 8.01 (d, J = 8.9 Hz, 1H), 7.98−7.91 (m, 2H), 7.54−7.47 (m, 2H), 7.41−7.35 (m, 2H), 7.09−7.03 (m, 2H), 7.02−6.94 (m, 2H), 5.29 (s, 1H), 3.84 (s, 3H), 3.27 (t, J = 5.1 Hz, 4H), 2.63 (d, J = 5.1 Hz, 4H), 2.50 (q, J = 7.2 Hz, 2H), 1.15 (t, J = 7.2 Hz, 3H). ^{13}C NMR (101 MHz, CDCl$_3$): 159.4, 151.3, 145.6, 142.7, 139.7, 133.9, 128.7, 128.6, 124.8, 121.5, 121.1, 119.9, 116.1, 114.4, 107.8, 55.5, 52.9, 52.5, 48.8, 12.1. LC-MS (ESI+): RT = 0.6−0.7 min, m/z = 413.49 (M+H$^+$).

Biology. *FRET-Based Assay.* Biochemical data was obtained via the Z′-LYTE kinase screening service (ThermoFisher).[51] Additional details can be found in the Supporting Information.

Expression and Purification of FGFR2. A dual plasmid containing WT FGFR2 (residues 461−763) and protein tyrosine phosphatase-1B (PTP-1B) (Addgene #8602) was transformed into competent BL21 (DE3) cells and the cells used to inoculate kanamycin- (50 μg/mL) and ampicillin- (50 μg/mL) treated Lysogeny broth (LB) agar plates. Single colonies were used to inoculate 100 mL LB and the media grown overnight at 37 °C, 200 rpm. This culture was used to inoculate 1L of LB and the LB grown at 37 °C, 200 rpm until OD$_{600}$ ∼0.7 and the cultures were induced using isopropyl β-D-1-thiogalactopyranoside (IPTG, 0.1 mM) and incubated at 16 °C overnight. Cultures were harvested and cell pellets were suspended in 5 mL of lysis buffer (20 mM Tris, pH 8.0, 300 mM NaCl, 10 mM imidazole, 2 mM tris(2-carboxyethyl)phosphone (TCEP)) and one protease tablet (cOmplete, EDTA-free Protease Inhibitor Cocktail-Sigma) and 5 μL of benzonase (≥250 U/μL-Sigma) were added and the cell mixture was lysed via sonication. Lysates were centrifuged at 4 °C, 20,000 rpm for 1 h and the supernatant loaded onto 5 mL cobalt

TALON resin (Clontech). The resin was washed and step-eluted with lysis buffer containing 250 mM imidazole. Fractions were analyzed by SDS-PAGE and dialyzed into 20 mM 4-(2-hydroxyethyl)-1-piperazineethanesulfonic acid (HEPES), pH 8.0, 100 mM NaCl, 1 mM TCEP and the His$_6$-tag removed by incubation with thrombin (1 U/μL) overnight. The mixture was then added to cobalt/benzamidine resin and mixed for 15 min to remove the His tag. Supernatant was further purified in a Superdex 100 column using buffer containing 20 mM HEPES, pH 7.5, 100 mM NaCl, 1 mM TCEP. Purified FGFR2 protein was concentrated to ∼10 mg/mL for direct use in crystallographic trials.

Expression and Purification of FGFR1. BL21 star (DE3) cells containing the FGFR1 kinase construct (residues 458−765, C488A, C548S) was kindly provided by Professor Alexander Breeze and used to inoculate 1 L of tetracycline- (12.5 μg/mL) and ampicillin- (100 μg/mL) treated Terrific broth (TB). Protein expression followed the same protocol as outlined for FGFR2. Purification of FGFR1 was carried out using a His-Trap High Performance column (GE Healthcare) Ni-NTA column connected to an ÄKTA prime. Appropriate fractions were pooled and dialyzed into ion exchange (IEX) buffer (20 mM Tris, pH 8.0, 1 mM TCEP) containing tobacco etch virus (TEV) protease (≥3000 U/mg-Sigma) overnight to cleave the His tag. Protein was loaded onto a 5 mL Q Sepharose column (GE Healthcare), washed with IEX buffer, and the protein was eluted with IEX buffer containing 1 M NaCl. IEX-purified fractions were directly loaded onto a Superdex 75 column and protein was eluted in buffer containing 20 mM Tris, pH 7.8, 20 mM NaCl, 2 mM TCEP. Protein was concentrated to ∼10 mg/mL for direct use in crystallographic trials.

Cocrystallization and Data Collection. FGFR2, at a concentration of 0.29 mM (10 mg/mL) in 20 mM HEPES, pH 7.5, 100 mM NaCl, 1 mM TCEP, was mixed with **38** ([]$_f$ 0.29 mM, 5% DMSO). Protein/ligand solutions (0.2 μL) were then mixed with 0.2 μL of 25% PEG 3350, 100 mM (NH$_4$)$_2$SO$_4$, 100 mM HEPES, pH 7.6. Crystals were then grown at 20 °C using the vapor diffusion method and crystals appeared between 2−4 weeks. The crystals were flash-cooled in liquid nitrogen after soaking for 30 s in mother liquor solution containing 25% (v/v) ethylene glycol as a cryo-protectant. X-ray diffraction data was collected at the European Synchrotron Radiation Facility (ESRF) on beamline ID30A-1 at 100 K. The diffraction images were indexed and integrated using DIALS[68] before subsequent scaling in AIMLESS[69] and data processing in the CCP4i2 suite.[70] The unit cell parameters for the crystal are a = b = 113.8 Å, c = 117.4 Å, α = β = γ = 90.0° in space group $P4_12_12$ with two FGFR2 molecules in the asymmetric unit cell. The structure was determined by molecular replacement using the program Phaser[71] with the human FGFR2 structure (PDB 2PVF) as the search model.[72] Iterative cycles of manual model building using both $2F_o$-F_c and F_0-F_c maps and refinement were carried out using WinCoot[73] and Refmac5,[74] respectively. The coordinate and the restraint dictionary files for the compound were generated using JLigand.[75] Ligands, sulfates, chloride ions, ethylene glycols, and waters were manually added into the density using WinCoot. Structural validations were carried out using MolProbity.[76]

FGFR1, at a concentration of 0.28 mM (10 mg/mL) in 20 mM Tris, pH 7.8, 20 mM NaCl, 2 mM TCEP, was mixed with **19**, **34**, and **38** ([]$_f$ 0.28 mM, 0.5% DMSO) and then crystals grown as outlined for FGFR2 using 0.185 M ammonium sulfate, 20% ethylene glycol, 16−22% PEG 8000, pH (6.2−6.8) as the crystallization conditions. Crystals were grown at 4 °C using the vapor diffusion method and crystals appeared between 1−2 weeks. Crystals were flash-cooled in liquid nitrogen and the data was collected at the Diamond Light Source (DLS) on beamline I04−1 at 100 K. Data reduction, structure determination, model building, and refinement were conducted in the same manner as FGFR2. The unit cell parameters for the FGFR1 crystals are a = 207.8 Å, b = 57.5 Å, c = 66.0 Å, β = 107.4° in space group $C2$ with two FGFR1 molecules in the asymmetric unit cell. The structures were determined by molecular replacement with the human FGFR1 structure (PDB 5A46) as the search model.[77]

CellTiter Blue Viability Assay. Human cell lines used in this work were: JMSU1, SUM52, VMCUB3. JMSU1 was obtained in 2003 from German Collection of Microorganisms and Cell Cultures (DSMZ) and authenticated in 2012 by short tandem repeats (STR) profiling. SUM52 was obtained from Professor Nick Turner, Institute for Cancer Research, London, in 2017. VMCUB3 was obtained in 2001 from the Institute of Cancer Studies (Leeds, UK) and was authenticated in 2012 by STR profiling. Cells were regularly tested for mycoplasma by PCR and cultured for a maximum of 10 passages from the authenticated stock.

JMSU1 and SUM52 cells were routinely cultured in Roswell Park Memorial Institute (RPMI)-1640 growth medium (Sigma) and VMCUB3 cells were cultured in Dulbecco's modified Eagle medium (DMEM) (Sigma), all containing 10% fetal calf serum (FCS, Biosera) and 2 mM GlutaMAX (Life Technologies), in a humidified incubator at 37 °C in an atmosphere of 5% CO_2. Cells were seeded at a density of 5×10^3 cells/well into a flat bottom 96-well plate (Corning) and incubated at 37 °C for 24 h. Medium was replaced with solutions of **38**, **41**, **42**, and PD173074 in medium (Sigma) at varying concentrations (0.1% $[]_f$ DMSO) and plates were incubated at 37 °C, 5% CO_2 for 72 h. Five wells were assayed per condition. Prewarmed CellTiter Blue reagent (Promega, 20 μL per well) was added, and plates were incubated at 37 °C, 5% CO_2 for 2 h in the dark. After incubation, 50 μL of 3% SDS was added to each well and the fluorescence immediately read (ex/em 540/590 nm) on a Berthold Mithras LB 940 Multimode plate reader. Wells were blanked with a medium-only control and then normalized to the DMSO vehicle control. Assays were repeated at least once using independent drug dilution series. Data were plotted using Origin 2016 and IC_{50} values calculated using a dose−response nonlinear curve fit.

Computational Modeling. Molecular modeling was performed with modules from the Schrödinger Small Molecular Drug Discovery Suite (Maestro), release 2021-2, using the OPLS4 force field for parametrization.[78] The X-ray crystal structure of FGFR1 (PDB 5B7V)[49] was imported from the PDB and prepared using the Protein Preparation Wizard using default settings. Ligands were drawn in Maestro and prepared using the LigPrep function. Docking was performed in a confined grid built 10 Å around the bound ligand CH5183284 and simulated using the extra precision setting in Glide.[79] Calculation of clogP and cell permeability potential was performed using QikProp and PerMM, respectively.[67] Output files were visualized in PyMol (version 2.0, Schrödinger, LLC) and used for figures throughout this manuscript.

Interference Compound Filter. All final compounds were examined for pan-assay interference potential using the ZINC patterns search (http://zinc15.docking.org/patterns/home) and no compounds were flagged.

■ ASSOCIATED CONTENT

Ⓢ Supporting Information

The Supporting Information is available free of charge at https://pubs.acs.org/doi/10.1021/acs.jmedchem.1c01163.

> Supporting schemes, figures, and tables; additional information: SPROUT modules, Z′-LYTE assay, and CellTiter Blue viability assay; Appendix One: FGFR1 analysis, FGFR2 analysis, and FGFR1 crystal; Appendix Two: Z′-LYTE IC_{50} curves, CellTiter Blue IC_{50} curves, HPLC chromatograms, and NMR spectra (PDF)

> Molecular formula strings (CSV)

Accession Codes

X-ray diffraction data, coordinates, and structure factors for the X-ray crystal structures were deposited with the PDB under accession codes 7OZF (FGFR1/**19**), 7OZD (FGFR1/**34**), 7OZB (FGFR1/**38**), and 7OZY (FGFR2/**38**). Authors will release the atomic coordinates and experimental data upon article publication.

■ AUTHOR INFORMATION

Corresponding Author

Colin W. G. Fishwick − *School of Chemistry, University of Leeds, Leeds LS2 9JT, U.K.;* ⓞ orcid.org/0000-0003-1283-2181; Email: c.w.g.fishwick@leeds.ac.uk

Authors

Lewis D. Turner − *School of Chemistry, University of Leeds, Leeds LS2 9JT, U.K.;* Present Address: Biosplice Therapeutics, Inc., 9360 Towne Centre Drive, San Diego, California 92121, United States; ⓞ orcid.org/0000-0003-0660-8247

Chi H. Trinh − *Astbury Centre for Structural Molecular Biology, Institute of Molecular and Cellular Biology, University of Leeds, Leeds LS2 9JT, U.K.*

Ryan A. Hubball − *School of Chemistry, University of Leeds, Leeds LS2 9JT, U.K.;* ⓞ orcid.org/0000-0001-6006-6114

Kyle M. Orritt − *School of Chemistry, University of Leeds, Leeds LS2 9JT, U.K.*

Chi-Chuan Lin − *Astbury Centre for Structural Molecular Biology, Institute of Molecular and Cellular Biology, University of Leeds, Leeds LS2 9JT, U.K.*

Julie E. Burns − *Leeds Institute of Medical Research at St James's, University of Leeds, Leeds LS9 7TF, U.K.*

Margaret A. Knowles − *Leeds Institute of Medical Research at St James's, University of Leeds, Leeds LS9 7TF, U.K.*

Complete contact information is available at:
https://pubs.acs.org/10.1021/acs.jmedchem.1c01163

Author Contributions

L.D.T conceptualized the study and performed chemical synthesis, protein expression, purification, crystallography, and cell viability assays. L.D.T and R.A.H carried out computational methods. C.H.T supervised FGFR1 expression and crystallography and performed data refinement. C.L supervised FGFR2 expression. J.E.B supervised cell viability assays. L.D.T wrote the original draft of the manuscript with input from C.H.T, R.A.H, and K.M.O, and all authors revised the final version. M.A.K and C.W.G.F acquired funding and supervised the study.

Notes

The authors declare no competing financial interest.

■ ACKNOWLEDGMENTS

■ ABBREVIATIONS

ACC, automated column chromatography; DFG, Asp-Phe-Gly; DLSF, Diamond Light Source Facility; DMEM, Dulbecco's modified Eagle's medium; DSMZ, Germain Collection of Microorganisms and Cell Cultures; ESRF, European Synchrotron Radiation Facility; FCS, fetal calf serum; FGFR, fibroblast growth factor receptor; HEPES, 4-(2-hydroxyethyl)-1-piperazineethanesulfonic acid; HER2,

human epidermal growth factor 2; IEX, ion exchange; IPTG, isopropyl ß-d-1-thiogalactopyranoside; LB, Lysogeny broth; ND, not determined; NP, normal phase; PLCγ, phospholipase C gamma; RP, reverse phase; RPMI, Roswell Park Memorial Institute; SD, standard deviation; STAB, sodium triacetoxyborohydride; STAT, signal transducer and activator of transcription proteins; STR, short tandem repeats; TCEP, tris(2-carboxyethyl)phosphone; TEV, tobacco etch virus

■ REFERENCES

(1) Groth, C.; Lardelli, M. The structure and function of vertebrate fibroblast growth factor receptor 1. *Int. J. Dev. Biol.* **2002**, *46*, 393−400.

(2) Eswarakumar, V. P.; Lax, I.; Schlessinger, J. Cellular signaling by fibroblast growth factor receptors. *Cytokine Growth Factor Rev.* **2005**, *16*, 139−149.

(3) Presta, M.; Dell'Era, P.; Mitola, S.; Moroni, E.; Ronca, R.; Rusnati, M. Fibroblast growth factor/fibroblast growth factor receptor system in angiogenesis. *Cytokine Growth Factor Rev.* **2005**, *16*, 159−178.

(4) Cross, M. J.; Claesson-Welsh, L. FGF and VEGF function in angiogenesis: signalling pathways, biological responses and therapeutic inhibition. *Trends Pharmacol. Sci.* **2001**, *22*, 201−207.

(5) Furdui, C. M.; Lew, E. D.; Schlessinger, J.; Anderson, K. S. Autophosphorylation of FGFR1 kinase is mediated by a sequential and precisely ordered reaction. *Mol. Cell* **2006**, *21*, 711−717.

(6) Lew, E. D.; Furdui, C. M.; Anderson, K. S.; Schlessinger, J. The precise sequence of FGF receptor autophosphorylation is kinetically driven and is disrupted by oncogenic mutations. *Sci. Signaling* **2009**, *2*, No. ra6.

(7) Ornitz, D. M.; Itoh, N. The fibroblast growth factor signaling pathway. *Wires. Dev Biol.* **2015**, *4*, 215−266.

(8) Di Martino, E.; Tomlinson, D. C.; Knowles, M. A. A decade of FGF receptor research in bladder cancer: Past, present, and future challenges. *Adv. Urol.* **2012**, *2012*, 429214.

(9) Byron, S. A.; Chen, H.; Wortmann, A.; Loch, D.; Gartside, M. G.; Dehkhoda, F.; Blais, S. P.; Neubert, T. A.; Mohammadi, M.; Pollock, P. M. The N550K/H mutations in FGFR2 confer differential resistance to PD173074, dovitinib, and ponatinib ATP-competitive inhibitors. *Neoplasia* **2013**, *15*, 975−988.

(10) Kim, S.; Dubrovska, A.; Salamone, R. J.; Walker, J. R.; Grandinetti, K. B.; Bonamy, G. M. C.; Orth, A. P.; Elliott, J.; Porta, D. G.; Garcia-Echeverria, C.; Reddy, V. A. FGFR2 promotes breast tumorigenicity through maintenance of breast tumor-initiating cells. *PLoS One* **2013**, *8*, No. e51671-e51671.

(11) Weiss, J.; Sos, M. L.; Seidel, D.; Peifer, M.; Zander, T.; Heuckmann, J. M.; Ullrich, R. T.; Menon, R.; Maier, S.; Soltermann, A.; Moch, H.; Wagener, P.; Fischer, F.; Heynck, S.; Koker, M.; Schöttle, J.; Leenders, F.; Gabler, F.; Dabow, I.; Querings, S.; Heukamp, L. C.; Balke-Want, H.; Ansén, S.; Rauh, D.; Baessmann, I.; Altmüller, J.; Wainer, Z.; Conron, M.; Wright, G.; Russell, P.; Solomon, B.; Brambilla, E.; Brambilla, C.; Lorimier, P.; Sollberg, S.; Brustugun, O. T.; Engel-Riedel, W.; Ludwig, C.; Petersen, I.; Sänger, J.; Clement, J.; Groen, H.; Timens, W.; Sietsma, H.; Thunnissen, E.; Smit, E.; Heideman, D.; Cappuzzo, F.; Ligorio, C.; Damiani, S.; Hallek, M.; Beroukhim, R.; Pao, W.; Klebl, B.; Baumann, M.; Buettner, R.; Ernestus, K.; Stoelben, E.; Wolf, J.; Nürnberg, P.; Perner, S.; Thomas, R. K. Frequent and focal FGFR1 amplification associates with therapeutically tractable FGFR1 dependency in squamous cell lung cancer. *Sci. Transl. Med.* **2010**, *2*, 62ra93.

(12) Babina, I. S.; Turner, N. C. Advances and challenges in targeting FGFR signalling in cancer. *Nat. Rev. Cancer* **2017**, *17*, 318−332.

(13) Liu, F.-T.; Li, N.-G.; Zhang, Y.-M.; Xie, W.-C.; Yang, S.-P.; Lu, T.; Shi, Z.-H. Recent advance in the development of novel, selective and potent FGFR inhibitors. *Eur. J. Med. Chem.* **2020**, *186*, 111884.

(14) Facchinetti, F.; Hollebecque, A.; Bahleda, R.; Loriot, Y.; Olaussen, K. A.; Massard, C.; Friboulet, L. Facts and new hopes on

(15) Luo, H.; Zhang, T.; Cheng, P.; Li, D.; Ogorodniitchouk, O.; Lahmamssi, C.; Wang, G.; Lan, M. Therapeutic implications of fibroblast growth factor receptor inhibitors in a combination regimen for solid tumors. *Oncol. Lett.* **2020**, *20*, 2525−2536.

(16) Weaver, A.; Bossaer, J. B. Fibroblast growth factor receptor (FGFR) inhibitors: A review of a novel therapeutic class. *J. Oncol. Pharm. Pract.* **2021**, *27*, 702−710.

(17) Yue, S.; Li, Y.; Chen, X.; Wang, J.; Li, M.; Chen, Y.; Wu, D. FGFR-TKI resistance in cancer: current status and perspectives. *J. Hematol. Oncol.* **2021**, *14*, 23.

(18) Roskoski, R. Classification of small molecule protein kinase inhibitors based upon the structures of their drug-enzyme complexes. *Pharmacol. Res.* **2016**, *103*, 26−48.

(19) Markham, A. Erdafitinib: First global approval. *Drugs* **2019**, *79*, 1017−1021.

(20) Kufareva, I.; Abagyan, R. Type-II kinase inhibitor docking, screening, and profiling using modified structures of active kinase states. *J. Med. Chem.* **2008**, *51*, 7921−7932.

(21) U.S. Food and Drug Administration. 2021 Notifications https://www.fda.gov/drugs/resources-information-approved-drugs/2012-notifications (accessed 13/06/2021).

(22) Tsimafeyeu, I.; Daeyaert, F.; Yin, W.; Ludes-Meyers, J.; Byakhov, M.; Tjulandin, S. 476 FGFR2 targeting with allosteric inhibitor RPT835. *Eur. J. Cancer* **2014**, *50* (6), 155.

(23) Tyulyandina, A.; Harrison, D.; Yin, W.; Stepanova, E.; Kochenkov, D.; Solomko, E.; Peretolchina, N.; Daeyaert, F.; Joos, J.-B.; Van Aken, K.; Byakhov, M.; Gavrilova, E.; Tjulandin, S.; Tsimafeyeu, I. Alofanib, an allosteric FGFR2 inhibitor, has potent effects on ovarian cancer growth in preclinical studies. *Invest. New Drugs* **2017**, *35*, 127−133.

(24) U.S. National Library of Medicine. Study of Alofanib in Patients With Metastatic Gastric cancer. https://clinicaltrials.gov/ct2/show/NCT04071184 (accessed 12/06/2021).

(25) Hah, J. M.; Sharma, V.; Li, H.; Lawrence, D. S. Acquisition of a "Group A"-selective Src kinase inhibitor via a global targeting strategy. *J. Am. Chem. Soc.* **2006**, *128*, 5996−5997.

(26) Hill, Z. B.; Perera, B. G.; Maly, D. J. A chemical genetic method for generating bivalent inhibitors of protein kinases. *J. Am. Chem. Soc.* **2009**, *131*, 6686−6688.

(27) Lamba, V.; Ghosh, I. New directions in targeting protein kinases: Focusing upon true allosteric and bivalent inhibitors. *Curr. Pharm. Des.* **2012**, *18*, 2936−2945.

(28) Zhou, W.; Hur, W.; McDermott, U.; Dutt, A.; Xian, W.; Ficarro, S. B.; Zhang, J.; Sharma, S. V.; Brugge, J.; Meyerson, M.; Settleman, J.; Gray, N. S. A structure-guided approach to creating covalent FGFR inhibitors. *Chem. Biol.* **2010**, *17*, 285−295.

(29) Brameld, K. A.; Owens, T. D.; Verner, E.; Venetsanakos, E.; Bradshaw, J. M.; Phan, V. T.; Tam, D.; Leung, K.; Shu, J.; LaStant, J.; Loughhead, D. G.; Ton, T.; Karr, D. E.; Gerritsen, M. E.; Goldstein, D. M.; Funk, J. O. Discovery of the irreversible covalent FGFR inhibitor 8-(3-(4-acryloylpiperazin-1-yl)propyl)-6-(2,6-dichloro-3,5-dimethoxyphenyl)-2-(methylamino)pyrido[2,3-*d*]pyrimidin-7(8*H*)-one (PRN1371) for the treatment of solid tumors. *J. Med. Chem.* **2017**, *60*, 6516−6527.

(30) Fumarola, C.; Bozza, N.; Castelli, R.; Ferlenghi, F.; Marseglia, G.; Lodola, A.; Bonelli, M.; La Monica, S.; Cretella, D.; Alfieri, R.; Minari, R.; Galetti, M.; Tiseo, M.; Ardizzoni, A.; Mor, M.; Petronini, P. G. Expanding the arsenal of FGFR inhibitors: A novel chloroacetamide derivative as a new irreversible agent with anti-proliferative activity against FGFR1-amplified lung cancer cell lines. *Front. Oncol.* **2019**, *9*, 179.

(31) Fairhurst, R. A.; Knoepfel, T.; Buschmann, N.; Leblanc, C.; Mah, R.; Todorov, M.; Nimsgern, P.; Ripoche, S.; Niklaus, M.; Warin, N.; Luu, V. H.; Madoerin, M.; Wirth, J.; Graus-Porta, D.; Weiss, A.; Kiffe, M.; Wartmann, M.; Kinyamu-Akunda, J.; Sterker, D.; Stamm, C.; Adler, F.; Buhles, A.; Schadt, H.; Couttet, P.; Blank, J.; Galuba, I.; Trappe, J.; Voshol, J.; Ostermann, N.; Zou, C.; Berghausen, J.; Del

Rio Espinola, A.; Jahnke, W.; Furet, P. Discovery of Roblitinib (FGF401) as a reversible-covalent inhibitor of the kinase activity of fibroblast growth factor receptor 4. *J. Med. Chem.* **2020**, *63*, 12542−12573.

(32) Liu, H.; Niu, D.; Tham Sjin, R. T.; Dubrovskiy, A.; Zhu, Z.; McDonald, J. J.; Fahnoe, K.; Wang, Z.; Munson, M.; Scholte, A.; Barrague, M.; Fitzgerald, M.; Liu, J.; Kothe, M.; Sun, F.; Murtie, J.; Ge, J.; Rocnik, J.; Harvey, D.; Ospina, B.; Perron, K.; Zheng, G.; Shehu, E.; D'Agostino, L. A. Discovery of selective, covalent FGFR4 inhibitors with antitumor activity in models of hepatocellular carcinoma. *ACS Med. Chem. Lett.* **2020**, *11*, 1899−1904.

(33) Hagel, M.; Miduturu, C.; Sheets, M.; Rubin, N.; Weng, W. F.; Stransky, N.; Bifulco, N.; Kim, J. L.; Hodous, B.; Brooijmans, N.; Shutes, A.; Winter, C.; Lengauer, C.; Kohl, N. E.; Guzi, T. First selective small molecule inhibitor of FGFR4 for the treatment of hepatocellular carcinomas with an activated FGFR4 signaling pathway. *Cancer Discovery* **2015**, *5*, 424−437.

(34) Chae, Y. K.; Ranganath, K.; Hammerman, P. S.; Vaklavas, C.; Mohindra, N.; Kalyan, A.; Matsangou, M.; Costa, R.; Carneiro, B.; Villaflor, V. M.; Cristofanilli, M.; Giles, F. J. Inhibition of the fibroblast growth factor receptor (FGFR) pathway: the current landscape and barriers to clinical application. *Oncotarget.* **2017**, *8*, 16052−16074.

(35) Krook, M. A.; Lenyo, A.; Wilberding, M.; Barker, H.; Dantuono, M.; Bailey, K. M.; Chen, H.-Z.; Reeser, J. W.; Wing, M. R.; Miya, J.; Samorodnitsky, E.; Smith, A. M.; Dao, T.; Martin, D. M.; Ciombor, K. K.; Hays, J.; Freud, A. G.; Roychowdhury, S. Efficacy of FGFR inhibitors and combination therapies for acquired resistance in FGFR2-fusion cholangiocarcinoma. *Mol. Cancer Ther.* **2020**, *19*, 847−857.

(36) Cleary, J. M.; Raghavan, S.; Wu, Q.; Li, Y. Y.; Spurr, L. F.; Gupta, H. V.; Rubinson, D. A.; Fetter, I. J.; Hornick, J. L.; Nowak, J. A.; Siravegna, G.; Goyal, L.; Shi, L.; Brais, L. K.; Loftus, M.; Shinagare, A. B.; Abrams, T. A.; Clancy, T. E.; Wang, J.; Patel, A. K.; Brichory, F.; Vaslin Chessex, A.; Sullivan, R. J.; Keller, R. B.; Denning, S.; Hill, E. R.; Shapiro, G. I.; Pokorska-Bocci, A.; Zanna, C.; Ng, K.; Schrag, D.; Janne, P. A.; Hahn, W. C.; Cherniack, A. D.; Corcoran, R. B.; Meyerson, M.; Daina, A.; Zoete, V.; Bardeesy, N.; Wolpin, B. M. FGFR2 extracellular domain in-frame deletions are therapeutically targetable genomic alterations that function as oncogenic drivers in cholangiocarcinoma. *Cancer Discov.* **2021**, *11*, 2488−2505.

(37) American Cancer Society. Key Statistics for Bile Duct Cancer. https://www.cancer.org/cancer/bile-duct-cancer/about/key-statistics.html (accessed 14/06/2021).

(38) Fernández-Nogueira, P.; Mancino, M.; Fuster, G.; López-Plana, A.; Jauregui, P.; Almendro, V.; Enreig, E.; Menéndez, S.; Rojo, F.; Noguera-Castells, A.; Bill, A.; Gaither, L. A.; Serrano, L.; Recalde-Percaz, L.; Moragas, N.; Alonso, R.; Ametller, E.; Rovira, A.; Lluch, A.; Albanell, J.; Gascon, P.; Bragado, P. Tumor-associated fibroblasts promote HER2-targeted therapy resistance through FGFR2 activation. *Clin. Cancer Res.* **2020**, *26*, 1432−1448.

(39) Casaletto, J.; Maglic, D.; Touré, B. B.; Taylor, A.; Schoenherr, H.; Hudson, B.; Bruderek, K.; Zhao, S.; O'Hearn, P.; Gerami-Moayed, N.; Moustakas, D.; Valverde, R.; Foster, L.; Gunaydin, H.; Ayaz, P.; Sharon, D.; Berstrom, D.; Watters, J. RLY-4008, a novel precision therapy for FGFR2-driven cancers desgined to potently and selectively inhibit FGFR2 and FGFR2 resistance mutations. In *American Association of Cancer Research Annual Virtual Meeting*, 2021.

(40) United States Securities and Exchange Commission. Form S-1 Registration Statement Relay Therapeutics, Inc (Pg 116). https://www.sec.gov/Archives/edgar/data/1812364/000119312520177746/d924757ds1.htm (accessed 12/06/2021).

(41) U.S National Library of Medicine. First-in-Human Study of Highly Selective FGFR2 Inhibitor, RLY-4008, in Patients with ICC and Other Advanced Solid Tumors. https://www.clinicaltrials.gov/ct2/show/NCT04526106?term=RLY-4008&draw=2&rank=1 (accessed 14/06/2021).

(42) Turner, L. D.; Summers, A. J.; Johnson, L. O.; Knowles, M. A.; Fishwick, C. W. G. Identification of an indazole-based pharmacophore

for the inhibition of FGFR kinases using fragment-led de novo design. *ACS Med. Chem. Lett.* **2017**, *8*, 1264−1268.

(43) Gillet, V.; Johnson, A. P.; Mata, P.; Sike, S.; Williams, P. SPROUT - A program for structure generation. *J. Comput.-Aided Mol. Des.* **1993**, *7*, 127−153.

(44) Gillet, V. J.; Newell, W.; Mata, P.; Myatt, G.; Sike, S.; Zsoldos, Z.; Johnson, A. P. SPROUT - Recent developments in the de-novo design of molecules. *J. Chem. Inf. Model.* **1994**, *34*, 207−217.

(45) Friesner, R. A.; Banks, J. L.; Murphy, R. B.; Halgren, T. A.; Klicic, J. J.; Mainz, D. T.; Repasky, M. P.; Knoll, E. H.; Shelley, M.; Perry, J. K.; Shaw, D. E.; Francis, P.; Shenkin, P. S. Glide: A new approach for rapid, accurate docking and scoring. 1. Method and assessment of docking accuracy. *J. Med. Chem.* **2004**, *47*, 1739−1749.

(46) Roth, G. J.; Binder, R.; Colbatzky, F.; Dallinger, C.; Schlenker-Herceg, R.; Hilberg, F.; Wollin, S. L.; Kaiser, R. Nintedanib: From discovery to the clinic. *J. Med. Chem.* **2015**, *58*, 1053−1063.

(47) Liu, J.; Peng, X.; Dai, Y.; Zhang, W.; Ren, S. M.; Ai, J.; Geng, M. Y.; Li, Y. X. Design, synthesis and biological evaluation of novel FGFR inhibitors bearing an indazole scaffold. *Org. Biomol. Chem.* **2015**, *13*, 7643−7654.

(48) Zhao, B.; Li, Y.; Xu, P.; Dai, Y.; Luo, C.; Sun, Y.; Ai, J.; Geng, M.; Duan, W. Discovery of substituted 1*H*-pyrazolo[3,4-*b*]pyridine derivatives as potent and selective FGFR kinase inhibitors. *ACS Med. Chem. Lett.* **2016**, *7*, 629−634.

(49) Nakanishi, Y.; Akiyama, N.; Tsukaguchi, T.; Fujii, T.; Sakata, K.; Sase, H.; Isobe, T.; Morikami, K.; Shindoh, H.; Mio, T.; Ebiike, H.; Taka, N.; Aoki, Y.; Ishii, N. The fibroblast growth factor receptor genetic status as a potential predictor of the sensitivity to CH5183284/Debio 1347, a novel selective FGFR inhibitor. *Mol. Cancer Ther.* **2014**, *13*, 2547−2558.

(50) Lee, C. Y.; Ahn, S. J.; Cheon, C. H. Protodeboronation of ortho- and para-Phenol Boronic Acids and Application to ortho and meta Functionalization of Phenols Using Boronic Acids as Blocking and Directing Groups. *J. Org. Chem.* **2013**, *78*, 12154−12160.

(51) ThermoFisher Scientific. Z′-LYTE Kinase Assay. https://www.thermofisher.com/us/en/home/industrial/pharma-biopharma/drug-discovery-development/target-and-lead-identification-and-validation/kinasebiology/kinase-activity-assays/z-lyte.html (accessed 15/06/2021).

(52) McBride, C. M.; Renhowe, P. A.; Heise, C.; Jansen, J. M.; Lapointe, G.; Ma, S.; Piñeda, R.; Vora, J.; Wiesmann, M.; Shafer, C. M. Design and structure−activity relationship of 3-benzimidazol-2-yl-1*H*-indazoles as inhibitors of receptor tyrosine kinases. *Bioorg. Med. Chem. Lett.* **2006**, *16*, 3595−3599.

(53) Yan, W.; Wang, X.; Dai, Y.; Zhao, B.; Yang, X.; Fan, J.; Gao, Y.; Meng, F.; Wang, Y.; Luo, C.; Ai, J.; Geng, M.; Duan, W. Discovery of 3-(5·-substituted)-benzimidazole-5-(1-(3,5-dichloropyridin-4-yl)-ethoxy)-1*H*-indazoles as potent fibroblast growth factor receptor inhibitors: Design, synthesis, and biological evaluation. *J. Med. Chem.* **2016**, *59*, 6690−6708.

(54) Liu, J.; Peng, X.; Dai, Y.; Zhang, W.; Ren, S.; Ai, J.; Geng, M.; Li, Y. Design, synthesis and biological evaluation of novel FGFR inhibitors bearing an indazole scaffold. *Org. Biomol. Chem.* **2015**, *13*, 7643−7654.

(55) Norman, R. A.; Schott, A. K.; Andrews, D. M.; Breed, J.; Foote, K. M.; Garner, A. P.; Ogg, D.; Orme, J. P.; Pink, J. H.; Roberts, K.; Rudge, D. A.; Thomas, A. P.; Leach, A. G. Protein-ligand crystal structures can guide the design of selective inhibitors of the FGFR tyrosine kinase. *J. Med. Chem.* **2012**, *55*, 5003−5012.

(56) Klein, T.; Tucker, J.; Holdgate, G. A.; Norman, R. A.; Breeze, A. L. FGFR1 kinase inhibitors: Close regioisomers adopt divergent binding modes and display distinct biophysical signatures. *ACS Med. Chem. Lett.* **2014**, *5*, 166−171.

(57) Tucker, J. A.; Klein, T.; Breed, J.; Breeze, A. L.; Overman, R.; Phillips, C.; Norman, R. A. Structural insights into FGFR kinase isoform selectivity: Diverse binding modes of AZD4547 and Ponatinib in complex with FGFR1 and FGFR4. *Structure* **2014**, *22*, 1764−1774.

(58) Chae, Y. K.; Hong, F.; Vaklavas, C.; Cheng, H. H.; Hammerman, P.; Mitchell, E. P.; Zwiebel, J. A.; Ivy, S. P.; Gray, R. J.; Li, S.; McShane, L. M.; Rubinstein, L. V.; Patton, D.; Williams, P. M.; Hamilton, S. R.; Mansfield, A.; Conley, B. A.; Arteaga, C. L.; Harris, L. N.; O'Dwyer, P. J.; Chen, A. P.; Flaherty, K. T. Phase II study of AZD4547 in patients with tumors harboring aberrations in the FGFR pathway: Results from the NCI-MATCH trial (EAY131) subprotocol W. *J. Clin. Oncol.* **2020**, *38*, 2407−2417.

(59) Guimarães, C. R. W.; Rai, B. K.; Munchhof, M. J.; Liu, S.; Wang, J.; Bhattacharya, S. K.; Buckbinder, L. Understanding the impact of the P-loop conformation on kinase selectivity. *J. Chem. Inf. Model.* **2011**, *51*, 1199−1204.

(60) Hari, S. B.; Perera, B. G. K.; Ranjitkar, P.; Seeliger, M. A.; Maly, D. J. Conformation-selective inhibitors reveal differences in the activation and phosphate-binding loops of the tyrosine kinases Abl and Src. *ACS Chem. Biol.* **2013**, *8*, 2734−2743.

(61) Miyake, M.; Ishii, M.; Koyama, N.; Kawashima, K.; Kodama, T.; Anai, S.; Fujimoto, K.; Hirao, Y.; Sugano, K. 1-tert-Butyl-3-[6-(3,5-dimethoxy-phenyl)-2-(4-diethylamino-butylamino)-pyrido[2,3-*d*] pyrimidin-7-yl]-urea (PD173074), a selective tyrosine kinase inhibitor of fibroblast growth factor receptor-3 (FGFR3), inhibits cell proliferation of bladder cancer carrying the FGFR3 gene mutation along with up-regulation of p27/Kip1 and G_1/G_0 arrest. *J. Pharmacol. Exp. Ther.* **2010**, *332*, 795−802.

(62) Morita, T.; Shimohara, N.; Honma, M.; Tokue, A. Establishment and characterization of a new cell-line from human bladder-cancer (JMSU1). *Urol. Res.* **1995**, *23*, 143−149.

(63) Tomlinson, D. C.; Lamont, F. R.; Shnyder, S. D.; Knowles, M. A. Fibroblast growth factor receptor 1 promotes proliferation and survival via activation of the mitogen-activated protein kinase pathway in bladder cancer. *Cancer Res.* **2009**, *69*, 4613−4620.

(64) Ethier, S. P.; Kokeny, K. E.; Ridings, J. W.; Dilts, C. A. erbB family receptor expression and growth regulation in a newly isolated human breast cancer cell line. *Cancer Res.* **1996**, *56*, 899−907.

(65) Tannheimer, S. L.; Rehemtulla, A.; Ethier, S. P. Characterization of fibroblast growth factor receptor 2 overexpression in the human breast cancer cell line SUM-52PE. *Breast Cancer Res.* **2000**, *2*, 311−320.

(66) Williams, R. D. Human urologic cancer cell-lines. *Invest. Urol.* **1980**, *17*, 359−363.

(67) Lomize, A. L.; Pogozheva, I. D. Physics-Based Method for Modeling Passive Membrane Permeability and Translocation Pathways of Bioactive Molecules. *J. Chem. Inf. Model.* **2019**, *59*, 3198−3213.

(68) Winter, G.; Waterman, D. G.; Parkhurst, J. M.; Brewster, A. S.; Gildea, R. J.; Gerstel, M.; Fuentes-Montero, L.; Vollmar, M.; Michels-Clark, T.; Young, I. D.; Sauter, N. K.; Evans, G. DIALS: implementation and evaluation of a new integration package. *Acta. Crystallogr. D. Struct. Biol.* **2018**, *74*, 85−97.

(69) Murshudov, G. N.; Skubák, P.; Lebedev, A. A.; Pannu, N. S.; Steiner, R. A.; Nicholls, R. A.; Winn, M. D.; Long, F.; Vagin, A. A. REFMAC5 for the refinement of macromolecular crystal structures. *Acta Crystallogr., Sect. D: Biol. Crystallogr.* **2011**, *67*, 355−367.

(70) Potterton, L.; Agirre, J.; Ballard, C.; Cowtan, K.; Dodson, E.; Evans, P. R.; Jenkins, H. T.; Keegan, R.; Krissinel, E.; Stevenson, K.; Lebedev, A.; McNicholas, S. J.; Nicholls, R. A.; Noble, M.; Pannu, N. S.; Roth, C.; Sheldrick, G.; Skubak, P.; Turkenburg, J.; Uski, V.; von Delft, F.; Waterman, D.; Wilson, K.; Winn, M.; Wojdyr, M. CCP4i2: the new graphical user interface to the CCP4 program suite. *Acta. Crystallogr. D. Struct. Biol.* **2018**, *74*, 68−84.

(71) McCoy, A. J.; Grosse-Kunstleve, R. W.; Adams, P. D.; Winn, M. D.; Storoni, L. C.; Read, R. J. Phaser crystallographic software. *J. Appl. Crystallogr.* **2007**, *40*, 658−674.

(72) Chen, H.; Ma, J.; Li, W.; Eliseenkova, A. V.; Xu, C.; Neubert, T. A.; Miller, W. T.; Mohammadi, M. A molecular brake in the kinase hinge region regulates the activity of receptor tyrosine kinases. *Mol. Cell* **2007**, *27*, 717−730.

(73) Emsley, P.; Lohkamp, B.; Scott, W. G.; Cowtan, K. Features and development of Coot. *Acta Crystallogr., Sect. D: Biol. Crystallogr.* **2010**, *66*, 486−501.

(74) Kovalevskiy, O.; Nicholls, R. A.; Long, F.; Carlon, A.; Murshudov, G. N. Overview of refinement procedures within REFMAC5: utilizing data from different sources. *Acta. Crystallog. D. Struct. Biol.* **2018**, *74*, 215−227.

(75) Lebedev, A. A.; Young, P.; Isupov, M. N.; Moroz, O. V.; Vagin, A. A.; Murshudov, G. N. JLigand: a graphical tool for the CCP4 template-restraint library. *Acta Crystallogr., Sect. D: Biol. Crystallogr.* **2012**, *68*, 431−440.

(76) Chen, V. B.; Arendall, W. B., 3rd; Headd, J. J.; Keedy, D. A.; Immormino, R. M.; Kapral, G. J.; Murray, L. W.; Richardson, J. S.; Richardson, D. C. MolProbity: all-atom structure validation for macromolecular crystallography. *Acta Crystallogr., Sect. D: Biol. Crystallogr.* **2010**, *66*, 12−21.

(77) Klein, T.; Vajpai, N.; Phillips, J. J.; Davies, G.; Holdgate, G. A.; Phillips, C.; Tucker, J. A.; Norman, R. A.; Scott, A. D.; Higazi, D. R.; Lowe, D.; Thompson, G. S.; Breeze, A. L. Structural and dynamic insights into the energetics of activation loop rearrangement in FGFR1 kinase. *Nat. Commun.* **2015**, *6*, 7877.

(78) Lu, C.; Wu, C.; Ghoreishi, D.; Chen, W.; Wang, L.; Damm, W.; Ross, G. A.; Dahlgren, M. K.; Russell, E.; Von Bargen, C. D.; Abel, R.; Friesner, R. A.; Harder, E. D. OPLS4: Improving Force Field Accuracy on Challenging Regimes of Chemical Space. *J. Chem. Theory Comput.* **2021**, *17*, 4291−4300.

(79) Friesner, R. A.; Murphy, R. B.; Repasky, M. P.; Frye, L. L.; Greenwood, J. R.; Halgren, T. A.; Sanschagrin, P. C.; Mainz, D. T. Extra precision glide: docking and scoring incorporating a model of hydrophobic enclosure for protein-ligand complexes. *J. Med. Chem.* **2006**, *49*, 6177−6196.